EXPERIMENTAL AND NUMERICAL STUDY OF STEEL FIBER REINFORCED CONCRETE STRUCTURES SUBJECTED TO INTERNAL EXPLOSION

By

Nikhil Vasant Moon

Supervised by

Dr. Raad Azzawi

Presented to the Faculty of the Graduate School of

The University of Texas at Arlington in Partial Fulfillment

of the Requirements for the Degree of

Master of Science in Civil Engineering

THE UNIVERSITY OF TEXAS AT ARLINGTON

May 2020

Acknowledgments

I would like to offer my sincere appreciation to Dr. Raad Azzawi for his guidance and support throughout my graduate academic career. Dr. Raad Azzawi has been a wonderful mentor to me, providing invaluable technical and academic guidance throughout this research. His knowledge and advice have always provided me with great inspiration and motivation in dealing with academic and personal challenges. I would also like to thank Ahmed Alateeq, Atheer Al Khafaji, Niraj Bora, Yash Patel, and Harshwardhan Sawaitul, who provided me with invaluable support and assistance throughout this project. Appreciations are also extended to Dr. Sharareh Kermanshachi and Dr. Recep Birgul for their valuable advice and guidance.

I would like to thank my parents and my two sisters, who have always provided great encouragement and support in helping me overcome some of the greatest challenges.

May 20, 2020

Abstract

The University of Texas at Arlington, 2020

By Nikhil Vasant Moon, Supervising Professor: Dr. Raad Azzawi

This research investigates the effect of an accidental explosion of a steam boiler in a boiler room on steel fiber reinforced concrete (SFRC) structure in an industrial facility, using nonlinear analysis in ABAQUS FEA software. The mechanical properties of SFRC are calculated through testing at the UTA Civil Engineering Laboratory Building. Steel fiber dosages in concrete at different volume fractions are examined for the mechanical properties of concrete. In total, 9 (4" x 8") cylindrical specimens for compressive strength and modulus of elasticity test, 9 (4" x 8") cylindrical specimens for tensile strength test, and 9 (6" x 6" x 21") beam specimens for modulus of rupture test were produced and tested after 28 days of curing. Modulus of Elasticity is found for the different volume fractions of SRFC by stress vs strain curve from experimental tests. Adding 1% of steel fiber in concrete can increase the modulus of elasticity by 11%, compressive strength by 22%, tensile strength by 42%, and modulus of rupture by 32 %. Using the concrete properties obtained from experimental results, numerical analysis is done to find the effect of the Steam Boiler explosion on SFRC boiler room using nonlinear analysis in ABAQUS FEA software. Dynamic/Explicit loading condition is considered for analysis. It's found that adding 1% steel fiber by volume fraction can increase the overall capacity of concrete structure by 26%, decrease strain by 21%, and decrease the deflection by 23%. Parametric studies are also carried out at 1% SFRC by different arrangements of Steam Boiler closed room – with a rigid roof, with a frangible roof and circular vent in the roof. It's found that the reflected pressure due to explosion can be significantly reduced on the surrounding walls. In case, roof with circular vent the stresses decrease by 50%, strain decrease by 70% and with frangible roof stress decrease by 31%, strain by 38% and strain decrease by 38%.

Table of Contents

List of illustrations

List of table

1 INTRODUCTION

Accidental explosions in the industrial facility such as the Steam Boiler explosion can cause catastrophic damage to the surrounding building's external and internal structural frames, collapsing of the walls. Besides, major catastrophes resulting from gas-chemical explosions result in large dynamic loads, greater than the original design loads, of many structures. The objective of this research is to assess the existing methods of structural analysis and study the effect of dynamic loads due to a steam boiler explosion on the steel fiber reinforced concrete structures. This research study is directed towards the effect of a possible Steam Boiler explosion inside a closed room in an industrial facility. The study includes evaluation of the equivalent TriNitroToluene (TNT) charge weight from the ignition of the fuel used in operating the boiler and utilizes 3-D models on the ABAQUS software package for the computation of the effect of this explosion on the surrounding steel fibers reinforced concrete (SFRC) walls. Steel Fiber-reinforced concrete (SFRC) is a composite material with small, discontinuous fibers of high tensile strength that are added during the mixing process in concrete. The fibers used in fiber reinforced concrete are classified according to the material they are made of like steel fibers, glass fibers, synthetic fibers, and natural fibers. Compared to the same concrete composition without fibers, fiber reinforced concrete has significantly higher fracture energy, compressive and tensile strengths. The main advantages of SFRC are visible in the post-peak response when the fibers bridge the cracks and contribute to the resistance and ductility. SFRC provides easier construction applications and gives architects/structural designers the capability to explore complex structures. This study capitalizes on experimental and numerical methods to research the strengths and performance of steel fiber-reinforced concrete (SFRC) structures under dynamic loading due to the explosion of Steam boiler in a Closed room in an industrial facility. The experimental result outcome includes the assessment of the

compression test, Modulus of Elasticity, tensile strength, and shear performance of 18-cylinder specimens of 4” diameter and 8” height and 9 beams specimens, 6”x6”x21” subjected to 28 days of standard curing. The numerical result outcome includes the reduced deflection and strain in the concrete structure under the effect of dynamic loads. Further, the results of different arrangements of the Steam Boiler - Closed room with a rigid roof, frangible roof, and circular vent in the roof are explored, which shows the reduction of the incident pressure wave on the surrounding walls and roof slab.

1.1 Objectives

The main objective of this research is composed of two primary goals. The first is to do the nonlinear analysis to find the effect of the steam boiler explosion on three cases with 0%, 0.5%, and 1% SFRC. To accomplish the first objective, a laboratory testing of the SFRC material is done to find the compression strength, modulus of elasticity, tensile strength, and modulus of rupture. The modulus of elasticity and tensile strength are the main parameters in FEA. The target for the study is to collect the stresses, strain, and deflection values on the surrounding walls of the Steam boiler room from FEA to see how steel fibers contribute to a change in structure’s strength. The second objective consists of a parametric study to mitigate the effect of reflected pressure generated due to a steam boiler explosion in Steam Boiler's closed room. It consists of the analysis with a different arrangement of the roof of Steam Boiler -a closed room mainly rigid roof, frangible roof and circular vent in the roof.

1.2 Research Contribution

Industrial Building design industries will benefit from the research development of this field to save cost and design efforts for structures under dynamic loadings due to accidental explosion. An explosion within nearby a building can cause catastrophic damage to the building's structure, loss of life, and injuries to occupants. This research contributes to mitigating these damages by improving the resistance of the concrete structure to an explosion. The improved mechanical properties of SRFC can be used to mitigate the effects of an accidental explosion. Various design codes such as ACI (American Concrete Institute), ASCE (American Society of Civil Engineers), AASHTO (American Association of State Highway and Transportation) and UFC 3-340-02 (Structures to Resist the Effects of Accidental Explosions) have limited research on the effect of explosion loading on SFRC structures. This research also helps in finalizing the conceptual design of the industrial buildings with the possible arrangement of the roof slab to reduce the reflected pressure developed due to an explosion causing more damages.

1.3 Outline for Dissertation

This thesis is organized into the five following chapters, respectively:

Chapter 1 – Introduction: Defines the two major studies that this research focuses on, and the approaches that will be taken to achieve each study.

Chapter 2 – Literature Review: Discusses how SFRC enhance current design methods in structural engineering. Explores past research that studies the effect of the dynamic loading due to accidental explosions on concrete structures.

Chapter 3 – Material Properties: Discusses the process of creating an SFRC mix design and performing ASTM standard compression, modulus of elasticity, tension, and modulus of rupture tests to determine material properties.

Chapter 4- Explosion Loading Calculation and Numerical Analysis (FEA) -Describes the quantification of load due to the accidental explosion of a Steam Boiler. Also, it describes the nonlinear analysis steps to model a Steam Boiler Closed Room in FEA software-ABAQUS under dynamic loading conditions. This chapter compares the results of concrete structure behavior at a different volume fraction of SFRC under the dynamic/explicit loading due to the explosion. Parametric studies are also discussed to reduce the reflected pressure developed in the closed room due to the explosion. Different arrangements of the Steam Boiler room are studied with a rigid roof, frangible roof, and circular vent in the roof.

Chapter 5- Conclusion: Concludes how the objectives of this research are met. It also provides further recommendations for this research and the overall benefits of SFRC under dynamic loading due to an accidental explosion in an industry.

2 LITERATURE REVIEW

2.1 Explosion Phenomenon

Although research into the effects of explosions started in 1870, most development to determine the effect of explosions on buildings and other similar structures was carried out in the 1950s and 1960s by the U.S. military. The first technical manual on blast loading titled “Structures to resist the effects of accidental explosions”, were released in 1959 by the US Department of the Army. This manual got revised in 1990 and named TM 5-1300 [1], which is most widely used by the military and civilian organization for designing structures to prevent the propagation of explosion and to protect loss of life and valuable equipment. Paper and publications like Newmark 1956 [33], Biggs 1964 [38], ASCE 1985, were published during that period, which also provided information for the design.

The most extensive and widely referenced publication for empirical design is UFC 3-340-02 [2] (formerly TM5-1300 - U.S. Department of Defense 2008). This design manual addresses accidental explosions related to munitions manufacturing, handling, and storage. This design manual provides the design procedures that apply to buildings and structures for the blast-explosion scenarios. UFC 3-340-02 provides load determination information on configurations, such as partially open cubicles and interior explosions. Information on empirical methods is available from other sources as well such as Biggs’s introduction to Structural Dynamics (Biggs 1964) [38], Mays and Smith’s Blast Effects on Buildings (Mays and Smith 1995)[39] and ASCE’s Structural Design for Physical Security and Design of Blast Resistant Buildings in Petrochemical Facilities (ASCE Physical Security 1999, ASCE Petrochemical 1997)[6].

Dr. Raad Azzawi's thesis research carried in 1992 on the "Dynamic behavior of RC barriers in industrial units subjected to the internal explosion" also explains the behavior of the concrete structures under dynamic loading especially confined internal explosion. It describes the quantification of the loading criteria of the reinforced concrete structure subjected to an internal explosion.

An accidental explosion creates a blast wave as a result of the atmosphere surrounding the explosion source being pushed back. In general, the pressure of the compressed air at the blast wave front decays as it moves away from the blast source. As discussed in many widely used books and publications (i.e., Smith and Hetherington [7], 1994, Kinney and Graham, 1985 [8], Dusenberry, 2010 [9], Bulson, 1997 [10], ASCE, 1997, and DOD, 2008 [2]), a typical blast wave, as observed at a location removed from the center of an explosion, reaches a peak value of overpressure and begins to decay exponentially (as shown in figure 1), eventually decreasing below atmospheric pressure. This peak overpressure decreases as the distance from the explosion source increases.

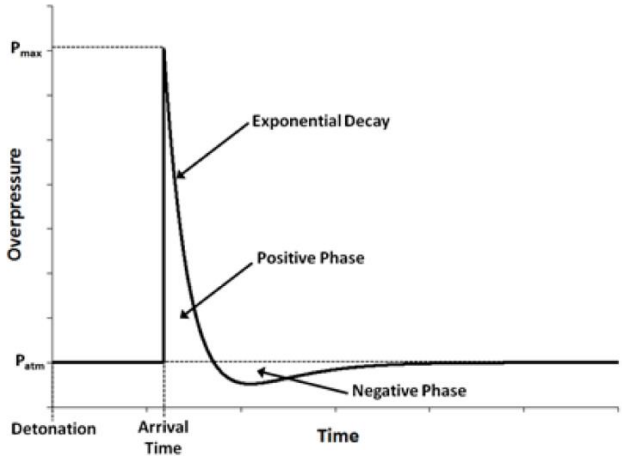

Figure 1 Typical overpressure amplitude for an accidental explosion

The amount of time it takes the blast wavefront to reach a given point is known as the arrival time. The overpressure profile can be divided into the positive pressure portion (positive phase) and a negative pressure portion (negative phase). Furthermore, the amount of time it takes the blast wave to decay below atmospheric pressure is known as the positive phase duration. The area under the curve during the positive phase duration is the positive blast wave impulse and is generally closely related to the damage capabilities of an accidental explosion. In many cases, this approximation is appropriate because the positive phase portion of the incident pressure wave is typically the most damaging. Accurately simulating a realistic blast wave acting on a structure for a given explosive scenario is challenging because the peak overpressure, positive phase duration, amount of explosive, and distance from the explosion source all affect the overpressure amplitude. Furthermore, accounting for reflection effects on a loading surface adds further complication to the blast loading model; generally, the structural response is fairly sensitive to capturing the correct incident wave reflection.

Several accidents have occurred in recent years due to steam boiler explosion such as St Mary's Hospital in New Jersey- the United States in 2006 and Dyeing factory in Muang district, Thailand in 2014, photos of the destructive damage is shown in Figure 2 & 3. The analysis and design of structures subjected to the Steam Boiler explosion require a detailed understanding of blast phenomena and the dynamic response of various structural elements. Excellent details are provided by the "Gas Explosion Handbook", published by Gexon Company in (2007) [11].

Figure 2 Boiler Explosion at St Mary's Hospital in New Jersey- United States

Figure 3 Boiler Explosion at a Dyeing factory in Muang district, Thailand

The mechanism of the gas clouds, ignition, heat of release rate, pool fire, combustion, and blast waves in free air is outlined, and an introduction to the different methods for the equivalent estimate of blast loads and structural response is presented. From a physical point of view, blasting demolition consists of two dynamic stages: The first stage is the

wave propagation and development of fracture network in the structure upon detonation of explosives, and the second stage is the collapse of the structure, weakened by dynamic fracture, due to the gravitational effect. Several studies on structural demolition by blasting has mainly handled the second stage [Mattern S (2006), Isobe (2006)].

The analysis and design of structures subjected to the Steam Boiler explosion require a detailed understanding of blast phenomena and the dynamic response of various structural elements. The paper presented by Mohamed F. Ibrahim, Hisham A. El-Arabaty, Ibrahim S. Moharram in Feb 2019 on “Effect of a steam boiler explosion on boiler room and adjacent buildings structure” [28] describes an in-depth explanation of the nature of Boilers explosions. FEA software is used to analyze the dynamic response of the structure under the explosion phenomenon. Abaqus/Explicit finite element techniques used to simulate blast loading due to internal steam boiler explosion is discussed herein; the conventional weapons effects blast loading model, or CONWEP (Hyde, 1988) [12]. CONWEP is well suited for simulating the overpressure wave associated with the detonation of conventional explosives. The underlying methodology of approach is discussed in this thesis.

2.2 Steel Fiber Reinforced Concrete (SFRC)

SFRC is an extremely advantageous innovation in structural engineering that helped strengthen the weaker mechanical properties of concrete like tensile and flexural strength. Concrete is known for its low strain capacity and little tensile strength during failure; the introduction of synthetic fibers into concrete’s matrix improves the material’s ductility and mechanical behavior. The American Concrete Institute recognizes the introduction of fibrous content into concrete to potentially improve the structural element’s capability in preserving its strength and reliability over its designed service life (ACI 544, 2002). Studies in the laboratory on Steel Fiber Reinforced Concrete (SFRC) specimens suggest that

dispersion of steel fibers in concrete improves the mechanical characteristics of the composite, notable resistance to dynamic loads (Banthia et al.)[13], shear strength (Khaloo and Kim,)[14], fatigue resistance (Johnston and Zemp,)[15] and post cracking strength (Elsaigh and Kearsley,).[16]. Steel fibers tend to interlock together and the vibration is encouraged to decrease the air void content and to improve the bond with reinforcement bars. Despite a stiff appearance, a well-adjusted fiber mixture can be pumped (ACI 544, 1993). Typically, normal concrete tends to be very brittle and not as ductile as steel. The low tensile strength in concrete allows the formation of "micro-cracks". The size of the fibers relative to that of the aggregates determines their distribution; it is recommended to choose fibers not shorter than the maximum aggregate size to be effective in the hardened state. Usually, the fiber length is 2-4 times that of the maximum aggregate size." (Johnston, 1996 and Coetze, 1990). Concrete typically has a lower modulus of rupture (fr). Therefore, concrete begins to crack more rapidly than steel, causing flexural failure. Extensive research performed on the application of steel fibers in concrete as a different method of reinforcing concrete for shear strength ultimately leads to the adoption of steel fibers for ACI's 2008 building code requirements (ACI 318-08, 2008).

Also, a comparative study carried out by A.M Shende et al. [17] on steel fiber reinforced concrete at a volume fraction of 0%, 1%, 2%, and 3% were used, and it was observed that compressive strength, tensile strength and flexural strength from steel fibers were on higher side from 3% fibers as compared to that produced from 0%, 1%, and 2% fibers. Through the utilization of steel fibers, the compressive strength increased from 11 to 28%, flexural strength increased from 18 to 58% and tensile strength from 9 to 29%.

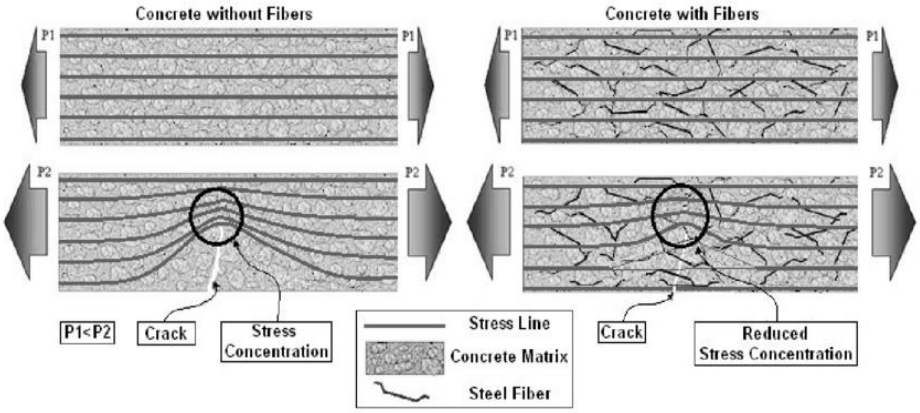

Figure 4 Steel Fibers in Concrete (Figueiredo -2005)

Steel fiber reinforced concrete (SFRC) appears stiffer compared with conventional concrete without fibers, even when the workability is the same (Johnston, 2001). Also, it is recommended to reduce the volume of coarse aggregates by 10% compared with plain concrete, and superplasticizer should be added to obtain the desirable workability (Johnston, 2001). The study carried by J. Mater [18] on the mechanical properties of SFRC indicates that fiber-matrix interaction contributes significantly to the enhancement of mechanical properties caused by the introduction of fibers. Extensive research performed on the application of steel fibers in concrete as a different method of reinforcing concrete for shear strength ultimately leads to the adoption of steel fibers for ACI's 2008 building code requirements (ACI 318-08, 2008). Another study shows that with increasing fiber content, the pre-peak ascending branch of the compressive stress-strain relationship is marginally improved, resulting in a slightly higher elastic modulus (Susetyo, 2009); this improvement results chiefly from the higher modulus of elasticity of steel fibers.

Ductility is the ability of concrete to undergo maximum plastic deformation before the collapse. It is considered a good warning indicator before failure. The ductility behavior of steel fiber on concrete beams studied by Mahalingam (2013). They used steel fiber content of 0.5, 1, and 1.5 % by volume. They concluded that the ultimate load-carrying capacity of

concrete beams was improved by 14, 20, and 32%, respectively, compared to the conventional reinforced concrete beam.

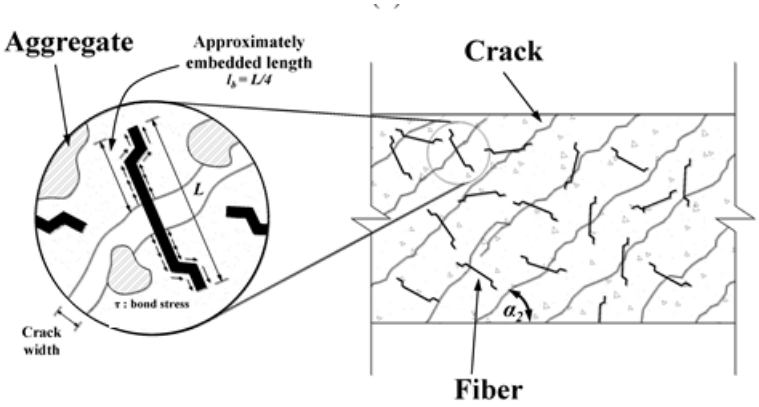

Figure 5 Steel Fibers tying cracks in Concrete

In 2015, Wan Jusoh [19] has proposed hybrid fiber-reinforced composite concrete (HYFRCC). Steel fiber (SF) was found to enhance the flexural and tensile strengths, and at the same time, it can able to resist the formation of macro cracking and concrete spalling. In 2016, Song and Yin [20] have conducted the compressive test and impact test, and then the hybrid effect between steel fiber (SF) and carbon fiber (CF) was evaluated by employing the hybrid effect index. Compressive toughness and impact toughness of (SFRC), carbon fiber reinforced concrete (CFRC), and hybrid fiber reinforced concrete. (HFRC) were explored at steel fiber volume fraction 0.5, 1, and 1.5%, and carbon fiber 0.1, 0.2, and 0.3%. Results showed that the addition of steel fiber and carbon fiber can increase the compressive strength. SF, CF, and the hybridization between them could increase the compressive toughness significantly.

In 2019, Dr. Raad Azzawi and Dr. Ali Abolmaali [4] conducted the research of steel fiber RC hollow columns under eccentric loading, which describes steel fiber enhances the strength capacity, ductility, and allowable stresses within the hollow column. Another research conducted by Dr. Raad Azzawi and Nancy Varughese [5] on the flexural behavior

of preflex SFRC encased steel joist composite beams explains adding 1% steel fibers by volume can increase the load capacity by 33% and decrease the midspan displacement by 70% in comparison to the same beam using plain concrete. The increase in steel fibers and cambering shows an improvement to the flexural capacity and cracking point of the beam, which can provide more strength to structures such as long-span bridges.

In short, the high tensile strength of the steel fiber used in high-strength SFRC contributes to the mitigation of cracking and to energy dissipation. Related research conducted by the author indicates the necessity for high-performance steel fiber to improve the toughness and flexural strength of high-strength concrete. Studies associated with the mechanical characteristics of high-strength SFRC, which focus on fiber content, aspect ratio, and tensile strength, are needed to ensure good performance without loss of workability due to the excessive fiber content in high-strength SFRC.

2.3 Finite Element Analysis

2.3.1 History and Progression of FEA

The FEA approach involves dividing an object such as a mechanical part or a building structure into small elements and then using the mathematical relationships between these elements to compute stresses and deflections caused by various loading conditions. Created as numerical techniques for finding approximate solutions to boundary value problems for partial differential equations, FEM is based on a problem domain's subdivision into simpler parts called finite elements, and on the calculus of variational methods to minimize an associated error function. In 1941-1942, Hrennikoff and Courant developed mesh discretization methods for solving elasticity and structural analysis problems in civil and aeronautical engineering. FEA technology evolved as an academic concept in the 1950s and soon caught the attention of structural analysts in the aerospace industry and

at NASA. From 1956 to 1960, Ray W. Clough published the first paper on the finite element method (FEM), General Motors, and IBM build the computer system DAC-1 (Design Augmented by Computers) to facilitate the design of cars. One of the first papers on this subject was published in 1956 in the Journal of Aeronautical Engineering by a group of Boeing engineers led by Jonathan Turner. Four academicians: J. H. Argyris, R. W. Clough, H. C. Martin, and O. C. Zienkiewicz are largely responsible for the “technology transfer” from the aerospace industry to a wider range of engineering applications of FEA during the 1950s and 1960s.

In 1965, NASTRAN (NASA Structural Analysis) was developed as a structural analysis solver tool. Another fundamental mathematical contribution to the FEM is represented by the book “An Analysis of the Finite Element Method” by Gilbert Strang and George Fix, first published in 1973. Since then, FEM has been generalized for the numerical modeling of physical systems in many engineering disciplines, including electromagnetism, heat transfer, and fluid dynamics. There are many approaches and advantages of this method, but the main purpose is to take any geometrical object and divide it into smaller elements to combine the solution of the elements by variational approximation. This computerized mathematical model could assemble 2D plate elements and create an in-plane stiffness matrix for different shapes such as rectangles and triangles. Some of the core benefits of FEM include “increased accuracy, enhanced design and better insight into critical design parameters, virtual prototyping, fewer hardware prototypes, a faster and less expensive design cycle, increased productivity, and increased revenue”. Throughout modern engineering history, FEM algorithms were embedded in many powerful design tools, contributing to raising the standards of engineering and significantly improving the design process.

2.3.2 Application of FEM in ABAQUS

FEA is a numerical method for solving partial differential equations as well as integral equations generated from the complex structure. It starts the analysis by dividing the interested object into many non-uniform regions (finite elements) that are connected to associated nodes. For each typical element, there exist dependent variables at the nodes such as displacement. An interpolation function is defined relative to the values of the dependent variables at the nodes associated with the element.

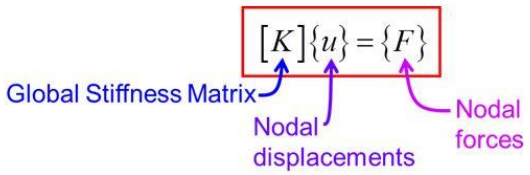

Figure 6 Fundamental Concept for Algebraic Equations in ABAQUS [23]

[K] is the global stiffness matrix, which is determined by geometry, material property, and element property. [u] is the displacement vector, which describes the motion of nodes under force. [F] is the force vector, which describes the force applied to the element. The functions of all the elements are assembled into the global matrix equation (governing algebraic equations) to represent the object we study. After applying the boundary condition, the governing algebraic equations can be solved for the dependent variable at each node. The strain and stress can be calculated based on the displacement of nodes associated with the element.

For this research, ABAQUS is the FEA software that models and analyzes the beam to find load-displacement under a static load. It does so by discretizing it into finer elements and formulating a solution from the given parameters and controlled variables. ABAQUS can model and analyze the solutions for various fundamental concepts such as elastic, thermal, fluid dynamics, electrostatics, etc. by taking the governing equation and applying the boundary conditions [22]. These analyses are performed through a set of simultaneous

algebraic equations. Jobs monitor the analysis, and the results are shown in 3D visualization for evaluation purposes. The equations used for basic analysis are from mechanics concepts and nonlinear finite element analysis. These equations set the requirements for finite rotations, deformation, stress, and strain [22].

For nonlinear analysis, the goal is to obtain a convergent solution with minimal effort. Once the model is ready for analysis, ABAQUS allows two approaches for setting up the step increments that will load the model. The first approach is the Direct user control of the increment size allows the user to set a number for the increments within one step that the analysis can increase steadily for. The second approach is Automatic control, where the user sets tolerances and error parameters for the steps [22]. Digital computation reduces a significant amount of time spent in labs trying to imitate the same results. FEA Software such as ANSYS, ABAQUS, FEA, Autodesk, etc. can be used to solve the complex structure's displacements, stresses, and other functions.

3 MATERIAL PROPERTIES

3.1 Concrete Mix Design

The material properties are found through lab testing based on ASTM C192/C192M procedure [26] before performing the numerical analysis using SFRC. The first step is to create a concrete mixture in the lab and add the volume fraction, Vf, of steel fibers. To do this, the following materials must go into the mix for a 27 cubic feet batch; coarse aggregate, fine aggregate, cement, and water. The mixture quantities are shown in Tables 1 through 3, and the type of steel fibers used is seen in Figure 7.

Table 1: Material Properties for Concrete Mix

Description	Cement	Fine Aggregate	Coarse Aggregate
Specific Gravity	3.15	2.82	2.5
Density (lb/ cf)	196	176	160.68

Table 2: Mix Proportions for 27 cubic feet Batch

Concrete Mix Description	Cement (lbs)	Water (lbs)	Fine aggregates (lbs)	Coarse Aggregates (lbs)	Water-cement ratio	% Steel Fiber	Steel Fiber (lb)
0.0% SFRC PC	680	306	1752	1263	0.45	0.0	0
0.5% SFRC	677	304	1743	1257	0.45	0.5	20.0
1.0% SFRC	674	302	1734	1251	0.45	1.0	40.0

Table 3: Material Properties of Steel Fibers

Length (in)	Diameter (in)	Tensile Strength (ksi)	Young's Modulus (ksi)
2.4	0.03	178	29000

Figure 7 Steel Fibers

The mixing process is done in a standard lab concrete mixer in the Civil Engineering Laboratory Building at The University of Texas at Arlington. There are three volume fractions of steel fibers in each concrete batch. The first batch has 0.0% Vf steel fibers, the second has 0.5%, and the third has 1.0%. After the concrete is made in the mixer, it is immediately put into the molds that ASTM specifies for each type of test [26]. The concrete molds for the compression test are 9 cylinders of 4" x 8". The next 9 molds are the rectangular beams that are 6" x 6" x 21" for the modulus of rupture test. The last set of 9 molds are for the cylinders that are 4" x 8" for the split test. Dry rodding helps consolidate the mix into the molds, and this process is important to ensure that the gaps created from the steel fibers do not remain once in the mold. Figures 8-14 show each SFRC mix design in the molds that will be tested.

Table 4: Framework of Experimental Study in Lab

Investigation of Mechanical Properties of SFRC Specimen			
Specimens	**0.0 % SFRC**	**0.5 % SFRC**	**1.0 % SFRC**
9 Flexure Beams ASTM C78 (6”x 6”x 21”)	3 Plain Concrete Beams (Plain Concrete)	3 Steel Fiber-Reinforced Concrete Beams with Vf = 0.5 % (SFRC = 0.5 %)	3 Steel Fiber-Reinforced Concrete Beams with Vf = 1.0 % (SFRC = 1.0 %)
9 Cylinders Compressive Strength Test ASTM C39 (4”x 8”)	3 Plain Concrete Cylinders (Plain Concrete)	3 Steel Fiber-Reinforced Concrete Cylinders with Vf = 0.5 % (SFRC = 0.5 %)	3 Steel Fiber-Reinforced Concrete Cylinders with Vf = 0.5 % (SFRC = 0.5 %)
9 Cylinders Tensile Strength Test ASTM C469 (4”x 8”)	3 Plain Concrete Cylinders (Plain Concrete)	3 Steel Fiber-Reinforced Concrete Cylinders with Vf = 0.5 % (SFRC = 0.5 %)	3 Steel Fiber-Reinforced Concrete Cylinders with Vf = 1.0 % (SFRC = 1.0 %)

Figure 8. 0.0% SFRC - Beam (6”x6”x21”) for Flexure and Cylinder Molds (4” x 8”) for Split Test

Figure 9. 0.0% SFRC - Cylinder Molds (4” x 8”) for Split Test

Figure 10. 0.0% SFRC - Beam Molds (6”x6”x21”) for Flexure Test

Figure 11. 0.5% SFRC - Cylinder Molds (4” x 8”) for Compressive Strength and Split Test

Figure 12. 0.5% SFRC - Beam Molds (6”x6”x21”) for Flexure Test

Figure 13. 1.0% SFRC - Cylinder Molds (4” x 8”) for Compressive Strength and Split Test

Figure 14. 0.0 %, 0.5% and 1.0% SFRC - Beam Molds (6”x6”x21”) for Flexure Test

A slump test is done to determine workability and consistency. A slump of 6.5 inch was found for 0.0% SFRC, 6 inch for 0.5% SFRC and 5.7 inch for 1.0% SFRC.

Figure 15. Slump Test on 0.5 % Steel Fiber Concrete Mix

Figures 16 show the cylinders and beams placed in the humidity-controlled room. Each Vf of steel fibers can be seen from red label markings. The textures of the concrete for each batch are very different depending on the percentage of steel fibers. The 0% concrete beams and cylinders have a much smoother surface. In the 0.5% and 1% beams and cylinders, this is not the case. Instead, they appear much more jagged and more porous since the fibers are drying into the concrete. This is because when the steel fibers mix into the concrete, there are two elements to combining, making the mix less consolidated and porous.

Figure 16. Humidity-Controlled Room (Specimens marked in white boxes)

3.2 Compression, Split, and Modulus of Rupture Tests

3.2.1 Compression Test

ASTM C39 provides the method for testing the small cylinders (4” x 8”) [24]. A 500 kip compression machine is used to perform the test in the Civil Engineering Lab Building, UTA. The cylinder is placed where its circular cross-section is directly in contact with the load. The process is done by a consistent incremental loading of 400 lb/sec until the cylinder reaches its ultimate load capacity. Figure 17 shows the machine used for testing.

Figure 17. Compression Testing Machine with 0.0% SFRC - Cylinder (4” x 8”)

This load is used to calculate the compressive strength, which can be found in equation 1 where fc' is the compressive strength, P represents the load capacity, and r is the radius of the cylinder. The elastic modulus of concrete is found through the stress vs strain curve by an experimental study in the lab discussed in part 3.2.1.1. Sample calculations for compressive strength and elastic modulus can be found in Appendix A. Figures 17 & 18 shows the setup of each compression test.

$$fc' = \frac{P}{\pi r^2} \qquad (Eq. 1)$$

Figure 18. 0.0% SFRC - Cylinder (4” x 8”) Collapses after testing

3.2.1.1 Concrete Strain Gauge

A strain gauge was installed on the surface of concrete cylinder molds, referred to as “*concrete strain gauges*” henceforth in this study. Concrete strain gauges used are single element strain gauge, utilized based on the failure mechanism dominating the area on which the gauge is to be installed. Therefore, a one strain gauge at every cylinder specimen was installed on the concrete surface of the 6 cylinders.

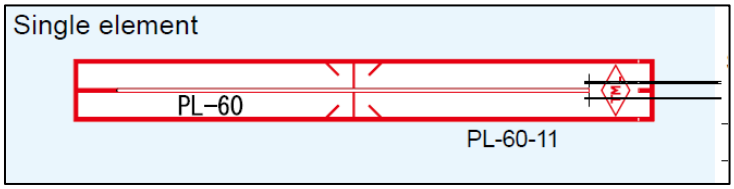

Figure 19. Single Element Strain Gauge

Applicable specimen	Concrete, Mortar
Operational temperature (°C)	-20 to +80 °C
Temperature compensation range (°C)	+10 to +80 °C
Applicable adhesive	CN-E, RP-2, PS
Backing	Polyester
Element	Cu-Ni (wire)
Strain limit at room temperature	2 % (20000 x 10^{-6} strain)
Fatigue life at room temperature	1 x 10^{5} (±1000 x 10^{-6} strain)

Figure 20. Strain Gauge Specification

Single Element- wire strain gauges utilize a transparent plastic backing impregnated with polyester resin. The gauge length used is 60 mm, so it is suited to the measurement of concrete strain. Since the backing is transparent, the bonding position can easily be checked in the installation works. Figure 19 & 20 shows the specification of concrete strain gauge.

A strain gauge was satisfactorily bonded to the surface of the concrete. Grit Blaster was used to remove any loose material on the surface of the concrete. A mild acidic solution (Figure 21) was applied in and around the gaging area and scrubbed with grit blaster to remove additional loose material. A strain gauge is then pasted on the gaging area with a strong adhesive.

A compression testing machine of 400 kip is used to perform the compression strength test with setup of strain gauge and LVDT.

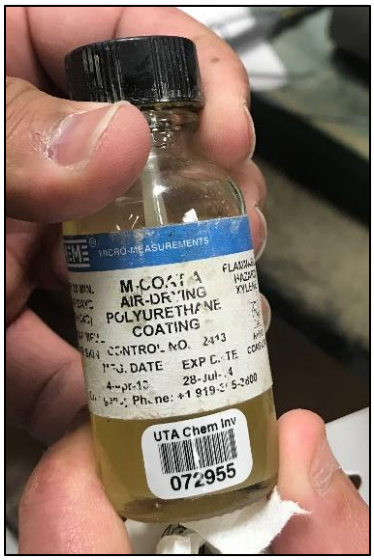

Figure 21. M Coat A applied on the surface of the concrete gaging area.

Figure 22. Strain Gauge assembled on Cylinder specimen.

Figure 23. 0.5% SFRC – Cylinder (4” x 8”) with a Strain gauge.

Figure 24. 0.5% SFRC Cylinder (4” x 8”) with Strain gauge and LVDT Test Setup

Figure 25. 0.5% SFRC - Cylinder (4” x 8”) with Strain gauge and LVDT for Compression Strength Test Setup

Figure 26. 0.5% SFRC - Cylinder (4” x 8”) after testing

Figure 27. 1.0 % SFRC Cylinder (4” x 8”) with Strain gauge and LVDT Test Setup

Figure 28. 1.0 % SFRC Cylinder (4” x 8”) collapses at 54.29 kips

Figure 29. 1.0 % SFRC - Cylinder (4” x 8”) with Strain gauge and LVDT for Compression Strength Test Setup

When comparing each cylinder, the 0%-cylinder from Figure 18 has significant fractures and cracks at an average of 44.24 kips. The uniaxial compression forms micro-cracks very early on, which over time expand in the same direction as the stress. In the 0.5%-cylinder, the steel fibers prove effective by maintaining the bond between the cracks and has a load capacity of 49.73 kips. The cracks shown in Figure 26 do not extend to the bottom, meaning although the cylinder reaches maximum load capacity, it is still able to resist pullout force on the steel fibers in some regions. The 1% fiber collapses at the largest load capacity of 54.29 kips, and it does not show significant fracturing like the other specimens as seen in Figure 28. The cracks propagate around the bottom and top of the cylinder, but the center remains intact from the steel fiber bond.

3.2.2 Split Test

Split tests are done according to ASTM C496 using 4” x 8” cylinders [27]. The 500-kips machine is used for determining the tensile strength of the specimen, as shown in Figure 30. The cylinder lies horizontally on the testing table as a diametral compressive force loads it along its length. The machine applies load at a rate of 150 lb/sec till the cylinder reaches failure along the vertical diameter. A steel plate with side plates is placed around the beam during this process to reduce the amount of compressive stress where the load will be applied. Once the ultimate load is recorded, the tensile strength is calculated according to equation 2. f_t is the tensile strength, P is the load capacity, L represents the length, and D is the diameter of the cylinder. Sample Calculations for tensile strength can be found in Appendix A.

$$f_t = \frac{2P}{\pi LD} \qquad (Eq. 2)$$

Figure 30. Split Tensile Setup- 0.0 % SFRC - Cylinder (4” x 8”)

For the split test in Figures 30, of the 0% large cylinder, the specimen broke at an average of 21.66 kips.

Figure 31. Split Tensile Setup- 0.5 % SFRC - Cylinder (4” x 8”)

Figure 32. Split Tensile Setup- 1.0 % SFRC - Cylinder (4” x 8”)

For the 0.5% cylinder (Figure 31), the specimen broke at 24.47 kips, and at 1% the cylinder broke at 30.76 kips (Figure 32).

3.2.3 Modulus of Rupture Test

Flexure tests are done using a rectangular beam (6”x6”x21”) as per ASTM C78 and placed lengthwise under the machine [25]. Loading will occur at the 1/3 points on the beam to exhibit pure bending in the middle portion. MTS machine of 55 kips capacity is used for the testing. The specimen is loaded at position rate at 0.04 inch/min, and fracture stress occurs in this middle portion called modulus of rupture. The machine records the ultimate load capacity, and equation 3 is used to find the modulus of rupture, fr. P is the load at failure, L is the length of the beam, D represents the depth and B the width. Sample calculations for the modulus of rupture can be found in Appendix A. Figures 33-38 show the setup and testing of 3 beams to determine the modulus of rupture.

$$f_r = \frac{PL}{BD^2} \qquad (Eq. 3)$$

Figure 33. 0.0% SFRC Beam-Modulus of Rupture Test Setup

Figure 34. 0.0% SFRC Beam at Failure Load 6.82 Kips

Figure 35. 0.5% SFRC Beam-Modulus of Rupture Test Setup

Figure 36. 0.5% SFRC Beam at Failure Load 7.57 Kips

Figure 37. 1.0% SFRC Beam-Modulus of Rupture Test Setup

Figure 38. 1.0% SFRC Beam at Failure Load 9.01 Kips

In comparison, Figures 34 and 36 show the improvement in flexural strength of the concrete when 0.5% volume steel fibers are added. In Figure 34, the beam cracks along the entire midspan section at a load of 6.82 kips. Once the steel fibers are in the concrete, the beam appears to harden like the 0% but performs better in flexure. This beam reaches its capacity at 7.57 kips for 0.5% volume steel fibers (Figure 36), which shows that the beam is improving with the addition of steel fibers. The cracking stops midway at the beam and does not fully collapse the beam. The 1% SFRC beam fails at 9.01 kips (Figure 38),

which shows that adding steel fibers into a normal concrete mix can improve the modulus of rupture of a beam.

Figure 39. Research Team during testing of beam

3.2.4 SFRC Material Properties

Tables 5 through 8 summarize the compressive, tensile, and modulus of rupture values found from the SFRC material lab testing.

Table 5: Concrete Compression Test

Concrete Compressive Strength, fc' (psi)			
Steel Fiber Volume (%)	0.0 %	0.5 %	1.0 %
Cylinder 1	3375.61	4155.11	4307.18
Cylinder 2	3619.83	3796.25	4143.47
Cylinder 3	3568.25	3922.96	4512.36
Average fc' (psi)	**3521**	**3958**	**4321**
% Increase	**0 %**	**12.41 %**	**22.72 %**

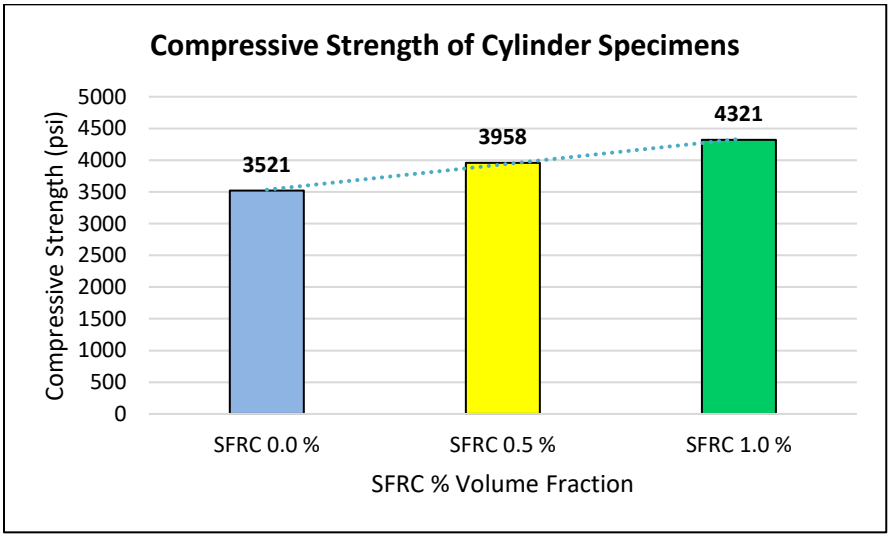

Concrete's compressive strength, fc', determines its ability to uniaxial loading. Table 5 shows that as the volume of fibers increases, so does the compressive strength. Steel fibers create a bond inside the concrete that postpones buckling and reduces cracking.

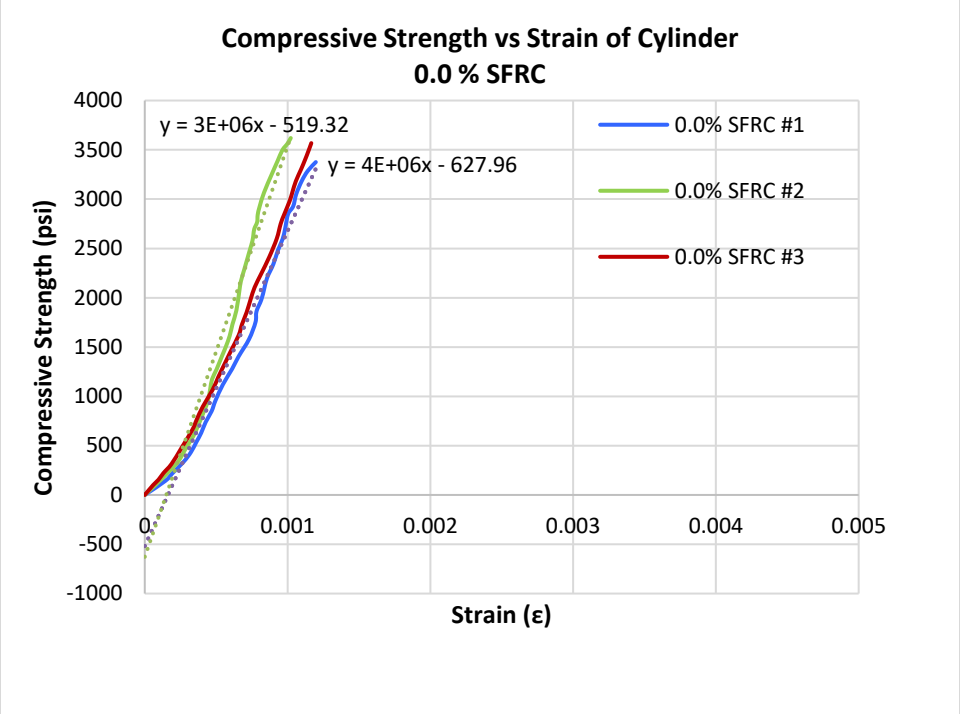

Figure 40 Compressive stress-strain curves for 0.0 % SFRC Concrete cylinders

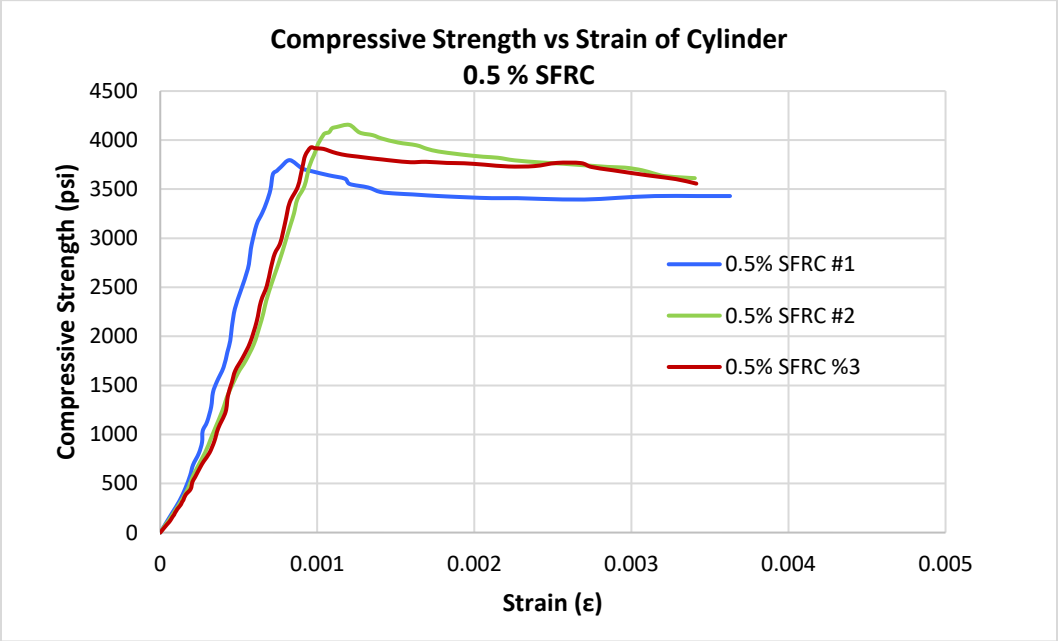

Figure 41 Compressive stress-strain curves for 0.5 % SFRC Concrete cylinders

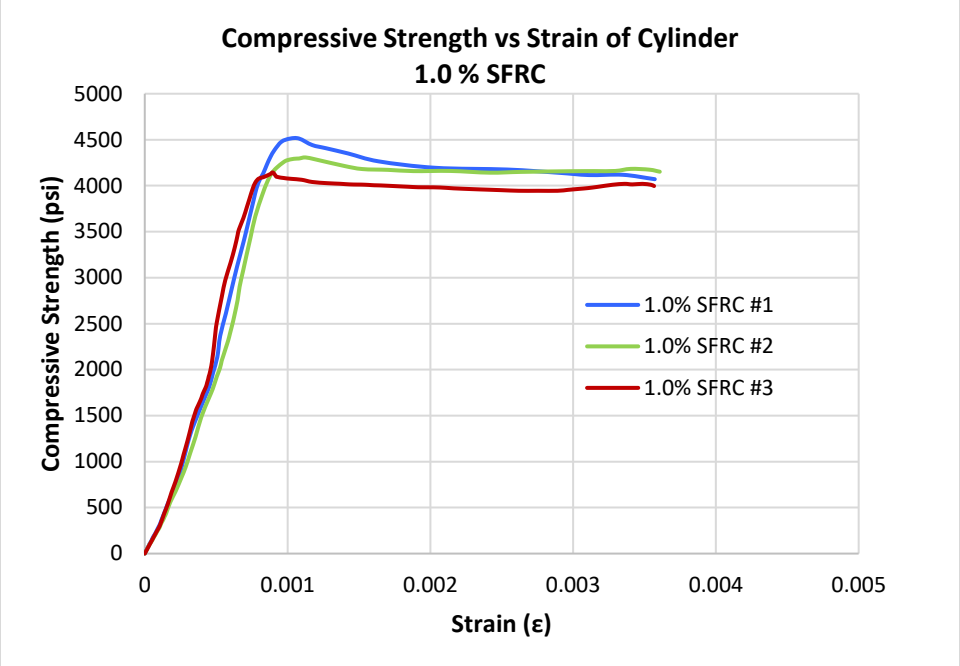

Figure 42 Compressive stress-strain curves for 1.0 % SFRC Concrete cylinders

From the compressive stress vs strain graphs Figure 40,41 and 42, average Modulus of Elasticity is calculated by the slope trendline.

Table 6: Modulus of elasticity of experimental specimens

Modulus of elasticity of experimental specimens			
% Fibers	0.0 %	0.5 %	1.0 %
Compressive strength, fc' (psi)	3521	3958	4321
Average Elastic Modulus, Ec (psi)	**3466823**	**3675670**	**3848020**
% Increase for *Ec*	**-**	**6.02 %**	**11.00 %**

Different elastic modulus equations were used to evaluate their accuracy with the experimental data and the database obtained from the literature. The equations equate the elastic modulus of concrete with steel fibers with the elastic modulus of normal concrete,

fiber's volume fraction, and/or fiber aspect ratio (fiber length divided by fiber diameter)—that is, Ezeldin and Balaguru [35], Gao et al. [36], and Padmarajaiah [37]. Table 7 summarizes all the elastic modulus equations in comparison with the experimental results. Modulus of elasticity of 0.5 % and 1.0 % SFRC obtained from experimental results are compared with the available elastic modulus equations obtained from the literature.

Equation of modulus of elasticity obtained from literature are as follows:

Ezeldin and Balaguru [35], $E_c = E_{cp} + 3105 V_f S_p$

Gao et al. [36], $E_c = E_{cp}(1 + 0.173 V_f S_p)$

Padmarajaiah [37] $E_c = E_{cp} + 2440.2\, V_f S_p$

Where E_c = Modulus of elasticity of concrete with Steel fibers,

E_{cp} = Modulus of elasticity of plain concrete,

V_f = Volume fraction of Steel fibers (%),

S_p = Aspect ratio for fiber (L_f/d_f), L_f = Length of steel fiber, d_f = diameter of steel fiber

Table 7: Modulus of Elasticity comparison with the equations

Comparison of Modulus of elasticity of experimental specimens with equations			
% Fibers	0.0 %	0.5 %	1.0 %
Results Obtained from Experiments, Average Elastic Modulus, Ec (psi)	**3466823.51**	**3675670.86**	**3848020.99**
Ezeldin and Balaguru [35] $E_c = E_{cp} + 3105 V_f S_p$	**3466823.51**	**3646960.70**	**3827097.90**
Gao et al. [36], $E_c = E_{cp}(1 + 0.173 V_f S_p)$	**3466823.51**	**3706727.72**	**3946631.88**
Padmarajaiah [37] $E_c = E_{cp} + 2440.2\, V_f S_p$	**3466823.51**	**3608392.20**	**3749960.89**

Modulus of elasticity obtained from experimental studies for 0.5 % and 1.0 % SFRC were more closely matched with the Ezeldin and Balaguru equation compared to other equations. Hence the results obtained from the experimental test are relevant to the Ezeldin and Balaguru equation.

Table 8: Concrete Split Test

Concrete Tensile Strength, f_t (psi)			
Steel Fiber Volume (%)	0.0 %	0.5 %	1.0 %
Cylinder 1	409.2	475.3	580.2
Cylinder 2	439.0	481.7	658.8
Cylinder 3	446.1	504.4	597.8
Average ft (psi)	**431**	**487**	**612**
% Increase	**-**	**13.00 %**	**42.00 %**

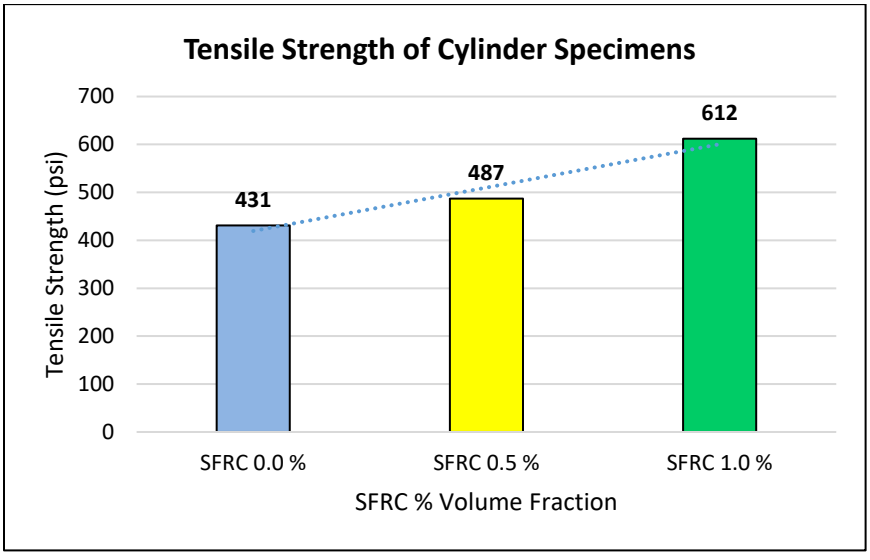

The change in concrete's tensile strength capacity can be seen in Table 8. The addition of fibers into the concrete mix increases the tensile strength of concrete by almost 42.00%.

Table 9: Concrete Modulus of Rupture Test

Concrete Modulus of rupture, f_r (psi)			
Steel Fiber Volume (%)	0.0 %	0.5 %	1.0 %
Beam 1	581.9	651.5	798.5
Beam 2	697.7	732.6	868.1
Beam 3	619.0	719.1	839.2
Average fr (psi)	**632**	**701**	**835**
% Increase	**-**	**11.00 %**	**32.12 %**

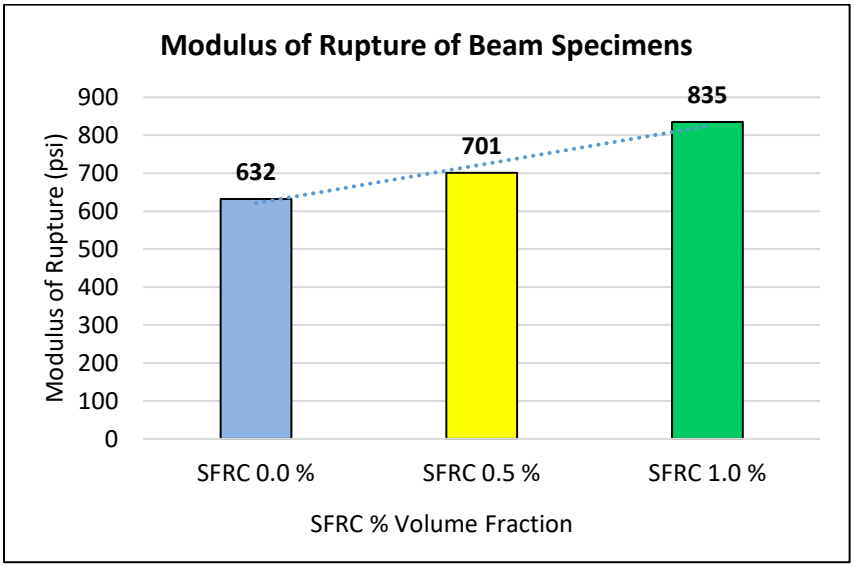

By the addition of steel fibers, concrete's modulus of rupture increases significantly. As seen from Table 9, fr for 1% volume of steel fibers increases the modulus of rupture around 32.12 %. This mechanical property can be increased if more steel fibers are added. Other factors should be considered when adding steel fibers, but the material properties prove that the beam should perform well under flexural stress because the steel is postponing micro-cracks from forming.

4 EXPLOSION LOAD CALCULATION & NUMERICAL ANALYSIS

4.1 Explosion Wave Characteristics

The primary step in the accidental explosion-resistant design of structures is to know how to define the explosion loading. The structures may be subjected to blast loading, which comprises ground shock, blast pressure, and fragment impact, particularly in the near-range region, whereas, in the far-field region, structures are subjected to only blast pressure. The present research focuses only on explosive-induced blast loading. Blast overpressure is expressed relative to ambient condition (P_0) rather than the absolute pressure. Figure 43 shows the typical blast-induced pressure wave profile produced from the ideal detonation about amplitude and frequency that governs the design of any structural component. An ideal blast wave representation and its characteristics are a function of the distance of a structure to the center of the charge, R, and time, t. The peak pressure is known as peak positive overpressure, P_{so}. A negative-phase follows, in which the pressure is lower than ambient pressure, known as P_{so}^- under pressure. The duration of peak positive overpressure and under pressure are known as positive (t_o) and negative (t_o^-) duration, respectively.

Several empirical approaches to compute and define the blast pressure profile have been proposed by many researchers and have been investigated extensively (Brode 1955 [29]; Henrych 1979; Baker 1983 [30]; Held 1983; Kingery and Bulmash 1984; Kinney and Grahm 1985; Ismail and Murray 1993; Smith and Hetherington 1994; Krauthammer and Altenberg 2000; Lam 2004; Bangash and Bangash 2006; Sadovskiy 2004; Baji_c 2007; Borgers and Vantomme 2008; Teich and Gebbeken 2010). Friedlander's equation is most commonly used to describe the blast wave profile owing to its simplicity versus the other empirical

relations. The original Friedlander's equation is independent of atmospheric

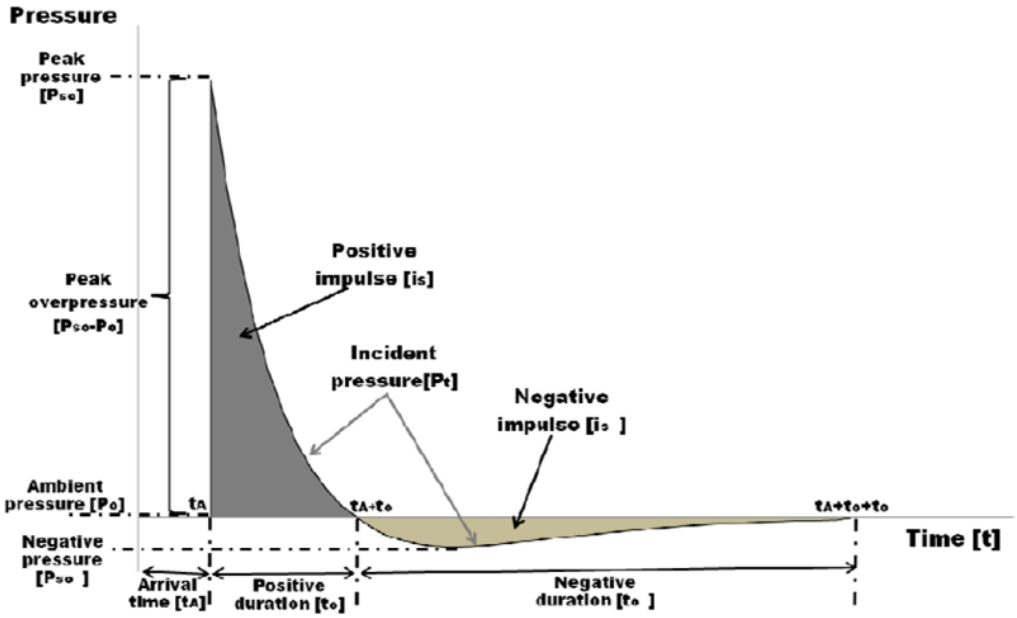

Figure 43 Ideal blast wave's pressure time history [31]

pressure. However, the modified Friedlander's equation (eq.4) (with atmospheric pressure, P_0) is widely used to model the blast wave, being comparatively more accurate and reasonably simpler in comparison with the others and given as

$$P_S(t) = P_0 + P_{so}\left(1 - \frac{t}{t_o}\right)e^{-b\left(\frac{t}{t_o}\right)} \qquad Eq.4$$

where P_{so} is the peak overpressure,

t_o is the positive-phase duration,

b is a decay coefficient of the wave-form and

t is the time elapsed, which is measured from the instant of blast arrival.

The decay coefficient b is calculated through a non-linear fitting of an experimental pressure-time curve over its positive-phase. Besides the peak-pressure, for designing purposes, an important parameter of the blast wave pulse is its impulse, which relates to

the total force (per unit area) that is applied to a structure due to the explosion. It is defined as the shaded area under the overpressure-time curve (Figure 43). The impulse is distinguished into positive i_s and negative i_s^-, according to the relevant phase of the blast wave time history. The expression is shown in equation 5 in the case of the positive impulse, which is more significant than its negative counterpart in terms of building collapse prevention [2],

$$i_s = \int_{t_A}^{t_A+t_o} P_S\,(t)dt \qquad Eq.5$$

For the above Friedlander equation, the positive impulse can be analytically calculated as

$$i_s = \frac{P_{so}t_o}{b^2}[b - 1 + e^{-b}] \qquad Eq.6$$

This equation constitutes an alternative way for solving iteratively for the decay parameter b when the values of the i_s, $P_{so,}$ and t_o are known from experimental data.

4.2 Blast Scaled Distance Laws

One of the most important parameters for explosion loading computations is the distance of the detonation point from the structure. The peak pressure value and velocity of the blast wave, which were described earlier, decrease rapidly by increasing the distance between the blast source and the target surface, as shown in Figure 44. In the figure, only the positive phases of the blast waves are depicted, whose durations are longer whenever the distance from the detonation point increases. The effect of distance on the blast characteristics can be taken into account by the introduction of scaling laws. These laws can scale parameters, which were defined through experiments, to be used for varying values of distance and charge energy release.

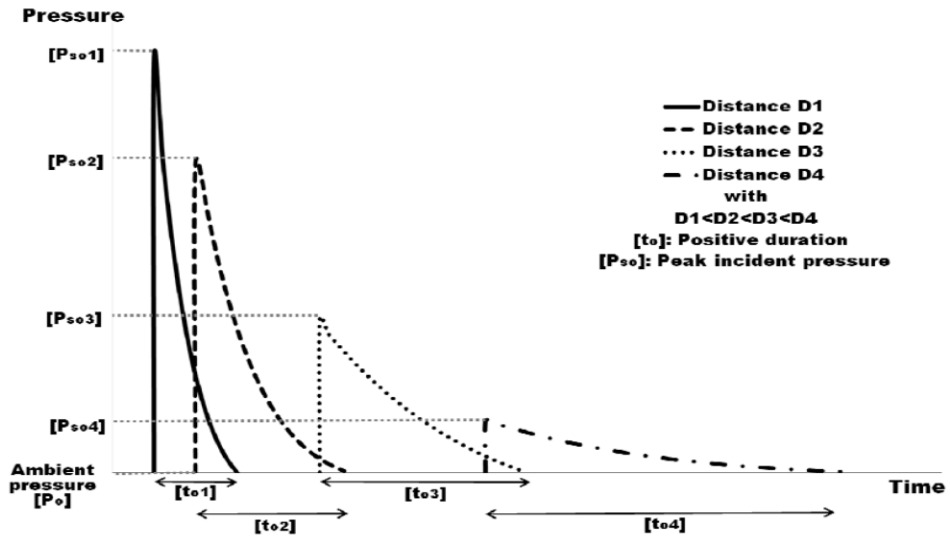

Figure 44 Influence of distance on the blast positive pressure phase.

The experimental results are, in this way, generalized to include cases that are different from the initial experimental setup.

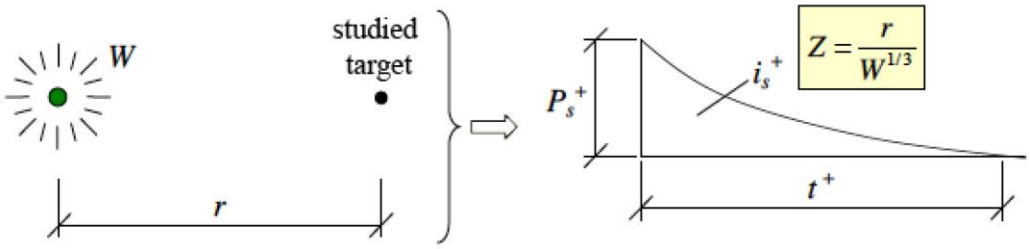

Figure 45 Hopkinson-Cranz scaling law graph

The blast scaling laws are the ones introduced by Hopkinson-Cranz and Sachs (figure 45). The idea behind both formulations is that during the detonation of two charges of the same explosive that have similar geometry but different weight and are situated at the same scaled distance from a target surface, similar blast waves are produced at the point of interest as long as they are under the same atmospheric conditions. Sachs scaling is

suitable in the case of different atmospheric conditions. According to Hopkinson-Cranz law, a dimensional scaled distance is described by equation [2],

$$Z = \frac{R}{\sqrt[3]{W}} \qquad Eq.7$$

where W is the weight (the mass) of the explosive [kg], and R is the distance from the detonation source to the point of interest [m].

4.3 TNT Equivalencies

The first step in the design of a building to sustain explosion loading is the weight and type of the explosive for which the design will be performed. The variety of explosives has led to the adoption of a universal quantity, which is used for all necessary computations of explosion parameters. TNT (Trinitrotoluene) was chosen as its explosion characteristics resemble most solid type explosives. An equivalent TNT weight is computed according to the equation that links the weight of the chosen design explosive to the equivalent weight of TNT by utilizing the ratio of the heat produced during detonation [2]:

$$W_e = W_{exp} \frac{H^d_{exp}}{H^d_{TNT}} \qquad Eq.8$$

where W_e is the TNT equivalent weight [kg],

W_{exp} is the weight of the actual explosive [kg],

$H^d_{exp}$is the heat of detonation of the actual explosive [MJ/kg], and

H^d_{TNT} is the heat of detonation of the TNT [MJ/kg].

Approximately one-third of the total chemical energy of the explosive is released by detonation. The rest is released at a slower rate as the heat of combustion through the burning of the explosive products mix with the surrounding air. Several tables describe the

heat output of most known explosives can be found in Table 10. These values can be used for the calculation of the equivalent TNT weight with the use of Equation 8.

Table 10: Indicative values of heat of detonation of common explosives.[2]

Name of explosive	Heat of Detonation (MJ/kg)
TNT	4.10-4.55
C4	5.86
NITROGLYCERIN	6.3
NITROMETHANE	6.4
NITROCELLULOSE	10.6
AMON./NIT.(AN)	1.59

Table 11 shows some predetermined TNT equivalent weight factors. These factors is used to determine the weight of TNT that produces the same blast wave parameters as the ones from another explosive of a certain weight.

Table 11: Indicative TNT equivalent mass factors [2]

Name of explosive	TNT Equivalent mass factor	
	Peak Pressure	Impulse
TNT	1.00	1.00
C3	1.08	1.01
C4	1.37	1.19
CYCLOTOL	1.14	1.09
OCTOL 75/25	1.06	1.06
TETRYL	1.07	1.05

The comparison of these blast wave parameters can be done either for pressure or impulse values; the table contains two factors depending on the used method [31]. The weight, W of an explosive is usually estimated by taking into account a relevant scenario, which would involve an accidental explosion of a steam boiler as well. The relevant regulations decide on the type of explosion like a steam boiler explosion that could be used, to be able to compute the equivalent weight of TNT for which the structure should be designed. Due to

a variety of uncertainties, it is recommended to apply a safety factor to the charge weights and augment them by approximately 20%. The same has been considered in the research paper by Mohamed F. Ibrahim, Hisham A. El-Arabaty, Ibrahim S. Moharram [28] to find the equivalent weight of TNT due to steam boiler explosion.

4.4 Explosion Loading

The type of explosion that is considered in this thesis is confined explosions. A confined or interior explosion involves more phenomena than an external explosion. In the internal explosion, there is first the direct incident shock as in an external explosion. This is followed by multiple shock reflections off the other surfaces that are confining the explosion. Finally, there is a longer duration gas pressure throughout the interior as the gaseous products of the detonation come to thermodynamic equilibrium.

The commonly used approach to obtain the blast pressure is the Conventional Weapons Effects Program (CONWEP) code developed by the U.S. Army based on the equations proposed by Kingery and Bulmash (1984) [32]. The time-dependent pressure, P(t), on the face is determined based on the input amount of trinitrotoluene (TNT) equivalent having molecular formula $C_7H_5(NO_2)_3$, the standoff distance, and angle of incidence, ϴ. The final pressure is computed using the following equation (CONWEP 2.00)

$$\boldsymbol{P(t) = P_r\, cos^2\theta + P_i\,(1 + cos^2\theta - 2cos\theta) + P_{reflected}(t)cos^2\theta, \qquad for\ cos\theta \geq 0}$$

where, P_r and P_i, reflected and incident pressures, respectively. To describe the combined effects of the standoff distance (R) expressed The CONWEP code provides the user with a peak pressure and impulse that can be used to apply load on the structure. The methods available for prediction of blast effects on structures can be grouped into three major categories, namely Empirical (or analytical) Methods, Semiempirical Methods, and Numerical (or first-principle) Methods.

Empirical approaches are developed based on extensive analysis of huge amounts of experimental data collected over a long period and thus limited by the extent of the experimental database and its accuracy over the techniques used at that time. Further, it is well known that the empirical equations do not present accurate results in near-field locations owing to the inapplicability of any sensing technique in this region. The common example of an empirical method–based guideline includes UFC 3-340-02 (2008) [2]. Semiempirical approaches are based on simplified models of physics of the phenomena. In these approaches, the focus is to model the governing physical processes in a much-simplified way. The approach essentially depends on extensive data and case studies, and the accuracy is generally better than that provided by the empirical approach. Numerical or first-principle approaches are governed by mathematical formulation, which depends on the physics of the problem. These mathematical formulations are developed by following the conservation of mass, momentum, and energy. Furthermore, the physical behavior of materials is described by constitutive relationships developed based on the experiments conducted on these materials. The Finite Element Method (FEM) offers the possibility to evaluate the response of the impulsively loaded structure using available software packages like ABAQUS. An explosion in the air forms a highly compressed gas mass that interacts with the surrounding air, generating an outward-propagating shock wave. Structures subject to air-blast loading can be analyzed efficiently using the CONWEP model. The model is known to yield good results in blast loading analyses. CONWEP loading allows to impose pressure loading due to an explosion. The loading is defined by the location of the explosion, the time of detonation, and the loading surfaces. Unlike an acoustic wave, a blast wave corresponds to a shock wave with discontinuities in pressure, density, etc. across the wavefront. Figure 46 shows a typical pressure history of a blast wave.

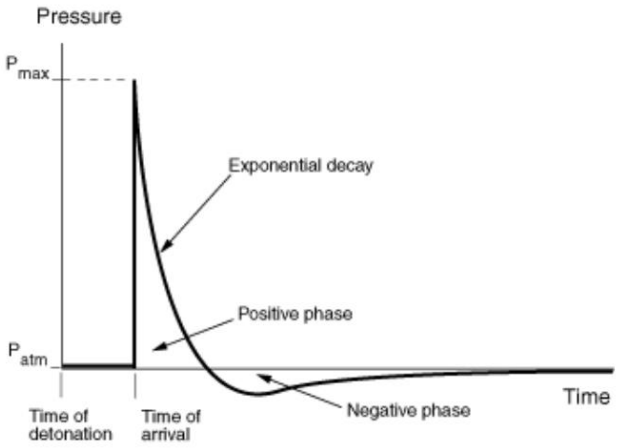

Figure 46 Pressure-time history of a blast wave

The CONWEP-ABAQUS model uses a scaled distance which is based on the distance of the loading surface from the source of the explosion and the amount of explosive detonated. For a given scaled distance, the model provides the following empirical data: the maximum overpressure (above atmospheric), the arrival time, the positive phase duration, and the exponential decay coefficient for both the incident pressure and the reflected pressure. Using these parameters, the entire time history of both the incident pressure and reflected pressure as shown in Figure 46 can be constructed.

A detonation time can be specified if the explosion does not occur at the start of the analysis. The detonation time needs to be given in total time; see conventions for a description of the time convention. The arrival time at a location is defined as the elapsed time for the wave to arrive at that location after detonation. The research paper by Mohamed F. Ibrahim et al. [28] is referred for the TNT equivalence loading of the steam boiler explosion in a closed room. Once a boiler explosion accident takes place, not only is the boiler itself destroyed but also other equipment and buildings around the boiler are damaged. Due to the complexity of overpressure generated from the boiler explosion and lack of systematic experimental data, it is common to describe the boiler explosion in terms

of an equivalent TNT charge. The diagram for TNT detonations has been used for the estimation of blasts from gas explosions, even though there are differences between the blasts from a gas explosion and a TNT detonation, Shepherd et al., (1991), Van den Berg, (1985). In a gas explosion, the local pressure may reach values as high as several bars. The blast pressure for TNT explosions is much higher closer to the charge. Such near-field data are, therefore, irrelevant for gas explosions.

For the present study, a standard steam boiler of *2000kg (2.0 ton)* capacity is considered. This type of boiler is most widely used in factories and all around the world. Estimating the pressure increase attributable to a confined explosion, the combustion process raises the temperature of a gaseous system and that, in turn, increases the pressure of the system by expanding the gases ZALOSH (1995). By comparing the two types of fuels and its equivalent TNT weight for the same Boiler type and same Boiler room and under the same environment conditions, a quick summary represented in Table 12.

Table 12: Summary of Different Types of Fuel Properties [28]

Fuel	Fuel Consumption	Density (kg/m3)	Mass of Spilled fuel	Burning Time (min)	WTNT (kg)
Diesel (Liquid Gas)	146 (kg/hr)	918	7.298	0.27	14.59
Natural Gas (Propane)	164 (m3/hr)	0.70	14.77	7.69	150.00

The pressure curve on the steam boiler room wall is compared in this case and with charge *TNT 150Kg*. The closed room is considered with a rigid foundation to know several effects of the *TNT 150 kg* explosion.

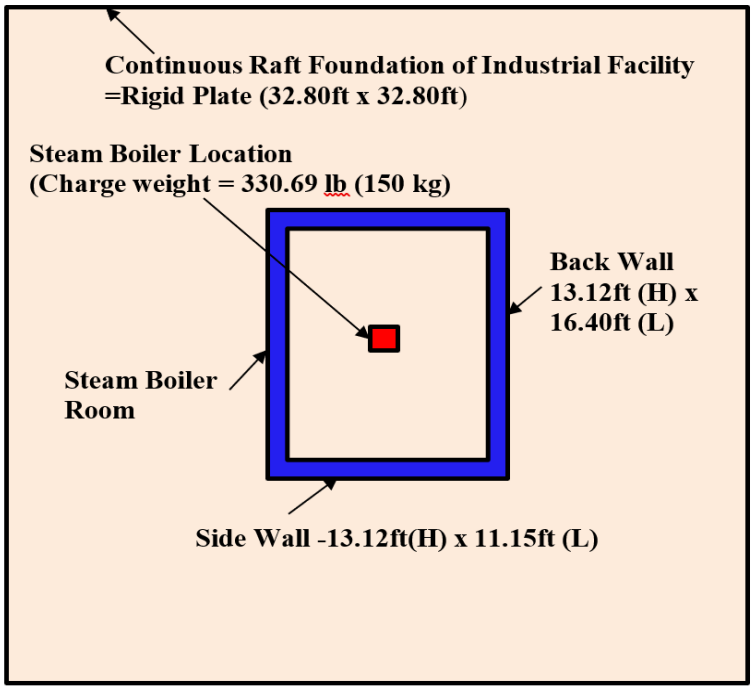

Figure 47 Plan of the Steam boiler Closed Room (Steam Boiler Capacity = 2000 kg)

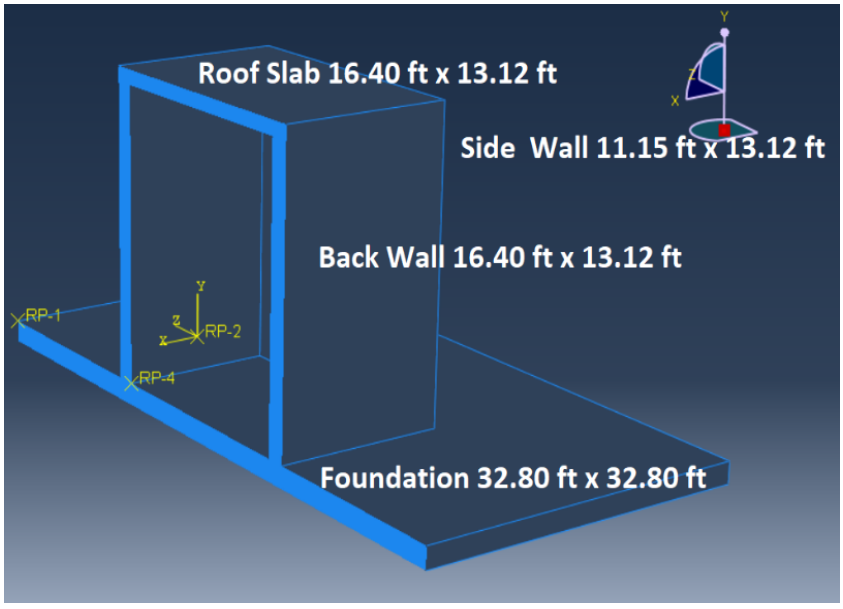

Figure 48 3D view – Section of Steam boiler room showing the charge weight location at Reference Point 2 (RP2).

The height of the back walls is 13.12 ft (4.0 m), and its length is 16.40 ft (5.0 m). The Side walls are 13.12 ft (4.0 m) high, and 11.15 ft (3.4 m) long. The thickness of all walls is 11.81 inch (0.30 m), and the roof slab thickness is 7.87 inch (0.20 m). A foundation of dimensions 32.80 ft x 32.80 ft (10.0 m x 10.0 m) is used to model the room floor. Charge weight 150kg TNT is located at Reference Point 2 (RP2) as shown in Figure 48, Reference Point 2 (RP2) is 3.6 ft (1.1 m) from the ground surface and 5.5 ft (1.7 m) from the back wall.

Positive shock wave parameters for an accidental explosion of the steam boiler are calculated. TNT equivalent charge weight of 150 kg is considered, as mentioned in Table 12. UFC 3-340-02 (2008) Chart -Positive Phase shock wave parameters for a TNT explosion is used to find the following parameters (Refer Appendix B for calculation):

- Scaled Distance, Z = 0.80653
- Peak side on overpressure, P_s = 1100 psi,
- Peak normally reflected pressure, P_r =11000 psi,
- Scaled incident impulse, $i_s / w^{1/3}$ = 15 psi-ms / $lb^{1/3}$,
- Incident impulse, i_s =103.728 psi-ms,
- Scaled reflected impulse, $i_r / w^{1/3}$ = 310 psi-ms / $lb^{1/3}$,
- Reflected impulse, i_r =2143.729 psi-ms,
- Scaled arrival time = $t_A / w^{1/3}$ = 0.06 ms / $lb^{1/3}$,
- Arrival time, t_A = 0.4149 ms,
- Scaled positive phase duration = $t_0 / w^{1/3}$ = 0.15 ms / $lb^{1/3}$,
- Positive phase duration, t_0 = 1.037 ms ≈ 1 ms (millisecond)
- Wave front velocity, U = 9 ft/ms
- Scaled wave length of positive pulse $L_w / w^{1/3}$ = 0.55 ft / $lb^{1/3}$
- Wave length of positive pulse = 3.80 ft.

An important parameter that is considered for the nonlinear analysis in ABAQUS FEA software is the positive phase duration of 1 millisecond. It can be noticed that the peak normally reflected pressure is 10 times the peak overpressure, which is more critical. It shows that the reflected pressure due to a steam boiler explosion is a critical load case and is considered for the analysis. Parametric studies are also done in Part 4.8 to reduce the effect of reflected pressure due to explosion by introducing different arrangements of the roof in a closed room – with a rigid roof, frangible roof and circular vent in the roof.

4.5 Modeling in ABAQUS

4.5.1 General

The finite element method (FEM) is used for solving problems of engineering and mathematical models. To solve a problem, the FEM subdivides a large system into smaller, simpler parts that are called finite elements. This concept uses many algebraic equations to find the most approximate solution for problems and yield an accurate representation of the results. This research focuses on analyzing the effect of a steam boiler explosion on Steel Fiber Reinforced Concrete closed room structure using an FEA tool called ABAQUS. ABAQUS is a Computer-Aided-Engineering software that helps model and performs tests on components to determine its various static and dynamic properties. This study investigates how steel fiber reinforced concrete can reduce the effect of blast loading. The experimental test results of the SFRC material were used in ABAQUS Modelling. Three different models in ABAQUS were made for the Steam Boiler accidental explosion in a closed room with 0.0%, 0.5%, and 1.0% volume fraction of steel fibers in concrete. The purpose of modeling and analyzing three different models in ABAQUS is to see how the stresses and strain in SFRC walls change under dynamic blast loading/steam boiler explosion loading.

Part one of the study is to find material properties of the SFRC at different volume fraction 0.0 %, 0.5 %, and 1.0 % from an available experiment. The second portion of the study is to find the effect of the Steam Boiler accidental explosion on the SFRC wall of the Steam boiler-closed room by numerical analysis in FEA software - ABAQUS. The modeled steam boiler -the closed room is meshed and dynamically loaded in ABAQUS to provide the stress, strain, and deflection at 0.0 %, 0.5 %, and 1.0 % of SFRC.

4.5.2 Creating Parts

The first step in ABAQUS is using the “Create Part” tool to model the geometry and regions of a steam boiler closed room parts. This tool models the dimensions and components for each part, as seen in Figure 49. ABAQUS interface creates the part on a coordinate grid, so the lines reference to the coordinate points. If a portion of the member needs to be cut or perforated, the “Create: Cut Extrude” tool is used.

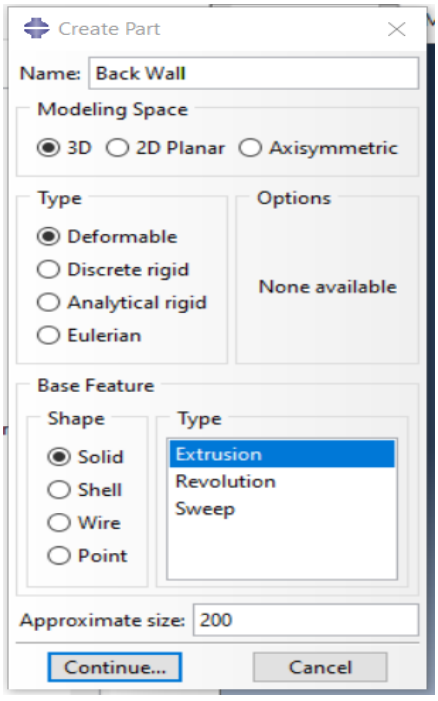

Figure 49 ABAQUS- Initial Step "Create Part"

4.5.2.1 Steam Boiler Closed Room Modeling

For this study, the steam boiler closed room's walls, roof and foundation are initially individual "Parts" in ABAQUS and then combine to form the steam boiler closed room. Parts of the model of the "Closed Room" are the Back walls, Side walls, Roof, and the foundation rigid plate (RP). The height of the back walls is 13.12 ft (4.0 m), and its length is 16.40 ft (5.0 m). The Side walls are 13.12 ft (4.0 m) high, and 11.15 ft (3.4 m) long. The thickness of all walls is 11.81 inch (0.30 m), and the roof slab thickness is 7.87 inch (0.20 m). A rigid plate with dimensions 32.80 ft x 32.80 ft (10.0 m x 10.0 m) is used to model the room floor. A summary of the dimensions for each component can be seen in Table 13.

Table 13: Dimensions of Steam Boiler Closed Room Parts

	Width, W (ft)	Height, H (ft)	Thickness, T (inch)
Back Wall 1	16.40	13.12	11.81
Back Wall 2	16.40	13.12	11.81
Side Wall 1	11.15	13.12	11.81
Side Wall 2	11.15	13.12	11.81
Roof Slab	16.40	13.12	7.87
Raft Foundation	32.80	32.80	11.81

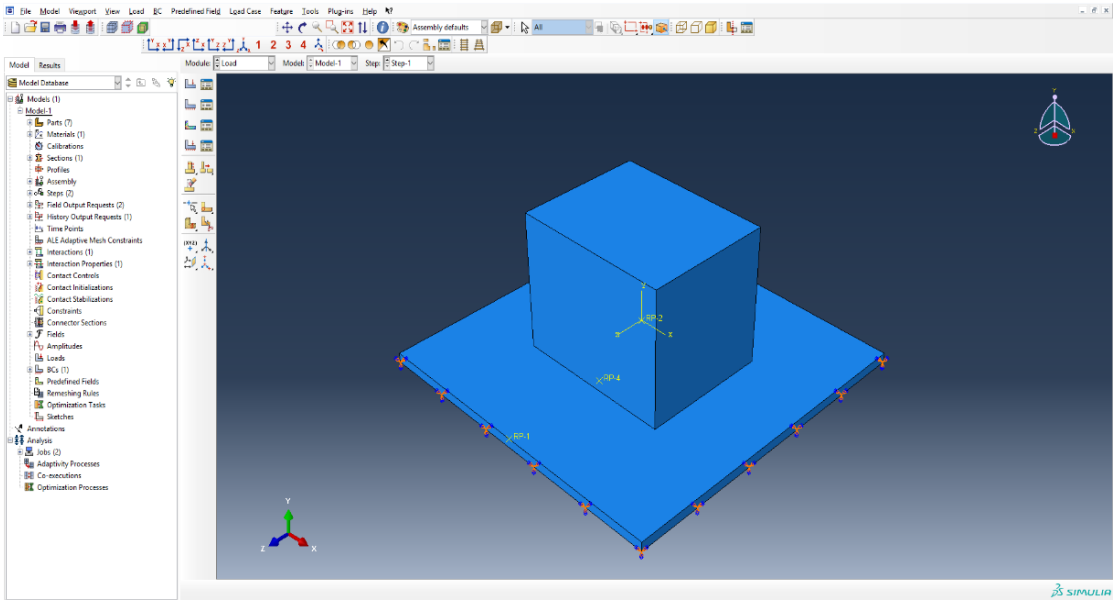

Figure 50 ABAQUS- Steam Boiler Closed Room

4.5.3 Meshing Components

A mesh is created on the closed room walls, roof, and foundation to discretize the model and form nodes on the components where the load will be distributed. Refining the mesh gives more degrees of freedom in the critical areas where stress occurs while a coarse mesh should be designed in general areas where there is not a high amount of stress. Four-node tetrahedral element (C3D4) element type is used for the meshing to get precise results as shown in Figure 51.

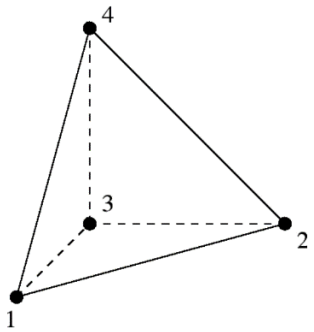

Figure 51 ABAQUS- 4-node tetrahedral element

Each type of mesh defines the cross-section of the discretized finite elements. For a 20 inch approximate global size mesh the finite element model generates about 4998 elements with individual nodes in the model. To determine the ideal number of elements for this model, a mesh convergence is done in Part 4.6. Figure 52 shows the meshed finite element model.

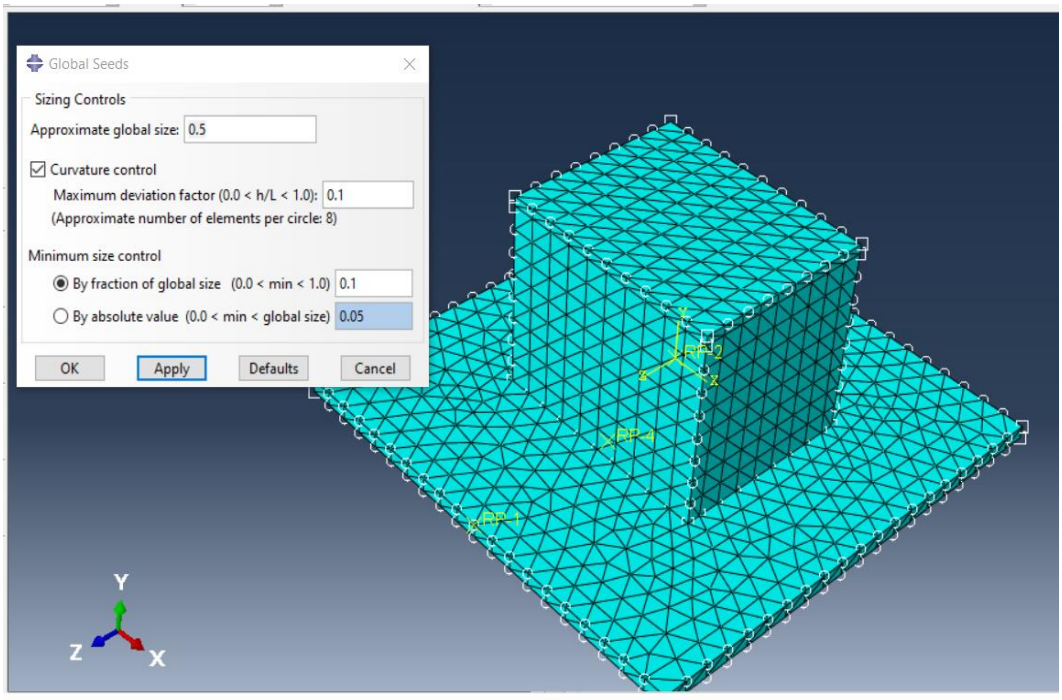

Figure 52 ABAQUS- 20-inch Global Size Mesh

4.5.4 Material Properties

The material properties of the Experiment Specimen obtained are used in ABAQUS. From the available experiment, for SFRC of 0.0 %, 0.5 %, and 1.0 %, the compressive strength of concrete is __psi, which can be used to determine an Elastic Modulus of psi. Values from the material properties tests, specifically the compressive strength f_c' and modulus of rupture f_r, are used in ABAQUS for each case. In both parametric studies f_c' and f_r are adjusted according to the 0%, 0.5%, and 1% cases. The Elastic modulus, which also

changes according to the percent of steel fibers, is also adjusted for each case. The material properties for SFRC of 0.0 %, 0.5 % and 1.0 % used in ABAQUS are shown in Table 14.

Table 14: Material Properties of SFRC Specimens

SFRC Parameters for ABAQUS			
% Fibers	0	0.5	1
Compressive strength, fc' (psi)	3521	3958	4321
Modulus Rupture Test, fr (psi)	632	701	835
Elastic Modulus, Ec (psi)	3466823	3675670	3848020

4.5.5 Concrete Damage Plasticity

Crack propagation is an important component in studying the flexural behavior of concrete. To set bounds for the SFRC structure in ABAQUS, tolerance values must be inputted into the Concrete Damage Plasticity (CDP).

Table 15: Concrete Damage Plasticity Parameters [11]

Dilation Angle	Eccentricity	fb0/fc0	K	Viscosity Parameter
31	0.1	1.16	0.667	0

4.5.6 Steps and Time Increments

The step tool defines each analysis step and the output requests for the ABAQUS model. In this study, the dynamic, explicit loading process is for analysis, as shown in Figure 53.

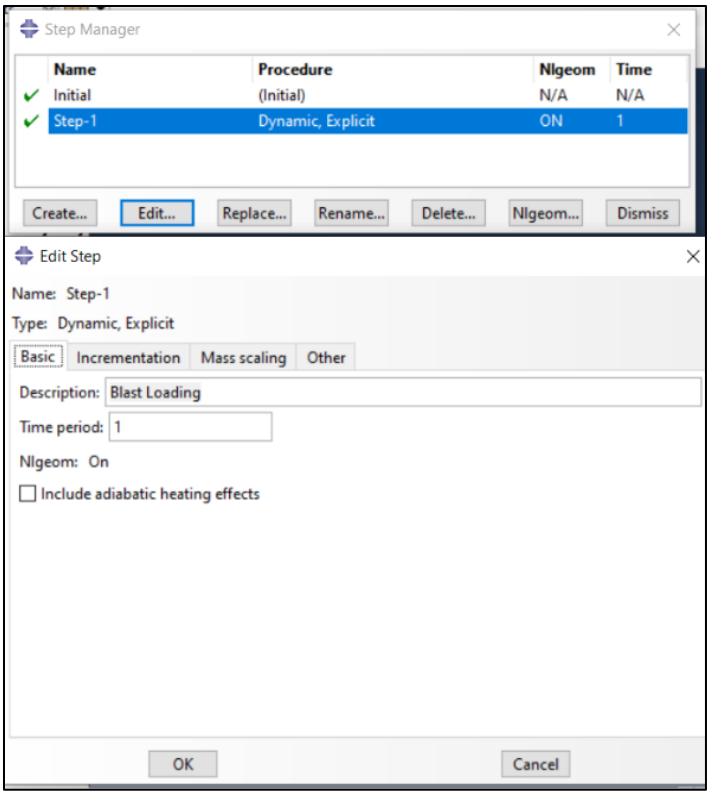

Figure 53 ABAQUS- Create Step for Dynamic, Explicit Loading

4.5.7 Loads and Boundary Conditions

CONWEP loading condition is used to apply dynamic blast loading on the wall, roof, and foundation. A reference point is created Reference Point 2 (RP2) (Figure 55) in the model, which is located at 3.6 ft (1.1 m) from the ground surface and 5.5 ft (1.7 m) from the back wall. Charge weight 150kg (1500 N) TNT is located at RP2 as shown in Figure 43, RP2 is 3.6 ft (1.1 m) from the ground surface and 5.5 ft (1.7 m) from the back wall. Rigid Boundary conditions are applied at the base of foundation, as shown in Figure 56.

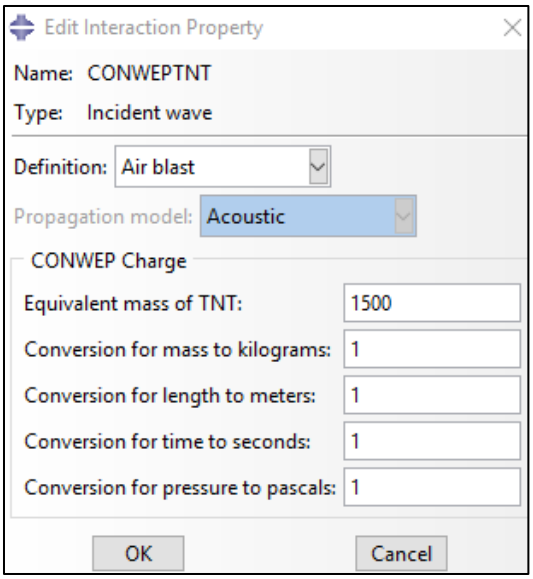

Figure 54 ABAQUS -150 kg (1500 Newton) TNT charge weight loading in CONWEP.

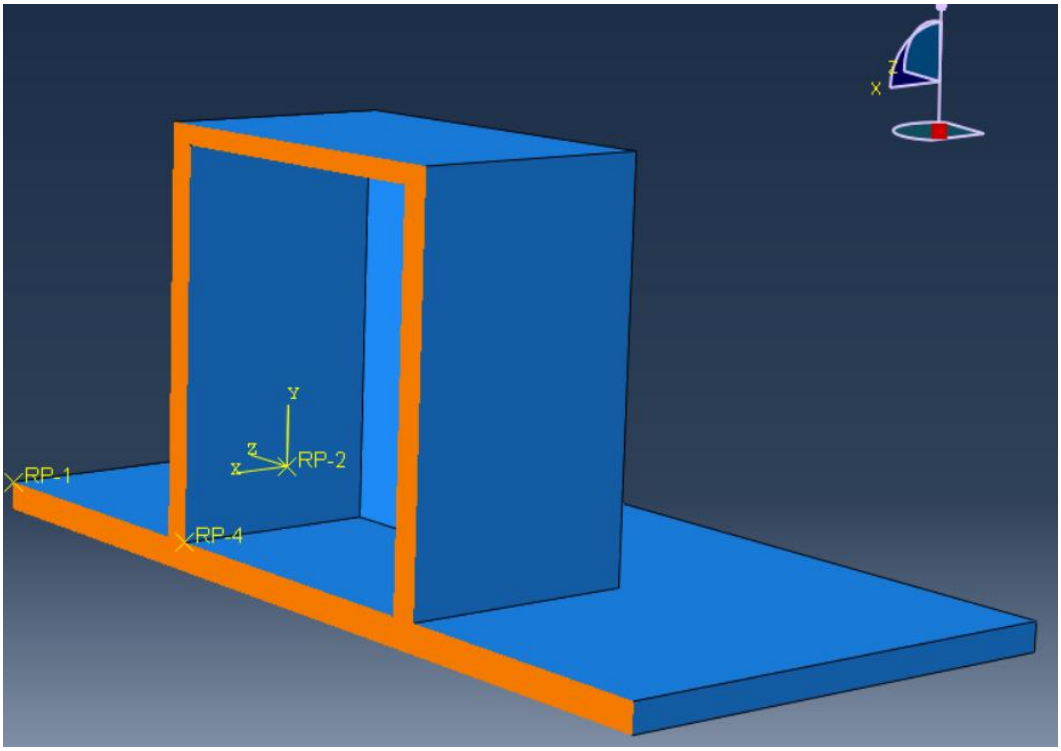

Figure 55 3D view – Section to show the charge weight location at RP2.

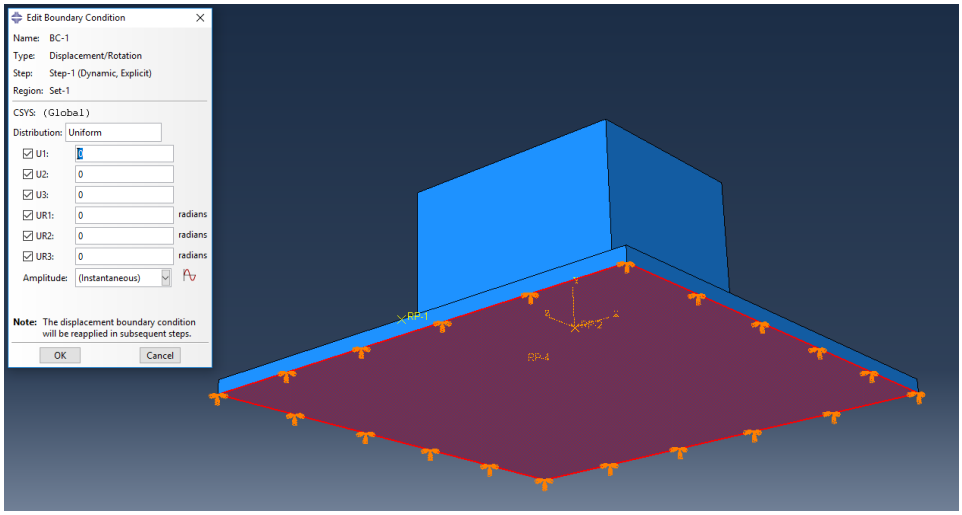

Figure 56 Rigid Boundary condition at the base of Foundation

4.5.8 3D Visualization

After the job is complete in ABAQUS, the interface allows the user to visualize the results in a 3D display as shown in Figure 57. The change in the model's behavior and physical properties are shown. The regions in the model have different shades of colors to show the distribution of stress and displacement.

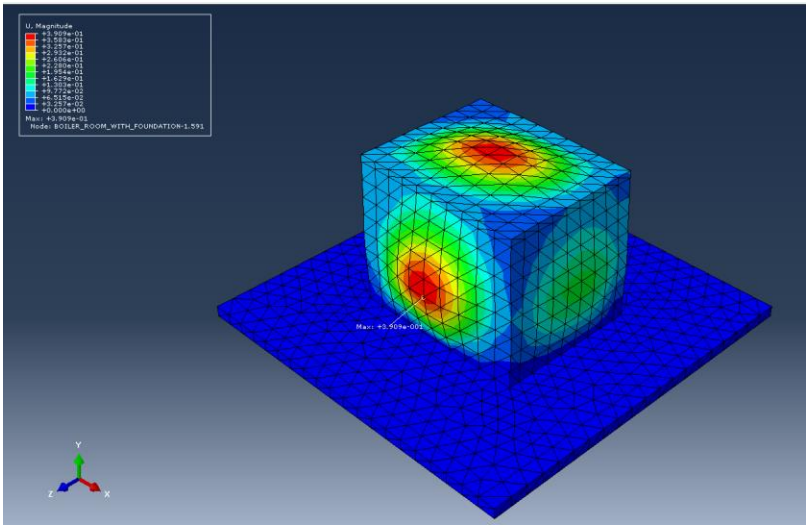

Figure 57 3D Visualization of Results

4.6 Mesh Convergence

To determine the most approximate amount of stresses and displacement experienced by the walls in the steam boiler-closed room, a mesh convergence study helps to choose the right number of elements. A finer mesh density discretizes the displacement area and the curvature inflection point. A specific geometrical cross-section is designed as the mesh depending on the optimal configuration by ABAQUS. A mesh convergence study is done to confirm what type and dimension of the mesh can allow for an accurate representation of the results. A mesh convergence study is done which helps to determine the ideal mesh size to achieve an accurate representation of the results.

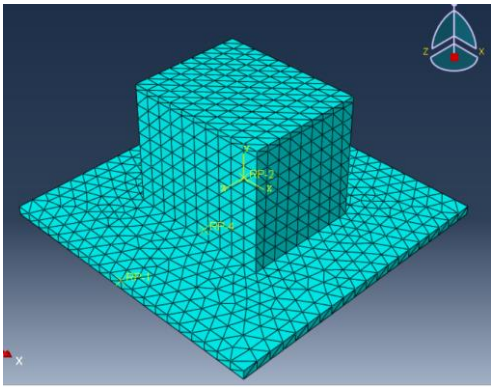

Figure 58 - 20-inch Mesh Size

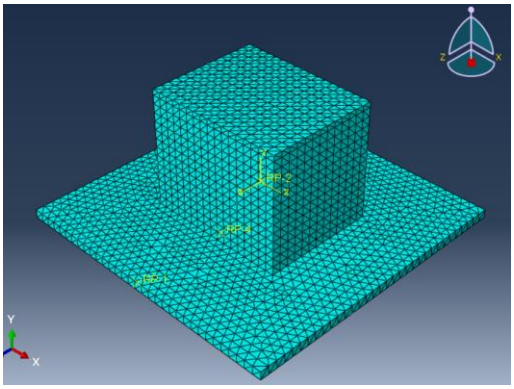

Figure 59 - 12-inch Mesh Size

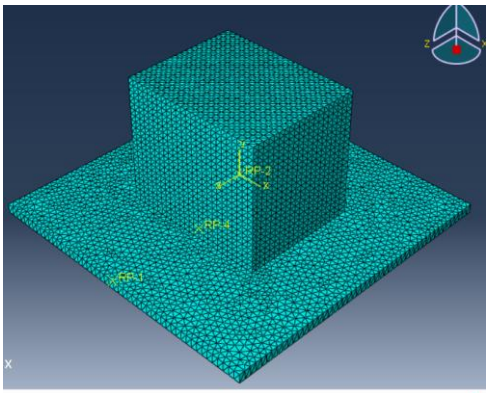

Figure 60 - 8-inch Mesh Size

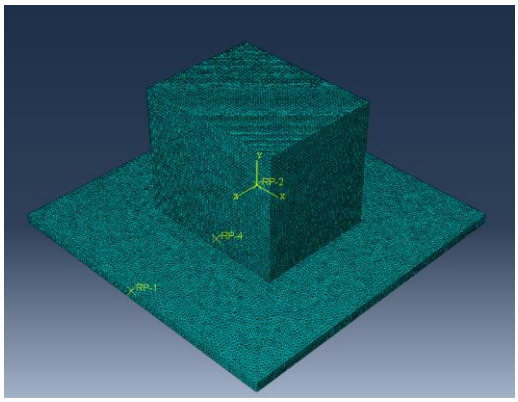

Figure 61 - 4-inch Mesh Size

Note that Figures 62 do not represent the results for this research and only shows how the data converges for different mesh sizes. Stress vs strain graph is studied at steam boiler closed room side wall mid-height for the convergence.

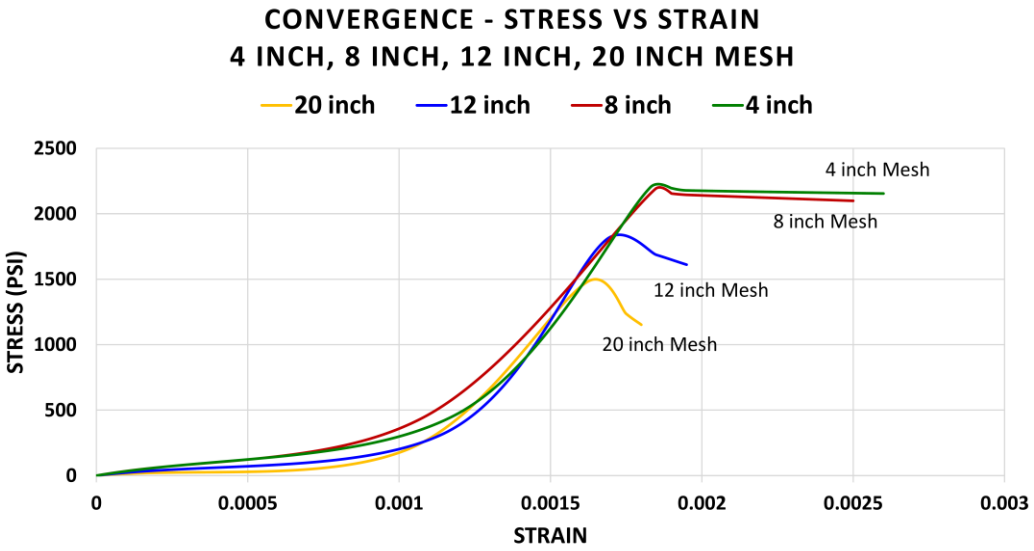

Figure 62 – Convergence for 4-inch, 8-inch, 12-inch & 20-inch Mesh Size

Figure 58 shows a 20-inch global size; the geometry creates a model with over 4998 finite elements. Figure 59 shows a 12-inch global size; the geometry creates a model with over 18234 finite elements. Figure 61 shows a 4-inch global size mesh for the steam boiler-closed room model; this geometry creates an extremely dense model with over 340359 finite elements. This causes a longer time for the software to process the elements. Figure 60 shows an 8-inch global size mesh; the geometry creates a model with over 51831 finite elements. The values show the convergence of results, which are closer to the 4-inch global size mesh results. Hence the 8-inch global size model is used for the analysis.

After analyzing the member with each mesh shown from Figures 58-61, a mesh of 8-inch global size mesh was chosen. A mesh of 8-inch global size mesh with 51831 elements is most optimal to determine the stress, strain, and displacement for the study.

4.7 Finite Element Analysis Results

In the first part of this research, the material properties of SFRC by different volume fraction of 0.0%, 0.5%, and 1.0% are found by experimental tests. The same material properties are used to carry out the nonlinear FEA studies. The Steam Boiler-Closed Room Model analysis is done in ABAQUS by using dynamic explicit loading. In FEA, the ABAQUS software use interpolation to determine the stresses, strain, and displacement value over a certain number of elements in different regions. The results of a steam boiler explosion-dynamic loading on the SFRC closed room structure is shown in this part.

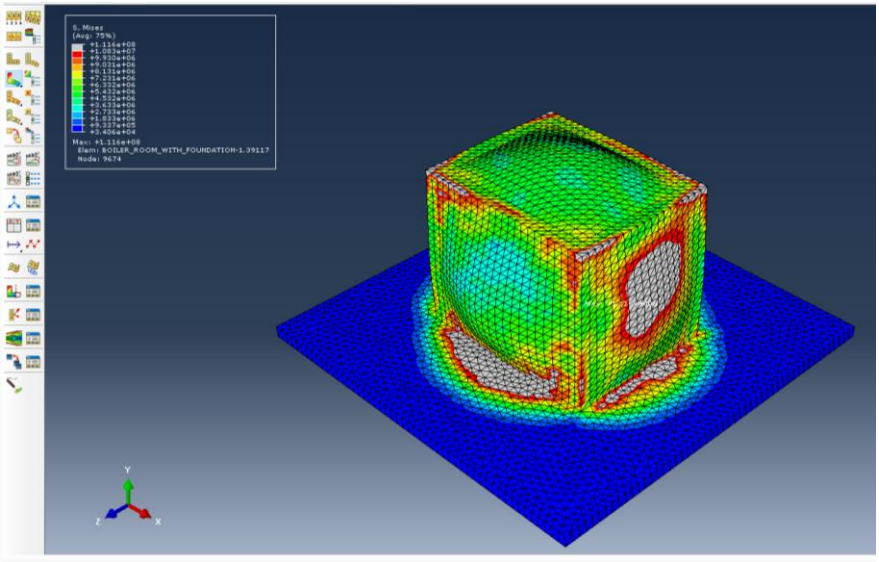

Figure 63 Steam Boiler Room ABAQUS Model showing Stresses developed due to a steam boiler explosion

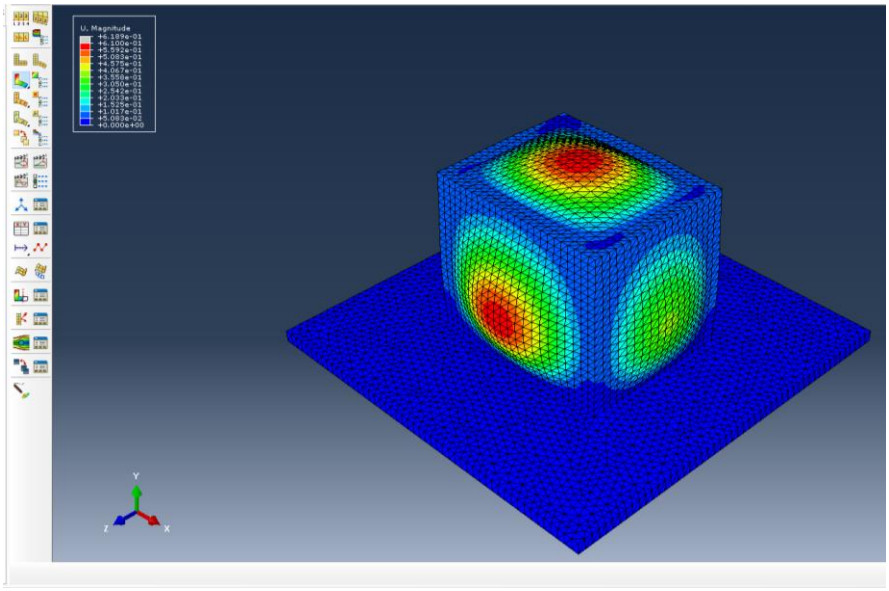

Figure 64 Steam Boiler Room ABAQUS Model showing deflection due to a steam boiler explosion

4.7.1 Results of Steam Boiler Room for 0.0%, 0.5% and 1.0% SFRC

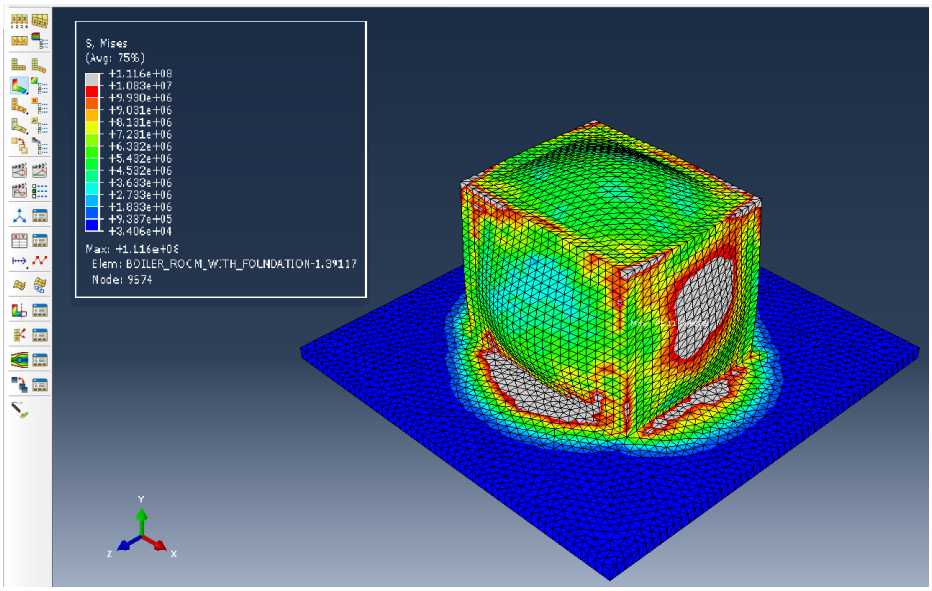

Figure 65 0.0% SFRC -Stresses (N/m^2) developed in Steam Boiler Room

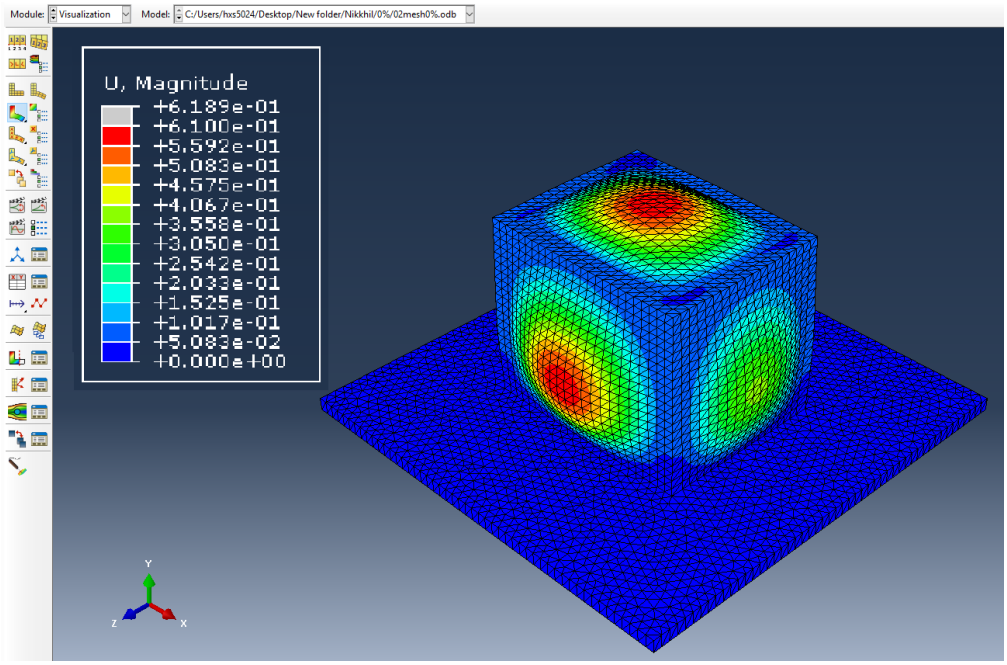

Figure 66 0.0% SFRC -Deflection (m) in Steam Boiler Room

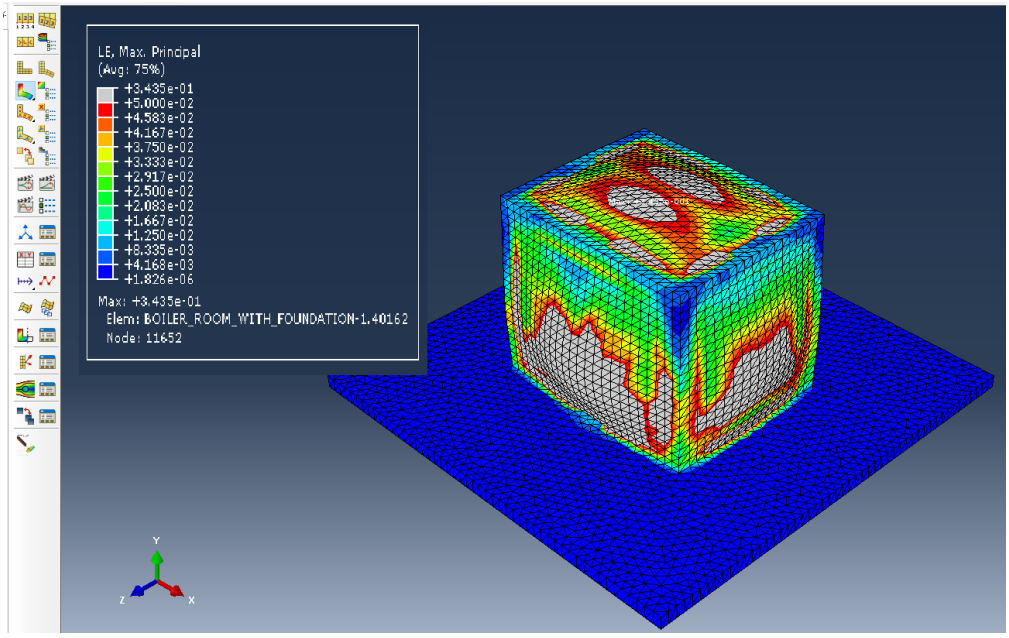

Figure 67 0.0% SFRC -Strain in Steam Boiler Room

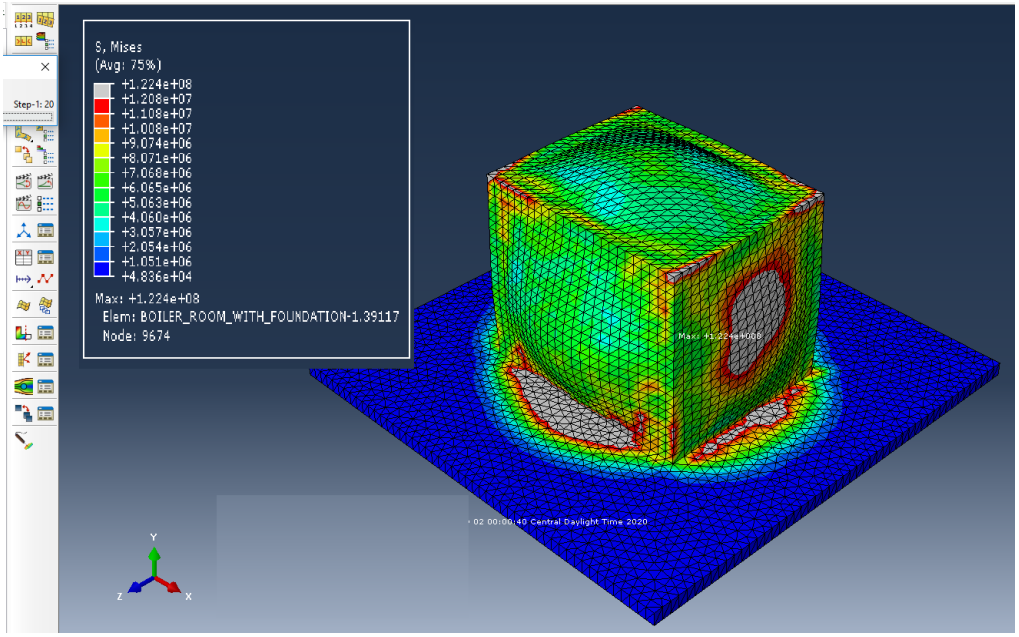

Figure 68 0.5% SFRC - Stresses (N/m^2) developed in Steam Boiler Room

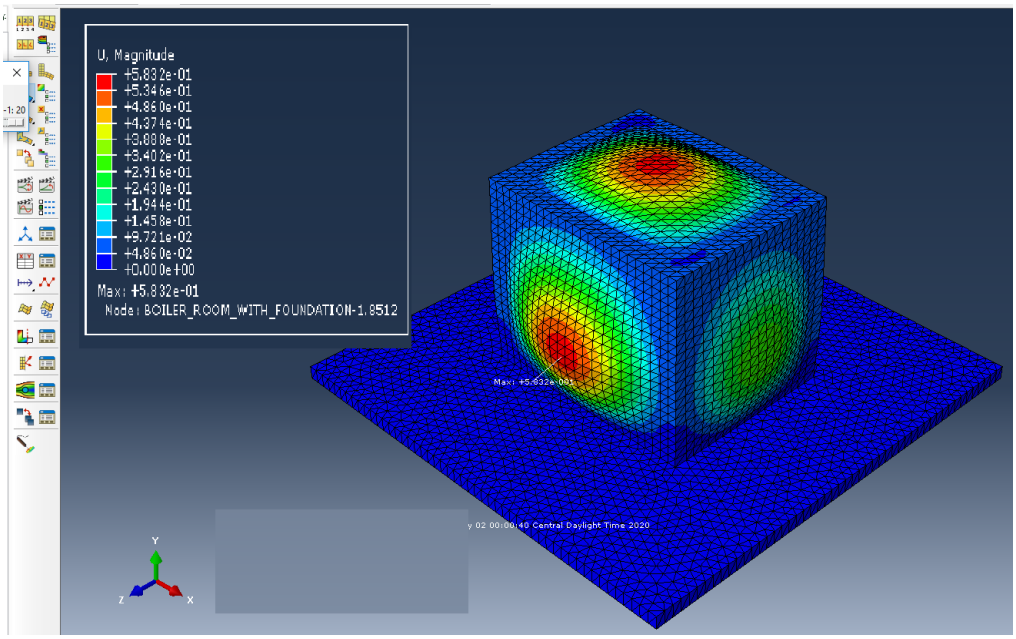

Figure 69 0.5% SFRC – Deflection (m) in Steam Boiler Room

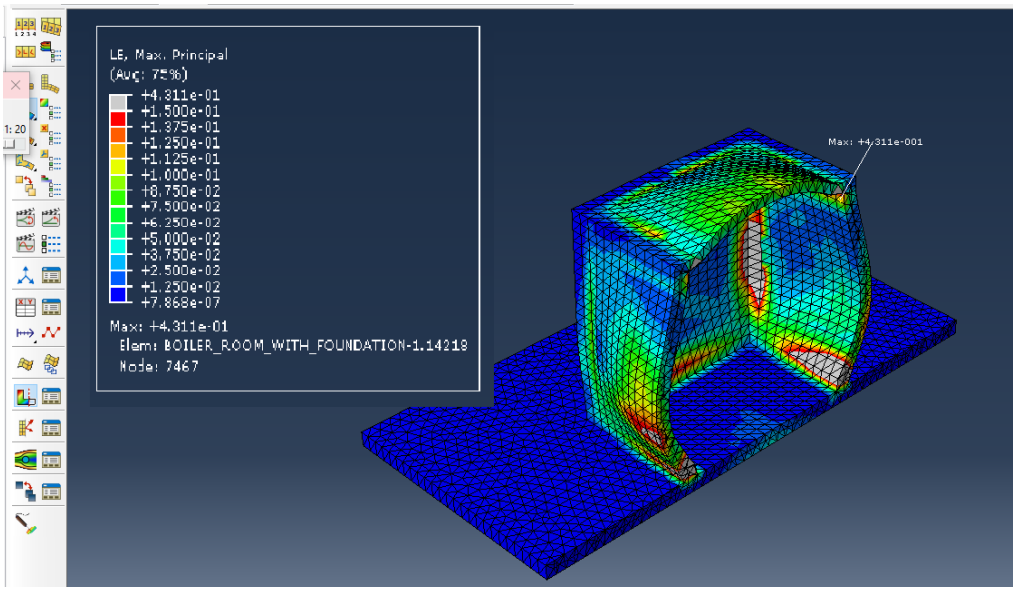

Figure 70 0.5% SFRC - Strain in Steam Boiler Room

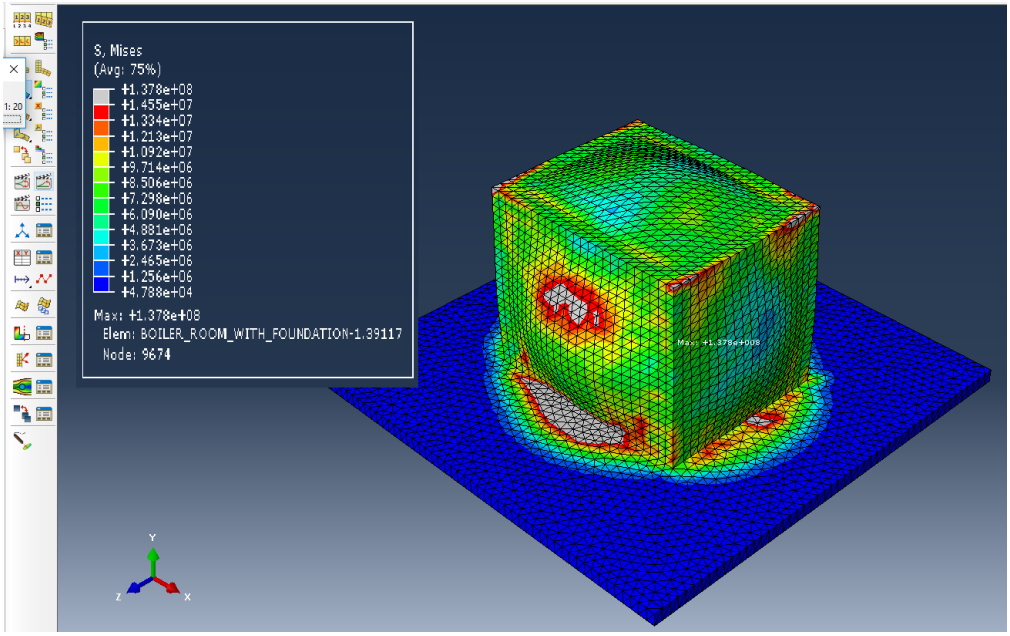

Figure 71 1.0% SFRC – Stresses (N/m^2) developed in Steam Boiler Room

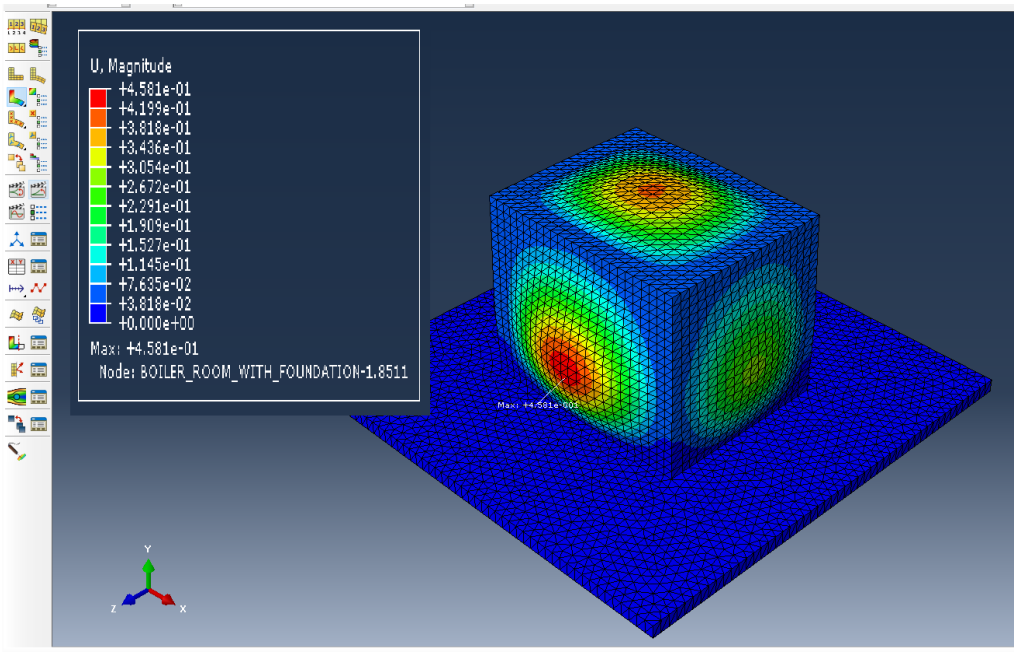

Figure 72 1.0% SFRC – Deflection (m) in Steam Boiler Room

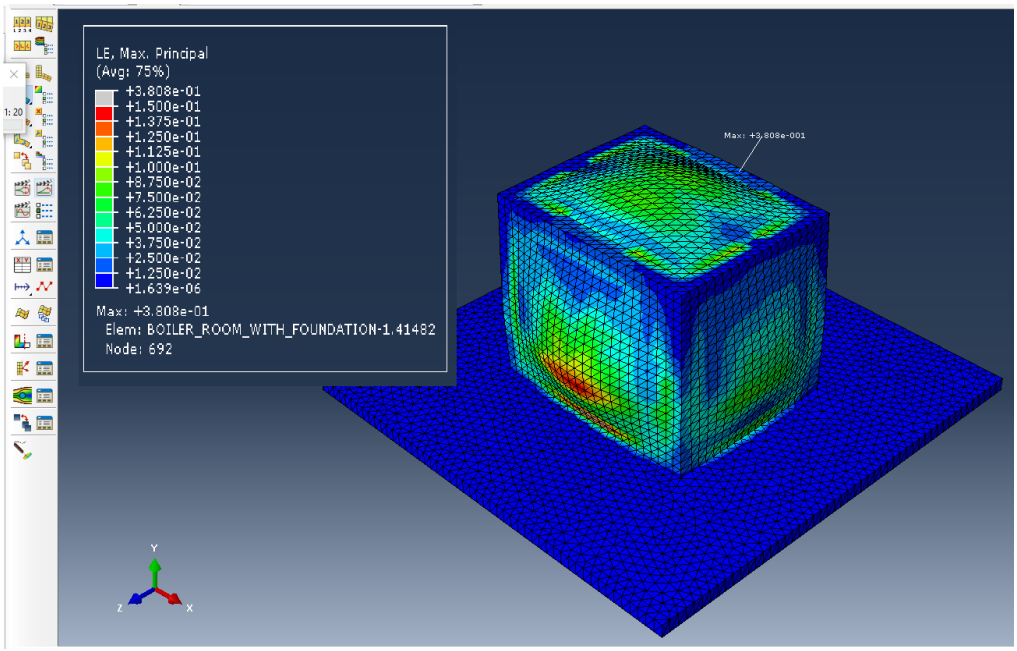

Figure 73 1.0% SFRC - Strain in Steam Boiler Room

Overall stresses developed in the Steam Boiler closed room structure for 1.0% SFRC is greater compared to the stresses for 0.0% SFRC. This shows the strength capacity of the 1.0 % SFRC structure is enhanced, and it can take more stress. Stresses developed in the structure are shared by concrete and steel fibers; hence it increased the capacity of the material. Also, the overall strain and deflection are reduced significantly in 1.0 % SFRC structure in comparison to 0.0% SFRC.

Stresses, strain, and deflection graphs are obtained for a time period of 8.3 milliseconds at the Steam Boiler closed room side wall and the roof slab for the comparison for different volume fractions of concrete.

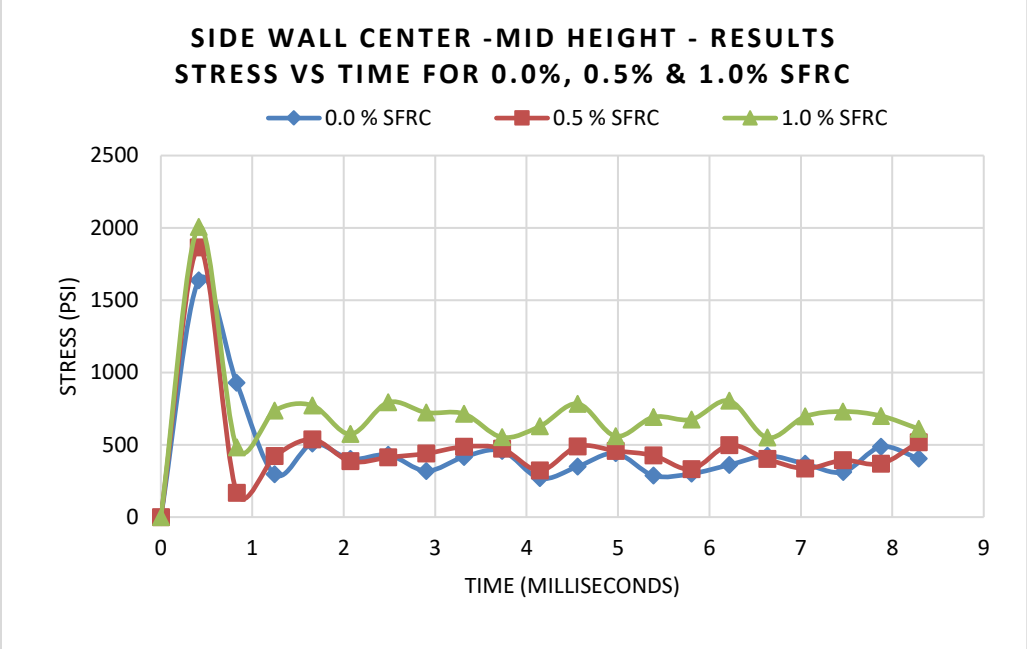

Figure 74 Side Wall -Maximum Stresses at node for 0.0%, 0.5% & 1.0% SFRC

The stress vs time graph shown in figure 74 shows the peak overpressure reaches the side wall at the arrival time of 0.4 milliseconds, and the stresses reduce drastically over a period of 8 milliseconds.

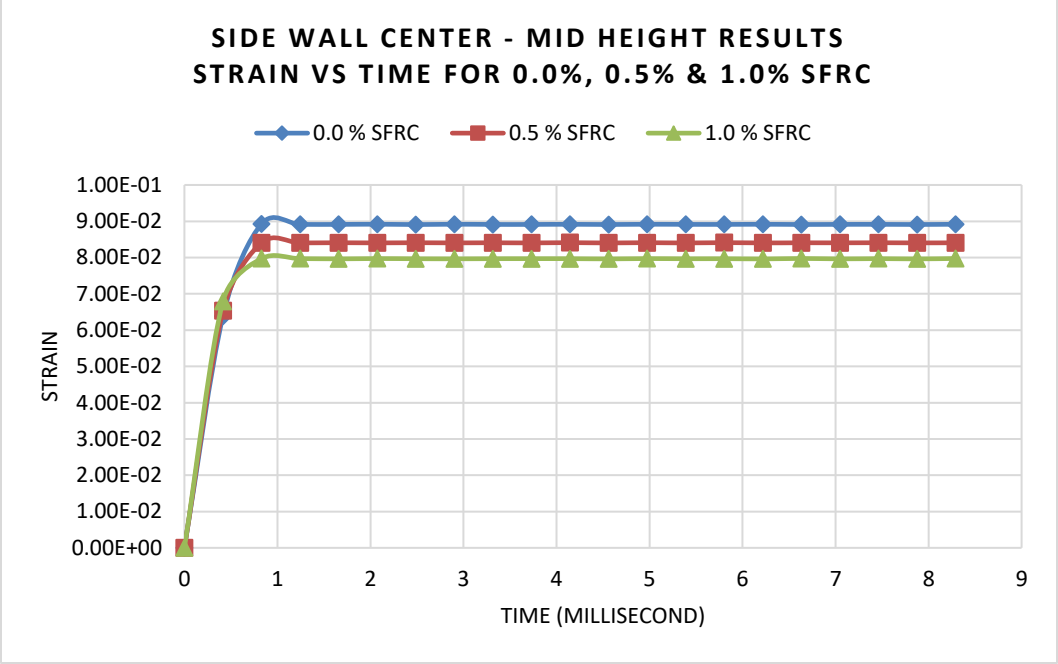

Figure 75 Side Wall -Maximum Strain node for 0.0%, 0.5% & 1.0% SFRC

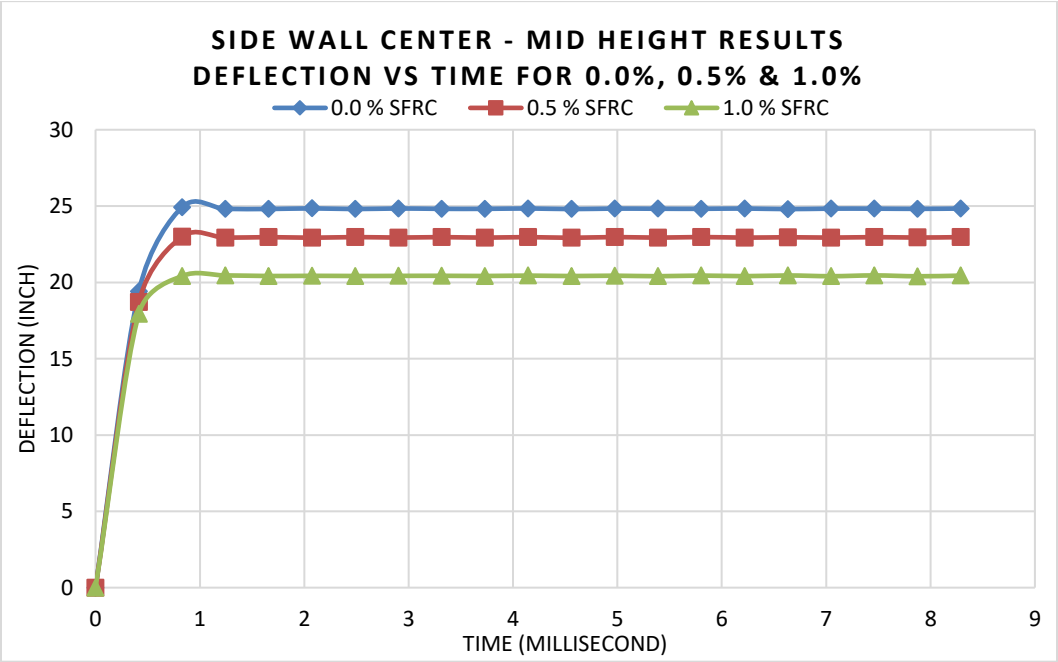

Figure 76 Side Wall -Maximum Deflection node for 0.0%, 0.5% & 1.0% SFRC

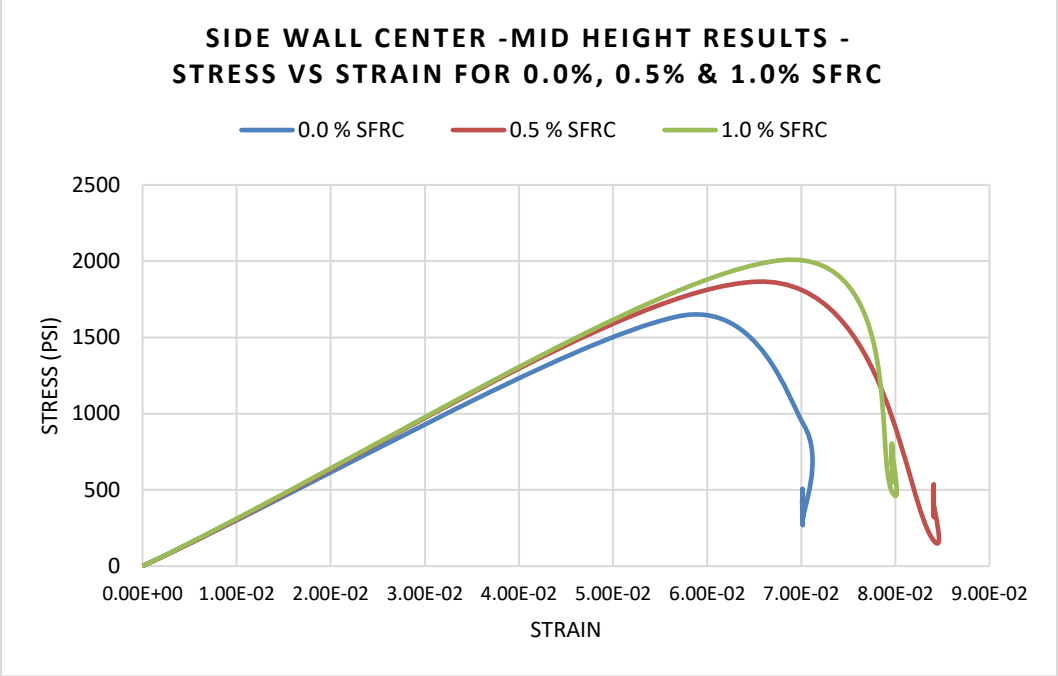

Figure 77 Side Wall – Mid Height -Stress Vs Strain for 0.0%, 0.5% & 1.0% SFRC

Table 16: Comparison for Side Wall Center - Mid-height - Results for different SFRC V_f

Side Wall- Mid Height Center – Stresses, Strain and Deflection Comparison of 0.0%, 0.5% & 1.0% SFRC			
	0.00%	0.50%	1.00%
Stresses (psi)	1637.806	1865.565	2006.677
% increase	-	**13.91%**	**22.52%**
Strain	0.0892	0.0841	0.0797
% decrease	-	**-7.73%**	**-17.93%**
Deflection (inch)	24.925	22.997	20.455
% decrease	-	**-5.77%**	**-10.66%**

At 1.0% SFRC structure side wall takes the maximum stresses; hence the capacity of the structure has increased to take more dynamic loads. Strain and deflection in the side wall – mid-height is significantly reduced by 17% and 10% with 1.0% SFRC. From figure 77, stress vs strain graph shows the maximum stress in the side wall reaches early at lower strain value for 0.0% SFRC, and for 1.0% its reaches maximum in higher strain value. In Table 16, a comparison is shown that the deflection and strain can be significantly reduced at 1.0% SFRC and it is found that the strength capacity has increased by 22%.

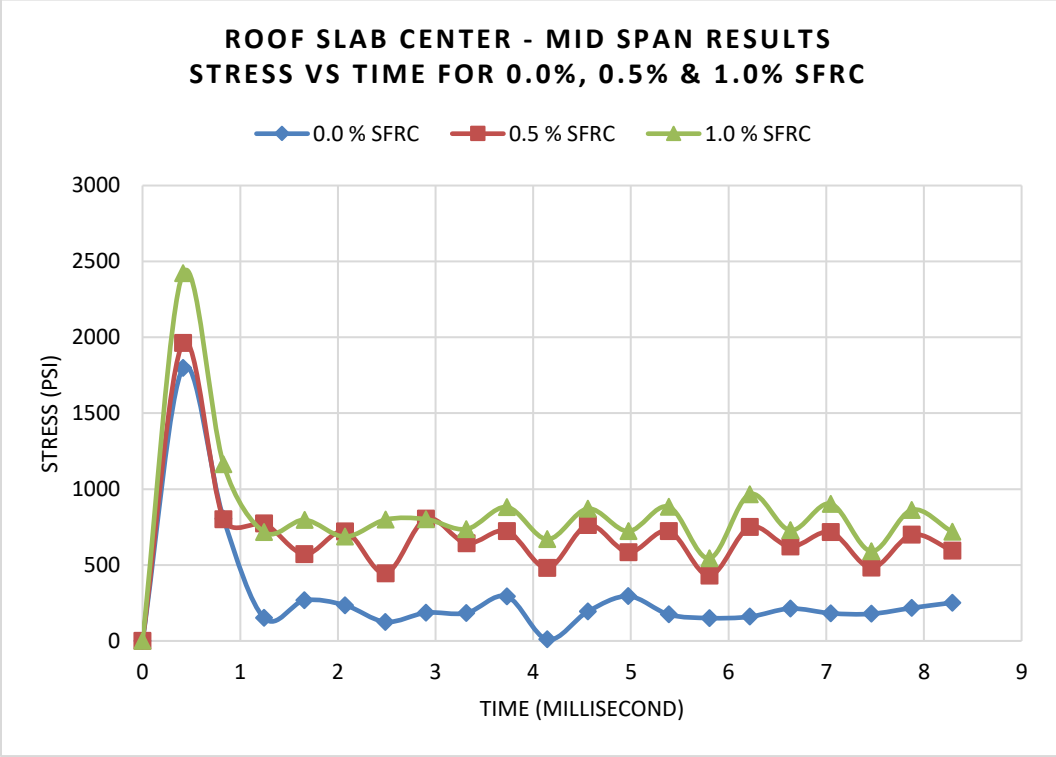

Figure 78 Roof -Maximum Stresses node for 0.0%, 0.5% & 1.0% SFRC

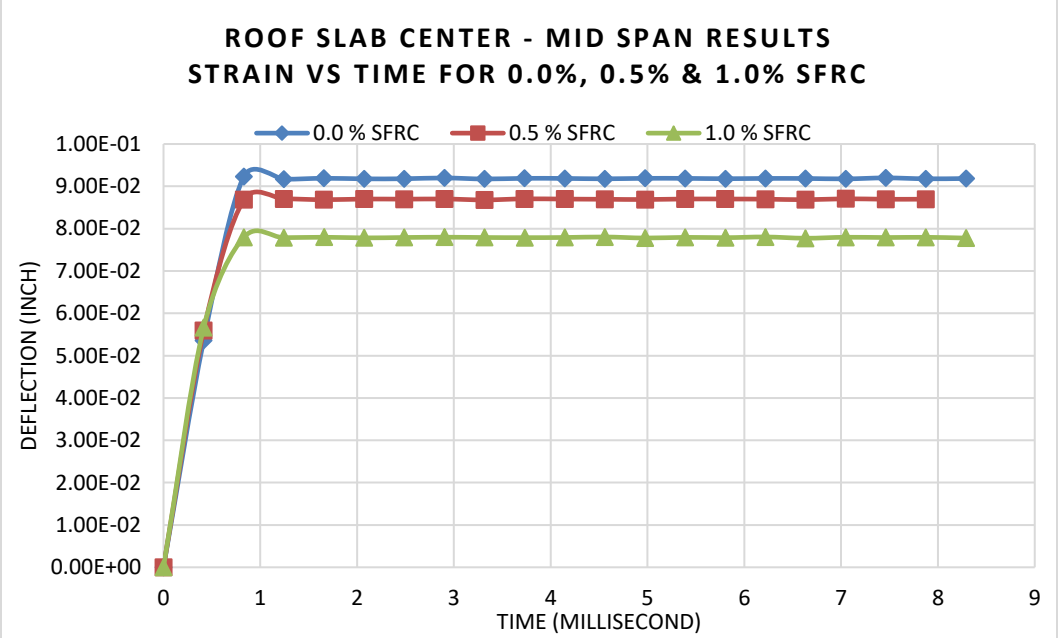

Figure 79 Roof -Maximum Strain node for 0.0%, 0.5% & 1.0% SFRC

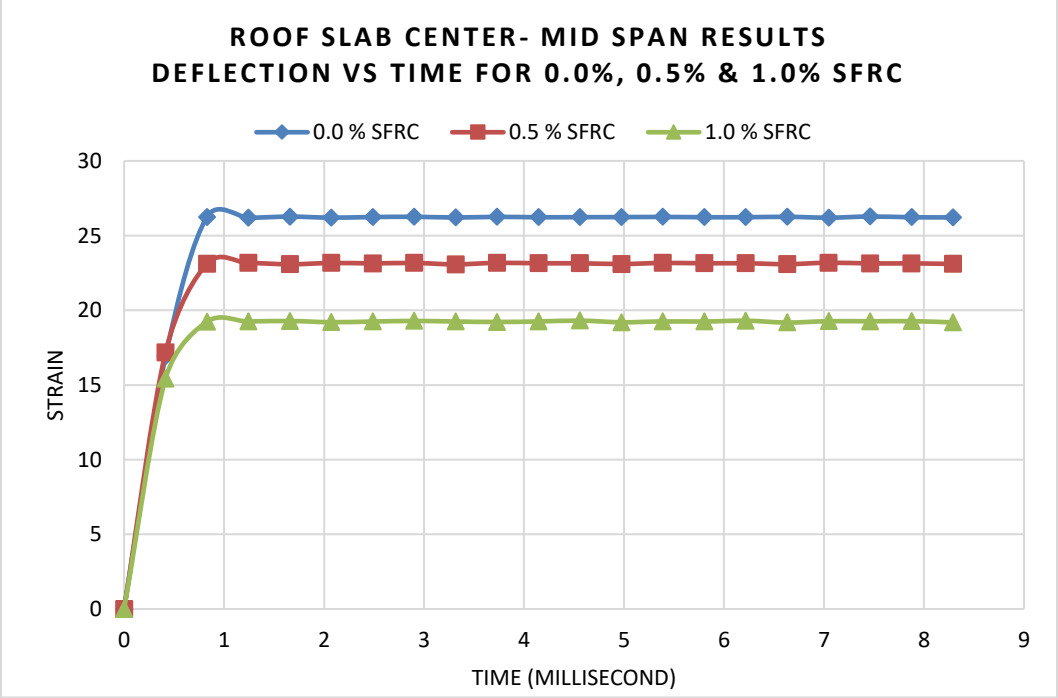

Figure 80 Roof -Maximum Deflection node for 0.0%, 0.5% & 1.0% SFRC

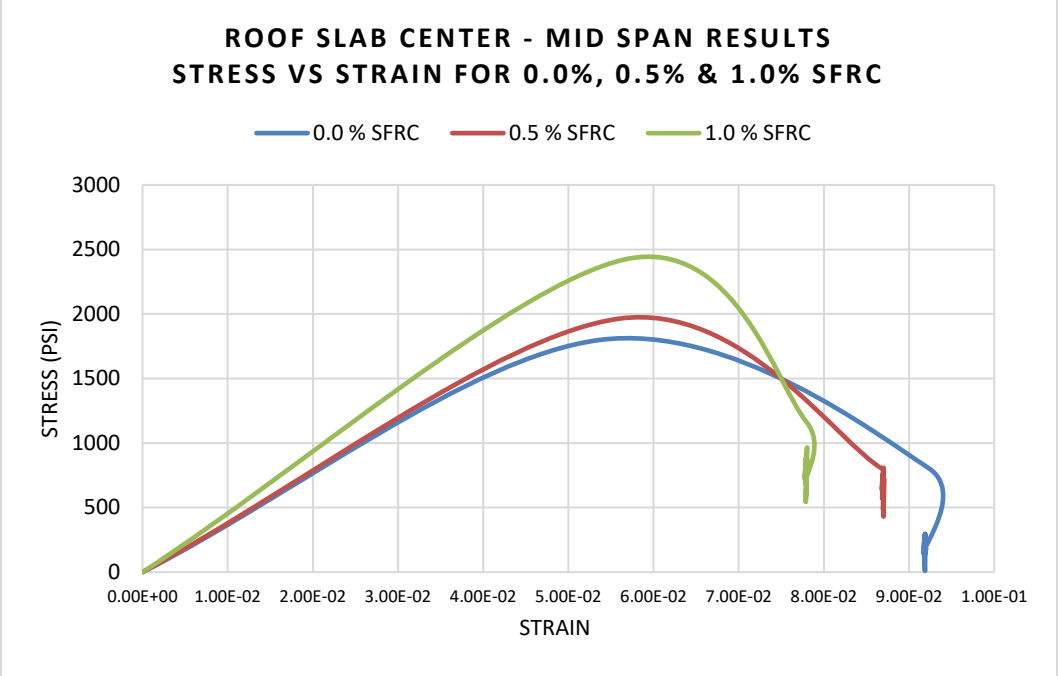

Figure 81 Roof -Stress Vs Strain at node for 0.0%, 0.5% & 1.0% SFRC

At 1.0% SFRC structure roof slab, strain, and deflection is reduced by 26% and 15% with 1.0% SFRC. From figure 81, the stress vs strain graph shows the maximum stress for 1.0% increased by 34% as it reaches to the maximum at higher strain value.

Table 17: Comparison for Roof Slab- Mid span center results for different SFRC V_f

Roof Slab - Mid Span Center – Stresses, Strain and Deflection comparison of 0.0%, 0.5% & 1.0% SFRC			
	0.00%	0.50%	1.00%
Stresses (psi)	1798.471	1963.637	2422.468
% increase	-	**9.18%**	**34.70%**
Strain	0.0922	0.0870	0.0780
% decrease	-	**-11.77%**	**-26.52%**
Deflection (inch)	26.276	23.183	19.306
% decrease	-	**-5.66%**	**-15.44%**

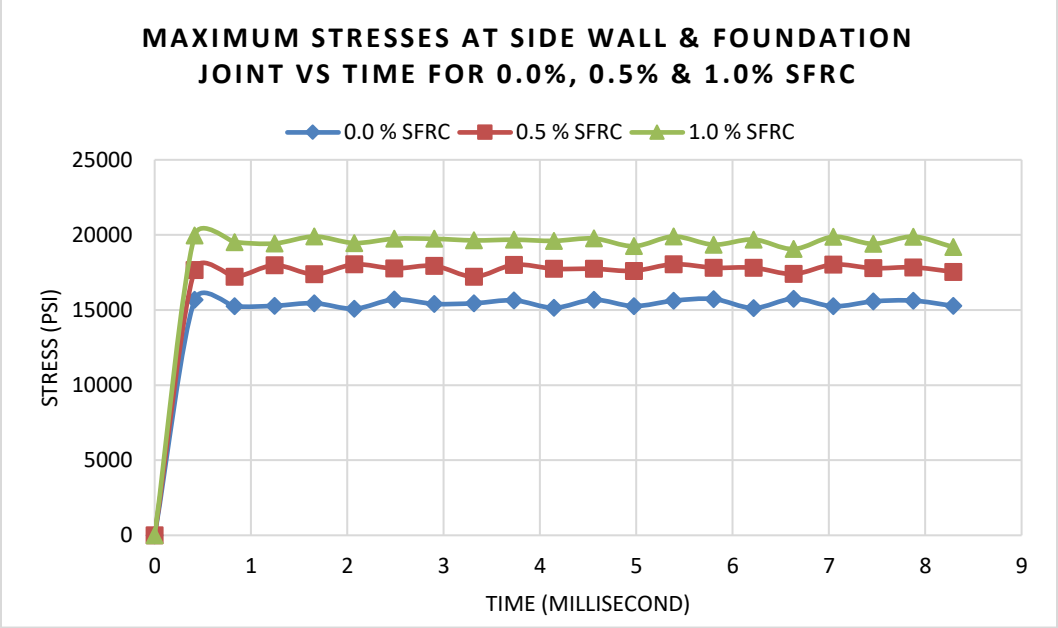

Figure 82 Steam Boiler Room -Maximum Stresses for 0.0%, 0.5% & 1.0% SFRC

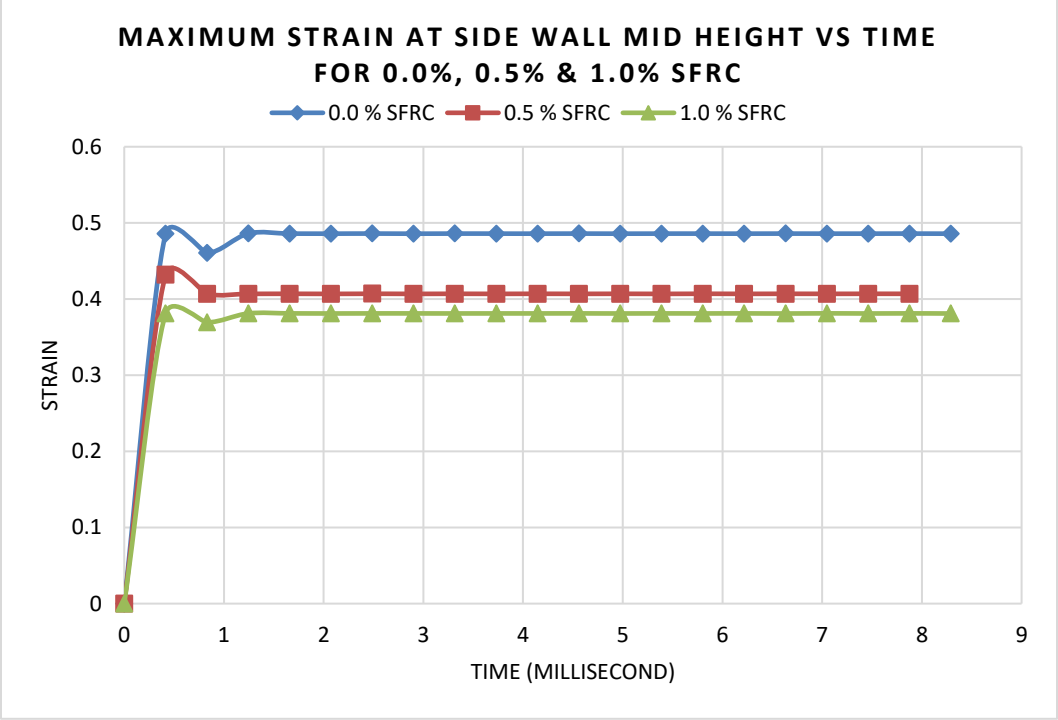

Figure 83 Steam Boiler Room -Maximum Strain for 0.0%, 0.5% & 1.0% SFRC

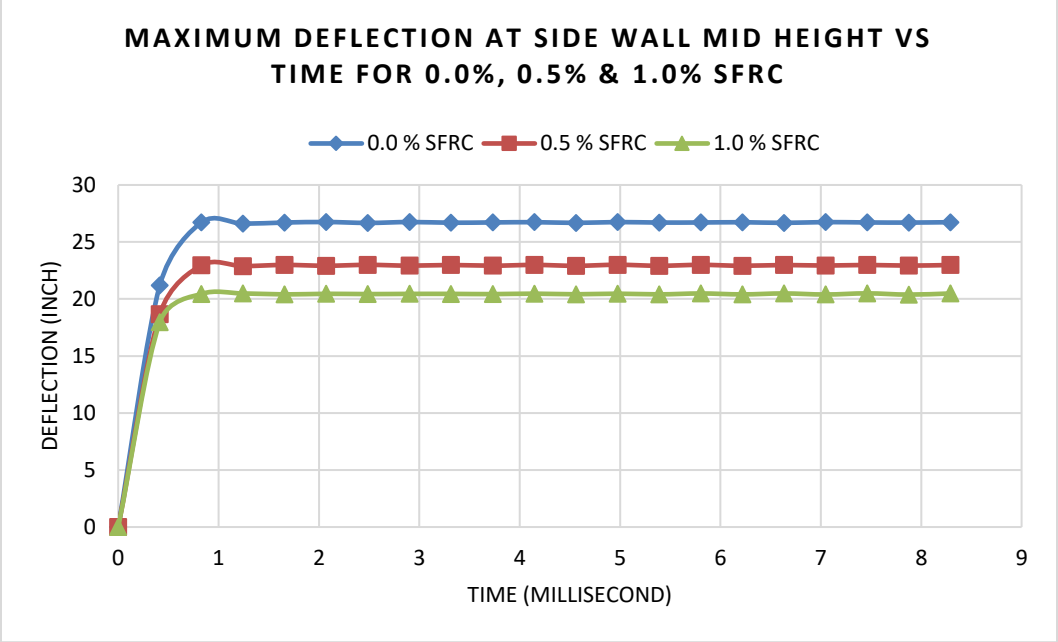

Figure 84 Steam Boiler Room -Maximum Deflection for 0.0%, 0.5% & 1.0% SFRC

Table 18: Comparison for Steam Boiler Room analysis results for different SFRC Vf

Stresses, Strain and Deflection Comparison of 0.0%, 0.5% & 1.0% SFRC			
	0.00%	0.50%	1.00%
Maximum Stresses (psi) at the Side Wall and Foundation joint	15748.700	18050.534	19957.200
% increase	**0**	**14.62%**	**26.72%**
Maximum Strain at Side Wall Mid Height	0.486	0.432	0.381
% decrease	**0**	**-11.09%**	**-21.57%**
Maximum Deflection (inch) at Side Wall Mid Height	26.751	22.999	20.492
% decrease	**0**	**-14.03%**	**-23.40%**

It is obtained from the results that the maximum stresses developed in the Steam boiler closed room are at the side wall and foundation joint as it offers rigidity to the structure. By adding 1.0% steel fiber to concrete, the overall capacity of structure can be significantly increased by 26%, the deflection reduced by 23%, and strain reduced by 21%. Although the failure criteria is assigned in ABAQUS's concrete damage plasticity specification, the stresses in the structure with 1.0% SFRC reach 20 ksi (Table 18), which is significantly higher than the compressive strength of concrete i.e. 4.3 ksi, hence the structure which fails at 4.3 ksi. This shows the structure has to be designed for 20 ksi stress; it can be done by providing reinforcement in structure or increasing the thickness of the wall.

4.8 Parametric Study Analysis

4.8.1 Parametric Study I- Steam Boiler Room with Frangible Roof

The first parametric study is carried out to reduce the reflected pressure, which damages the structure critically. It can be achieved by providing a frangible roof in the structure, which helps to release the energy due to explosion and reduce the reflected pressure exerted on surrounding walls. The roof slab made free to move along the vertical direction by assigning boundary conditions. As concluded from the study for 0.0%, 0.5%, and 1.0% SFRC that 1.0% SFRC significantly reduces the deflection, strain, and increases the strength capacity of the structure, hence 1.0% SFRC is considered for this study. All the parameters like mesh, concrete properties, steps, and dynamic loading conditions (CONWEP) are kept the same for this study.

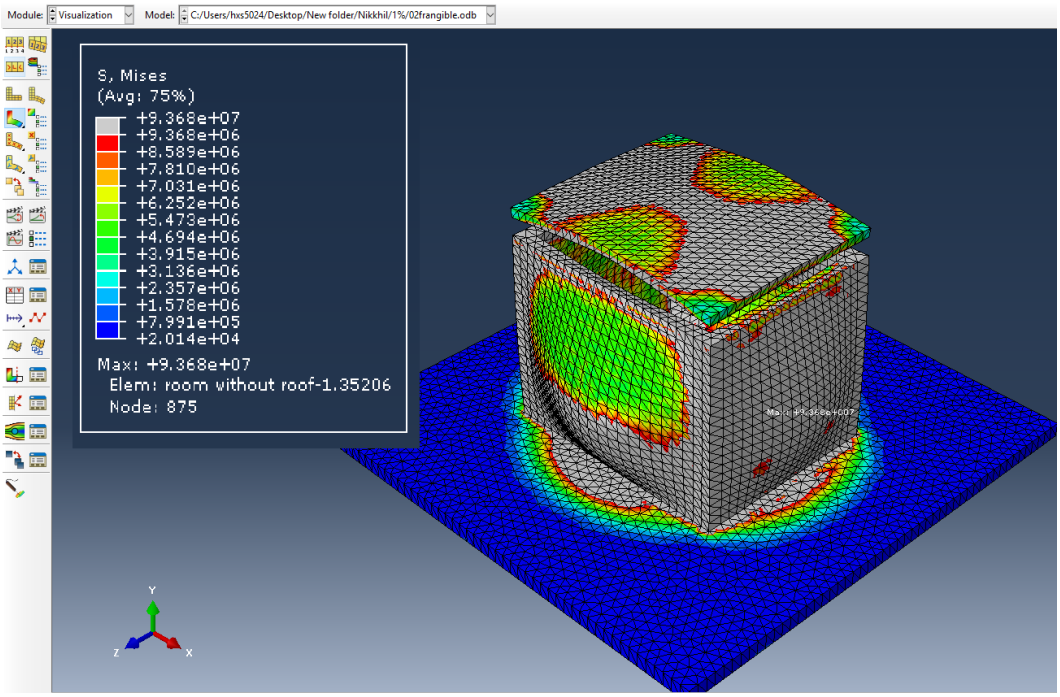

Figure 85 1.0% SFRC - Stresses (N/m^2) developed in Steam Boiler Room

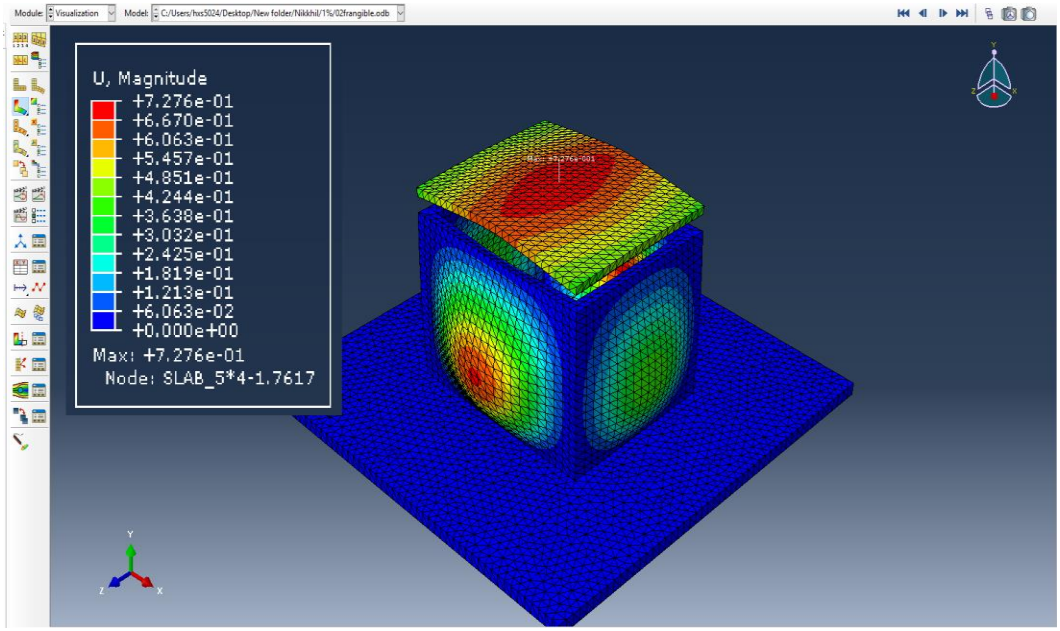

Figure 86 1.0% SFRC – Deflection (m) in Steam Boiler Room with Frangible Roof

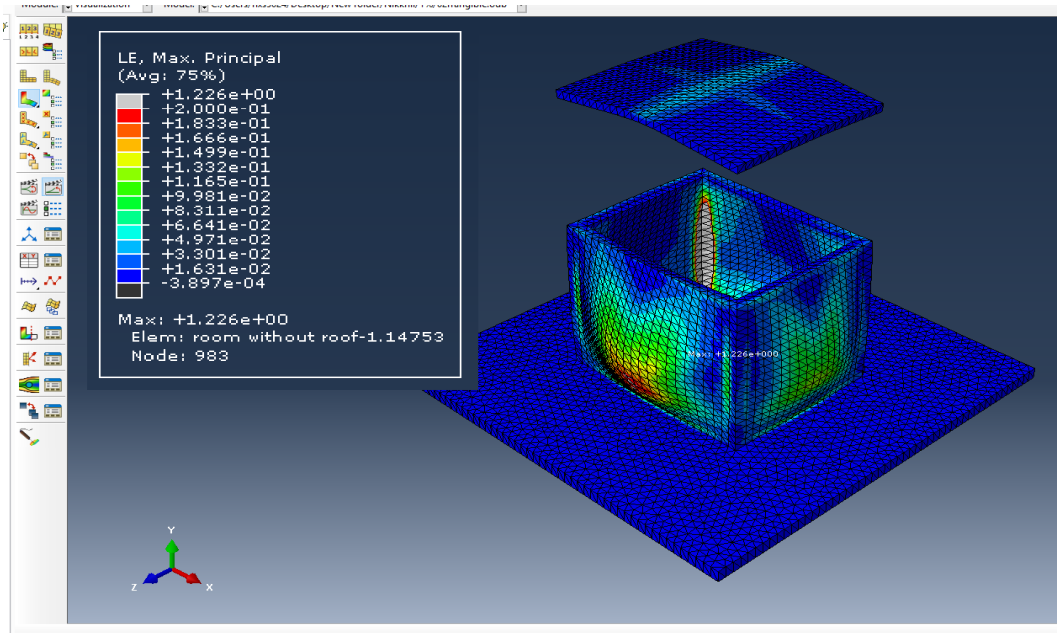

Figure 87 1.0% SFRC - Strain in Steam Boiler Room with Frangible Roof

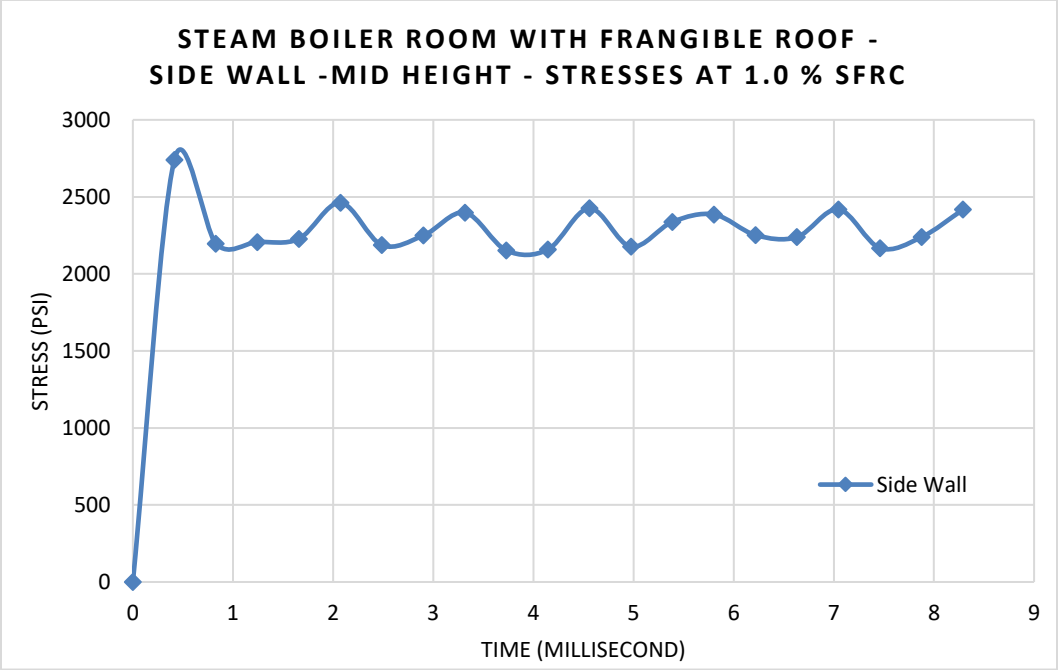

Figure 88 Boiler Room with Frangible Roof – Stresses at Side Wall at 1.0% SFRC V_f

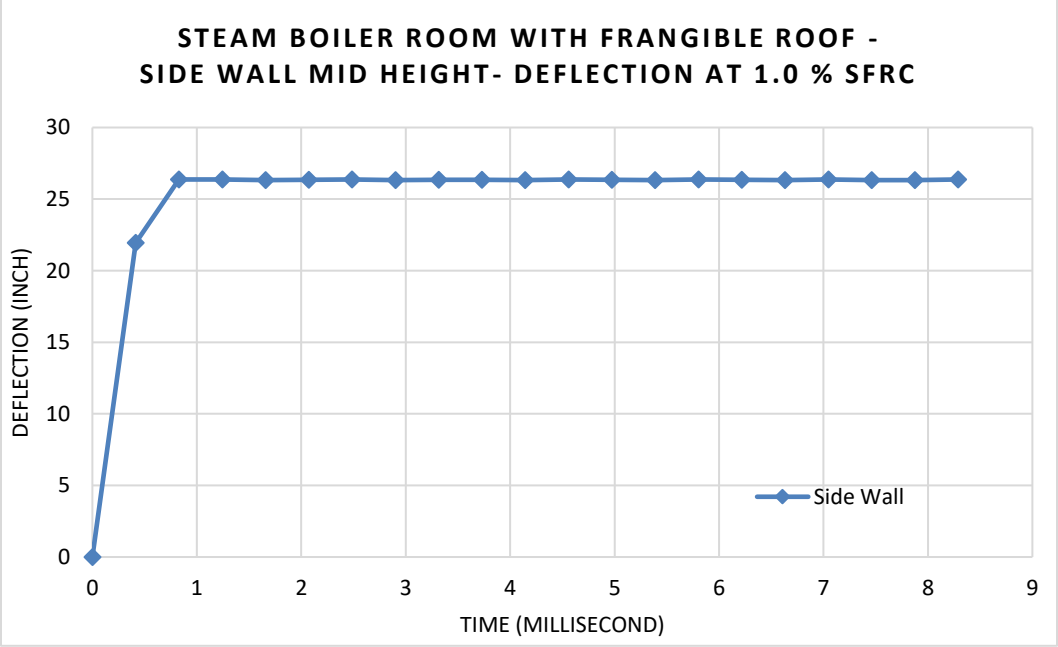

Figure 89 Boiler Room with Frangible Roof – Deflection at Side Wall at 1.0% SFRC V_f

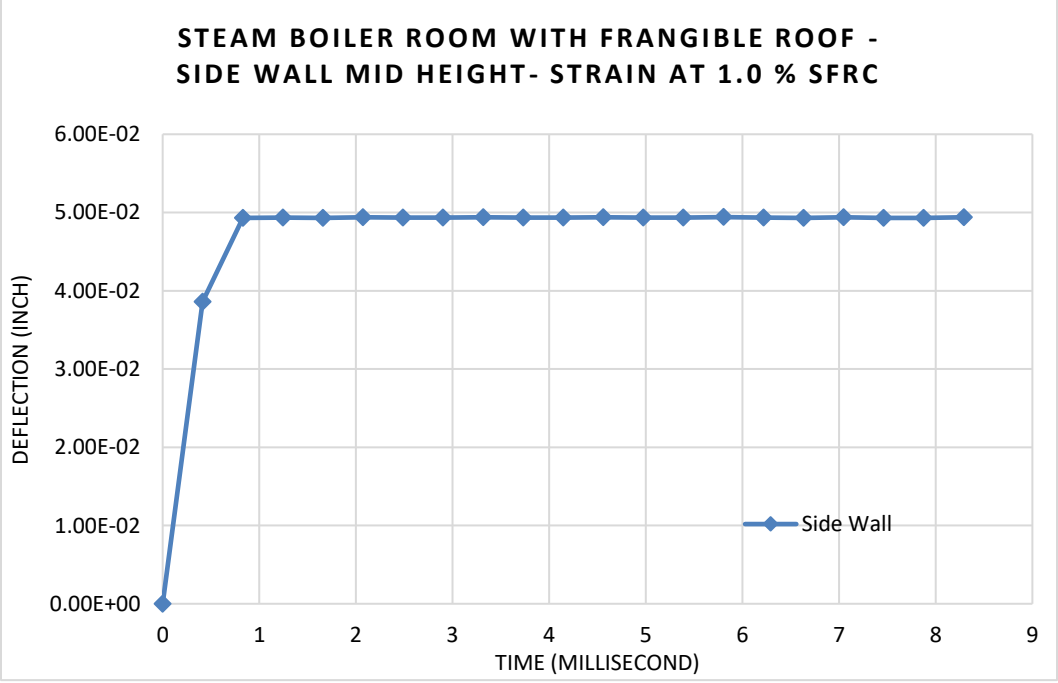

Figure 90 Steam Boiler Room with Frangible Roof – Strain at Side Wall at 1.0% SFRC V_f

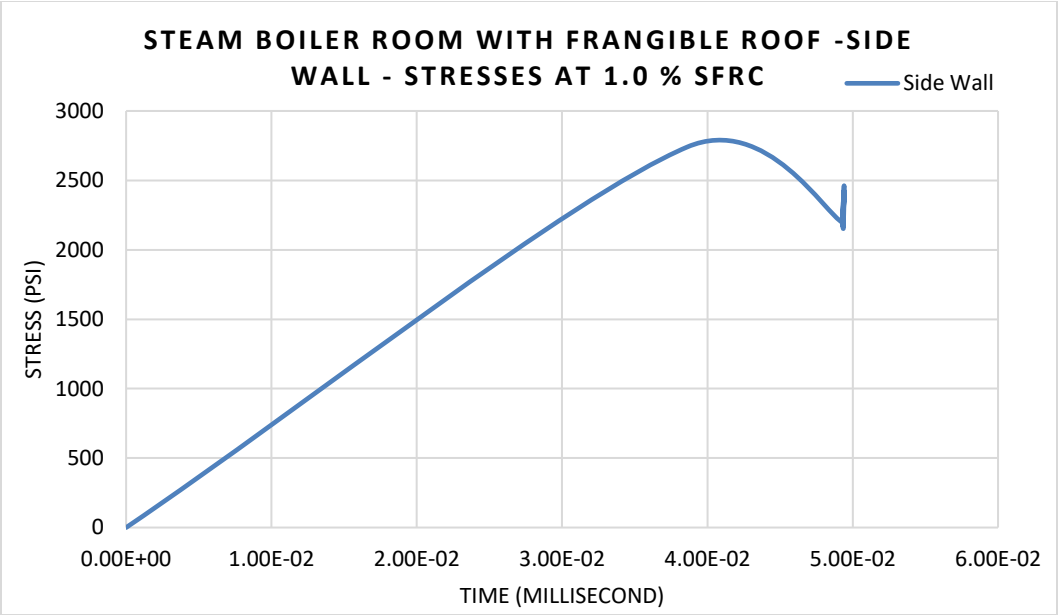

Figure 91 Steam Boiler Room with Frangible Roof – Stress Vs Strain at Side Wall at 1.0% SFRC V_f

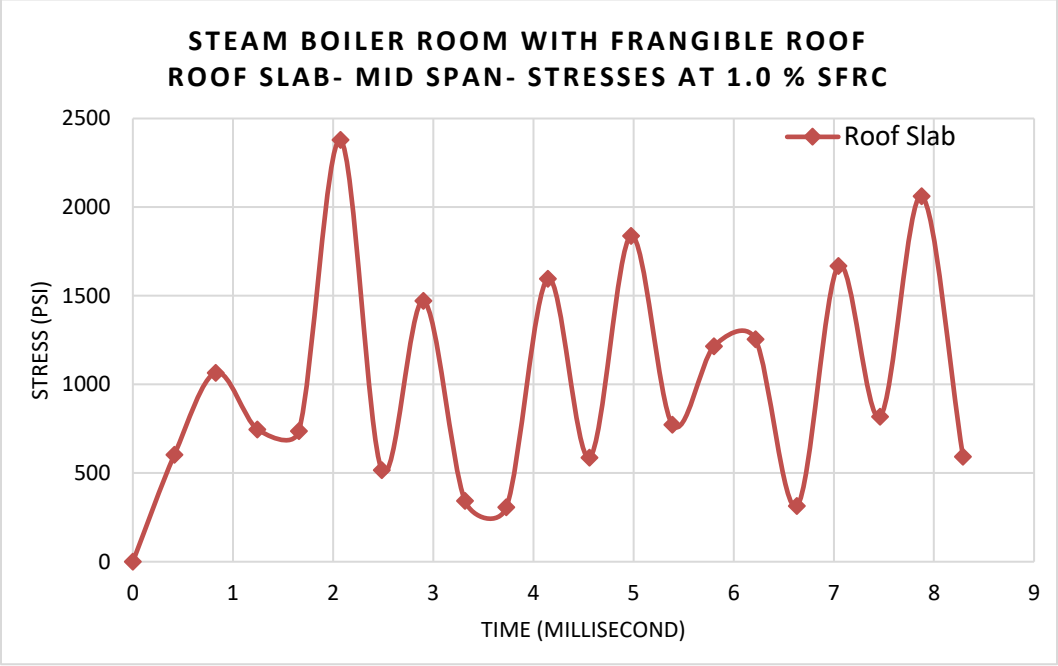

Figure 92 Boiler Room with Frangible Roof – Stresses at Roof Slab at 1.0% SFRC Vf

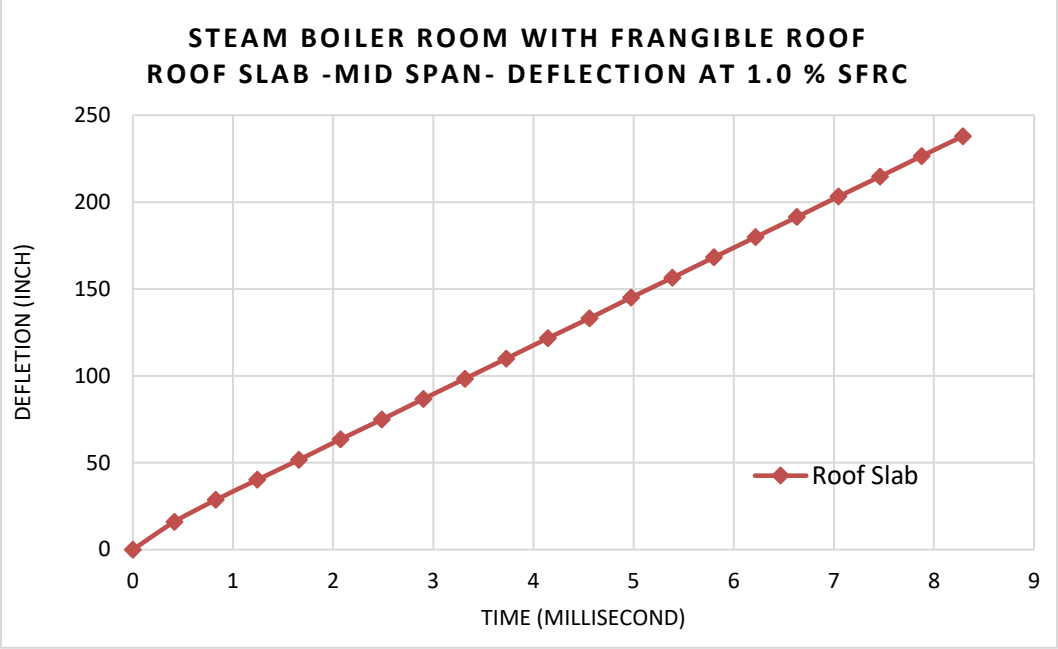

Figure 93 Boiler Room with Frangible Roof – Deflection at Roof Slab at 1.0% SFRC Vf

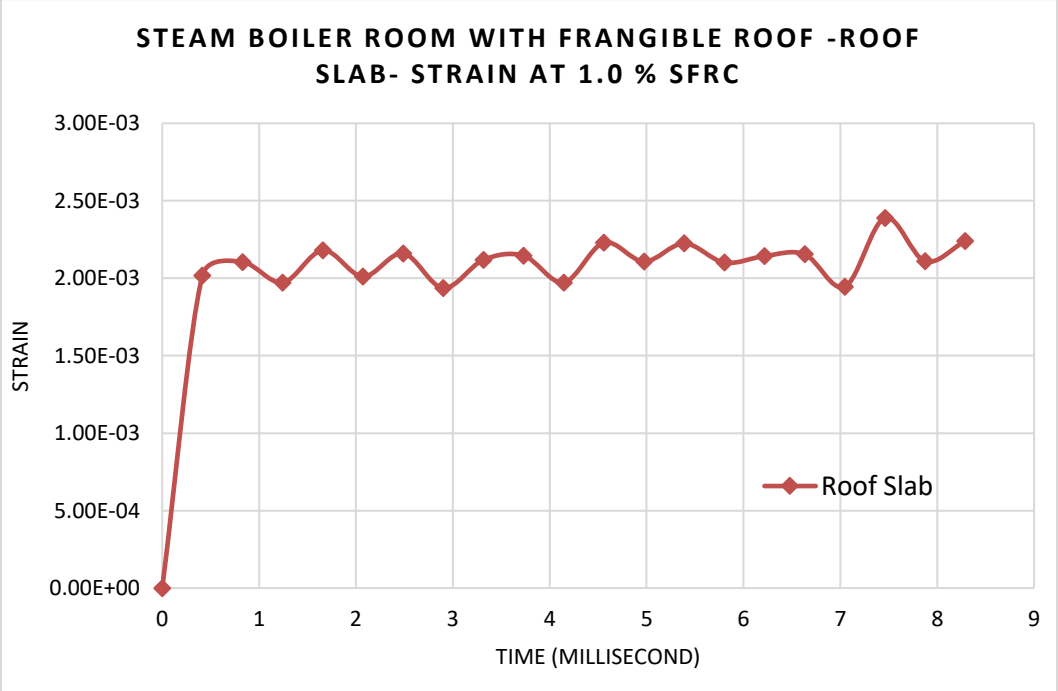

Figure 94 Steam Boiler Room with Frangible Roof – Strain at Roof Slab at 1.0% SFRC Vf

4.8.2 Parametric Study II-Steam Boiler Room with a 4 ft diameter circular vent in the roof

The second parametric study is again carried out to reduce the reflected pressure, which damages the structure critically. It can be achieved by providing a circular vent of 4 ft in roof slab in the structure, which helps to release the energy due to explosion and reduce the reflected pressure exerted on surrounding walls. As concluded from the study for 0.0%, 0.5%, and 1.0% SFRC that 1.0% SFRC significantly reduces the deflection, strain, and increases the strength capacity of the structure, hence 1.0% SFRC is considered for this study. All the parameters like mesh, concrete properties, steps, and dynamic loading conditions (CONWEP) are kept the same for this study.

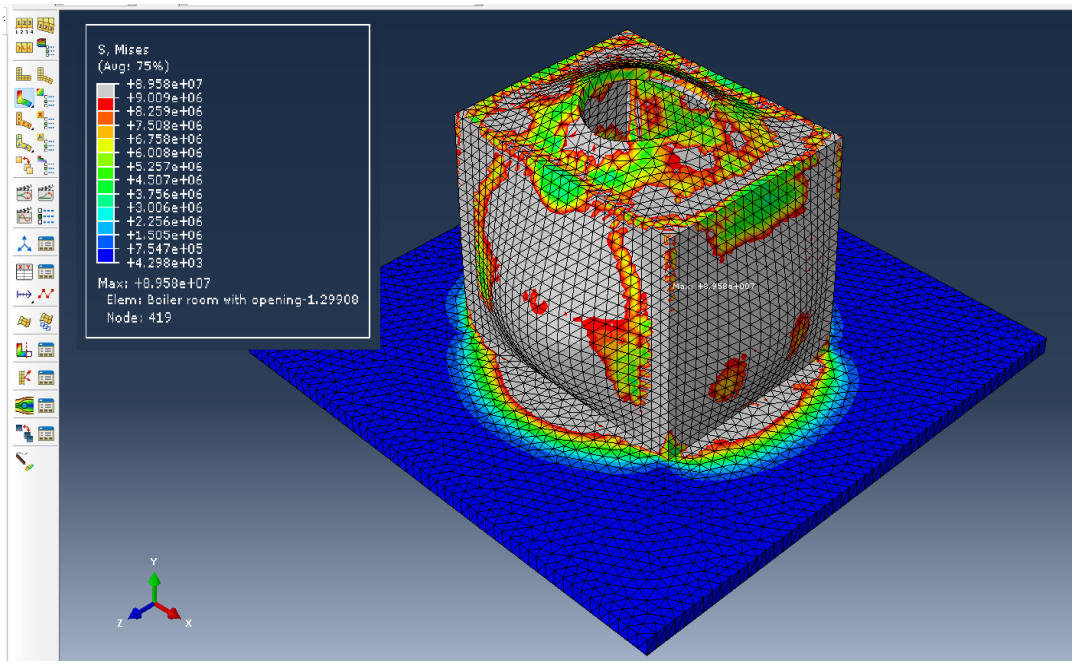

Figure 95 1.0% SFRC – Stresses (N/m^2) in the Boiler Room with a circular vent in the roof

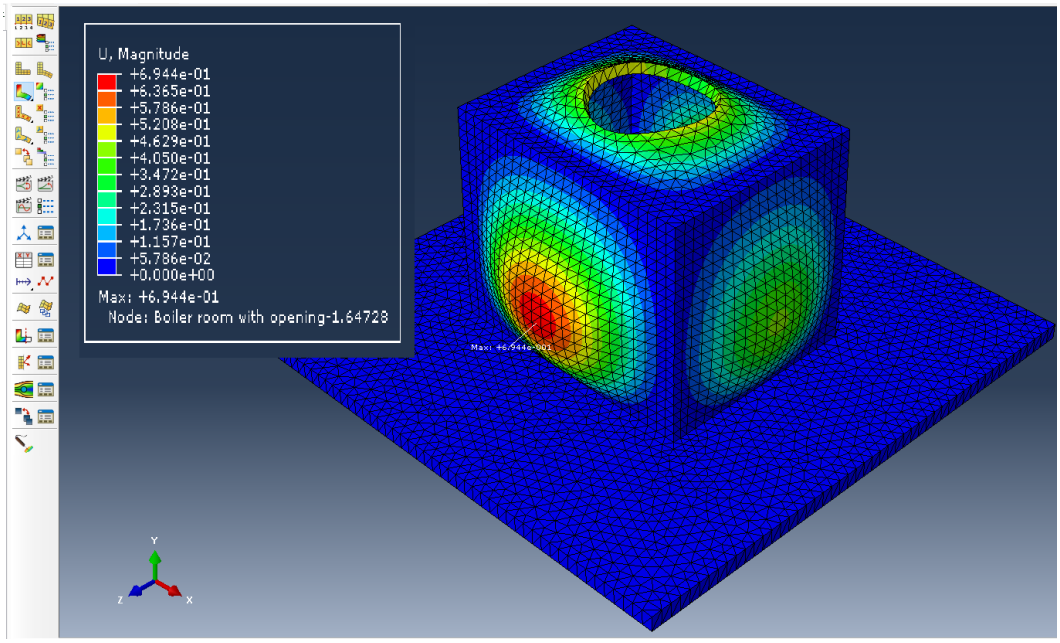

Figure 96 1.0% SFRC - Deflection (m) in the Boiler Room with Circular Vent in Roof

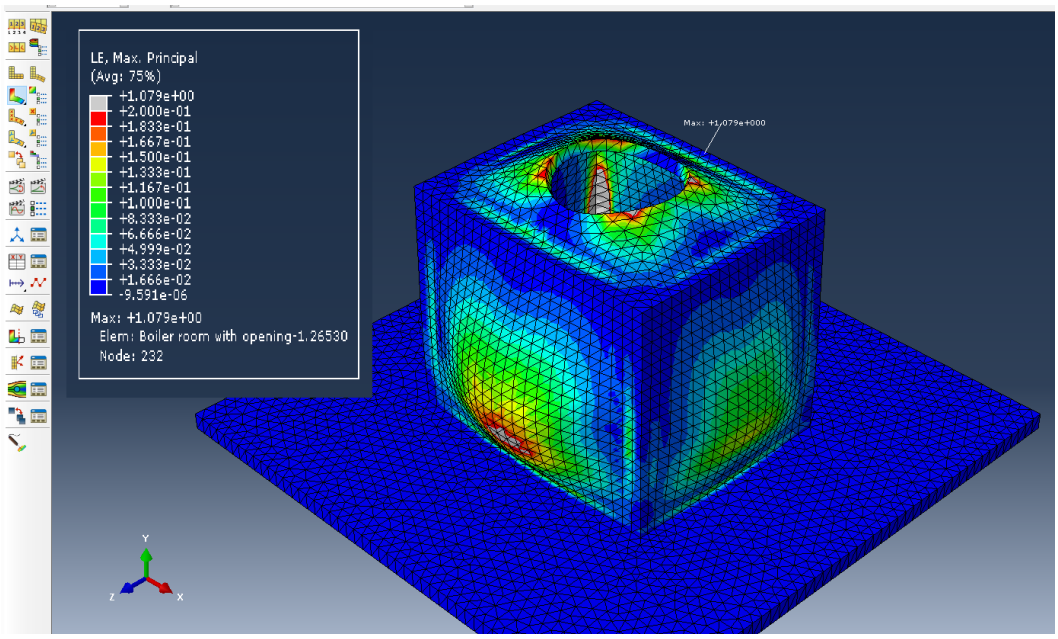

Figure 97 1.0% SFRC - Strain in Steam Boiler Room with Circular Vent in Roof

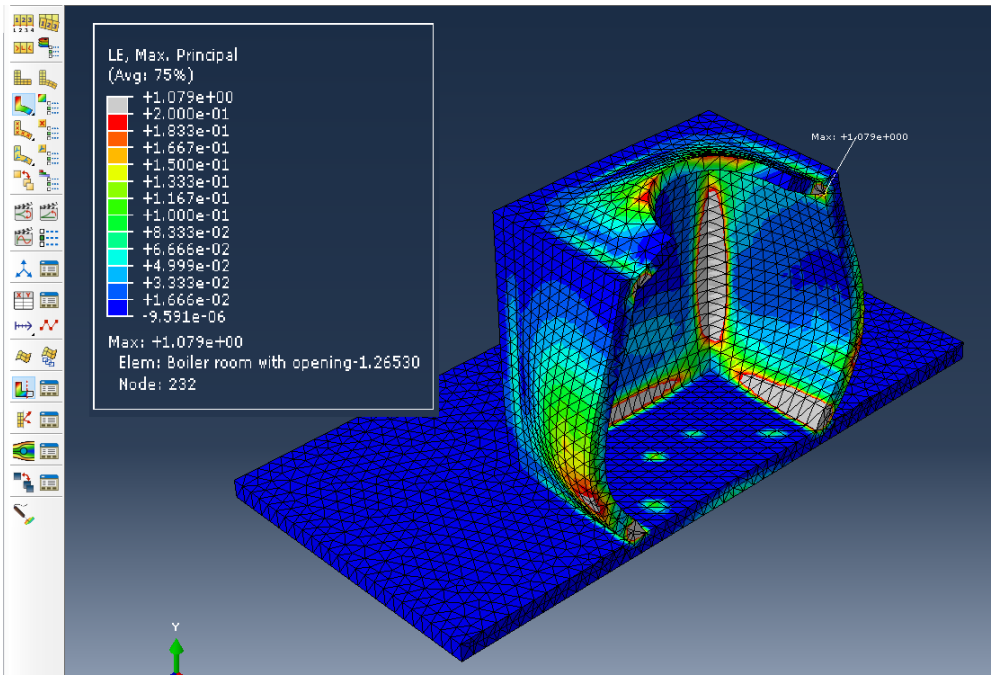

Figure 98 1.0% SFRC - Strain in Steam Boiler Room with Circular Vent in Roof

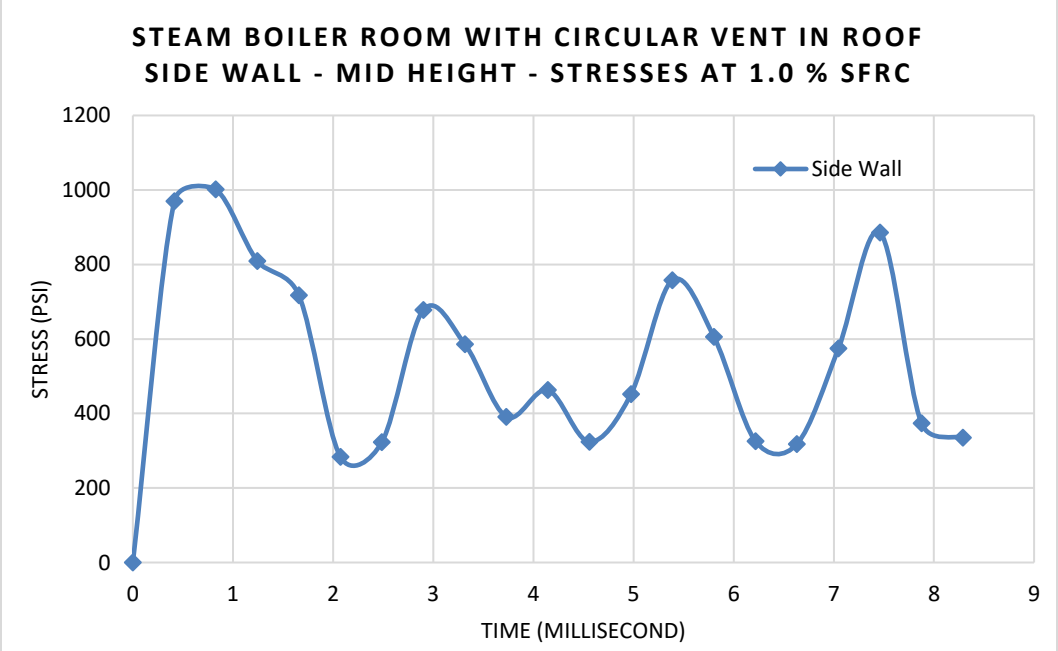

Figure 99 Circular vent in the roof – Stresses at Side Wall at 1.0% SFRC V_f

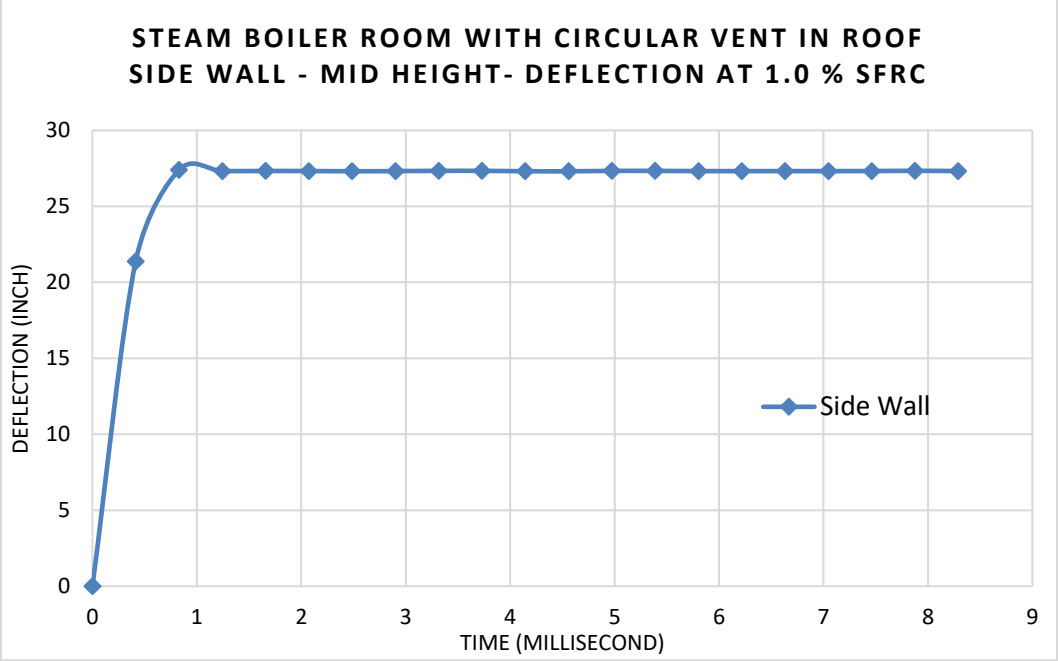

Figure 100 Circular vent in the roof – Deflection at Side Wall at 1.0% SFRC V_f

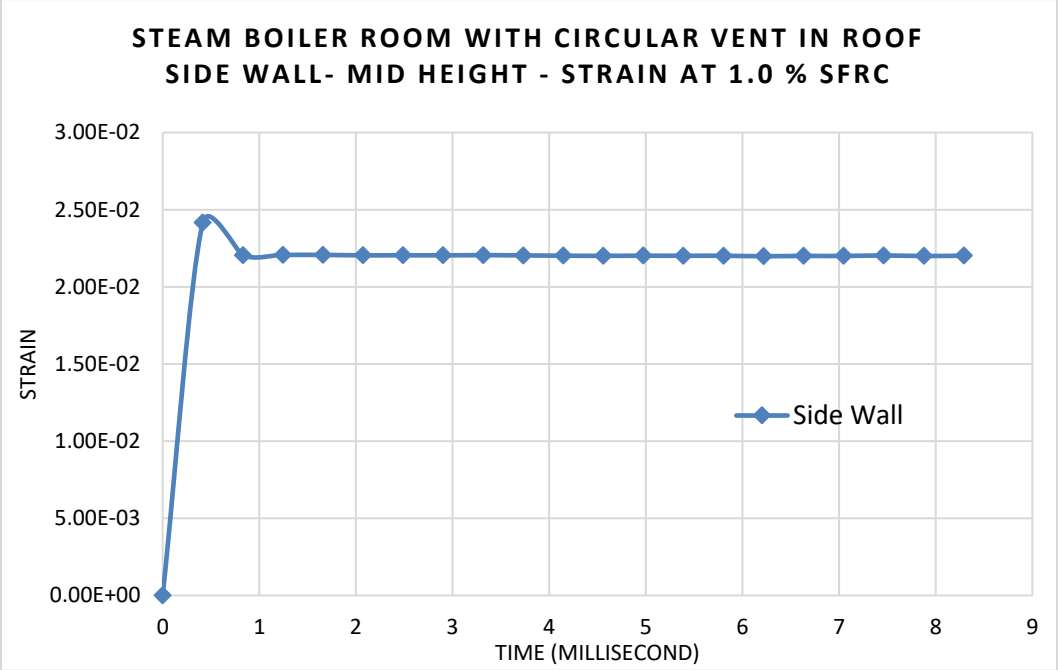

Figure 101 Circular vent in the roof – Strain at Side Wall at 1.0% SFRC V_f

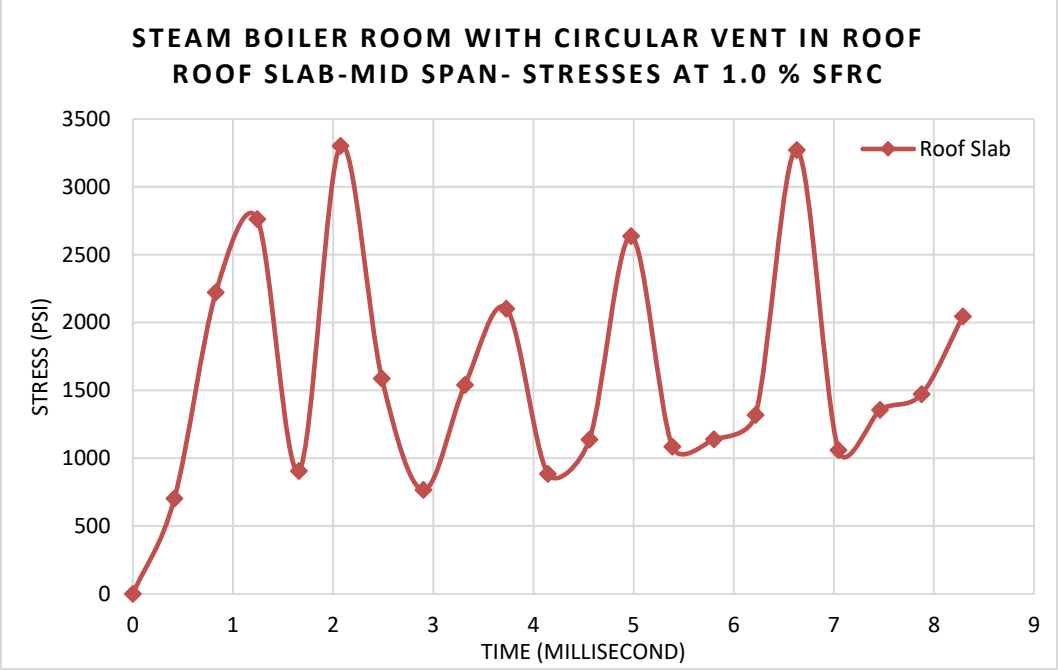

Figure 102 Circular vent in the roof – Stresses at Roof Slab at 1.0% SFRC V_f

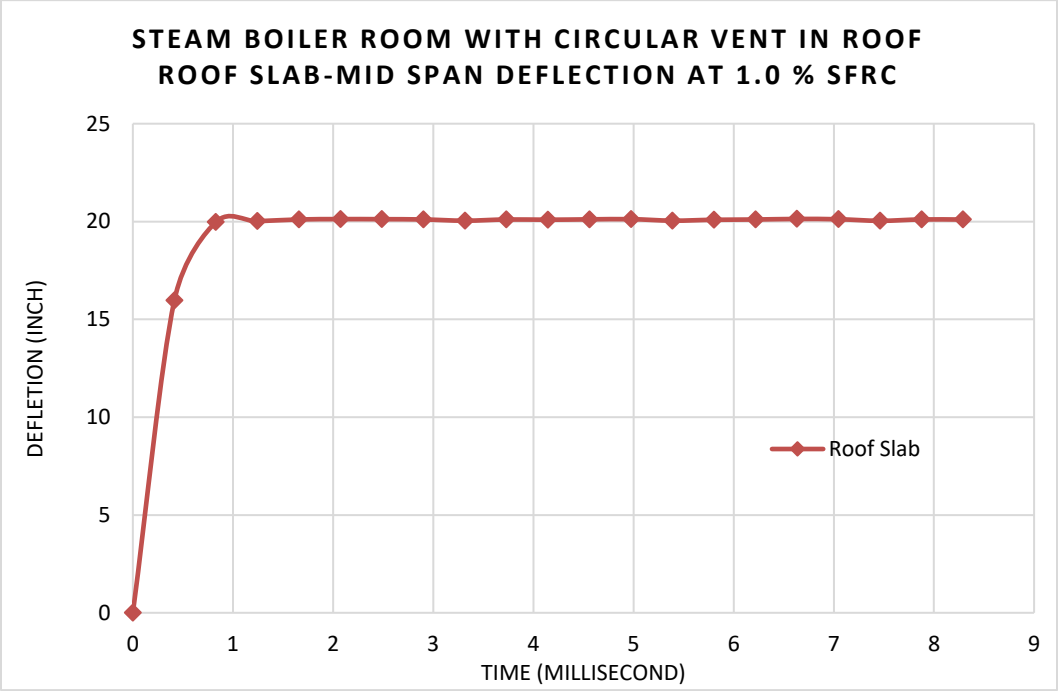

Figure 103 Circular vent in the roof – Deflection at Roof Slab at 1.0% SFRC V_f

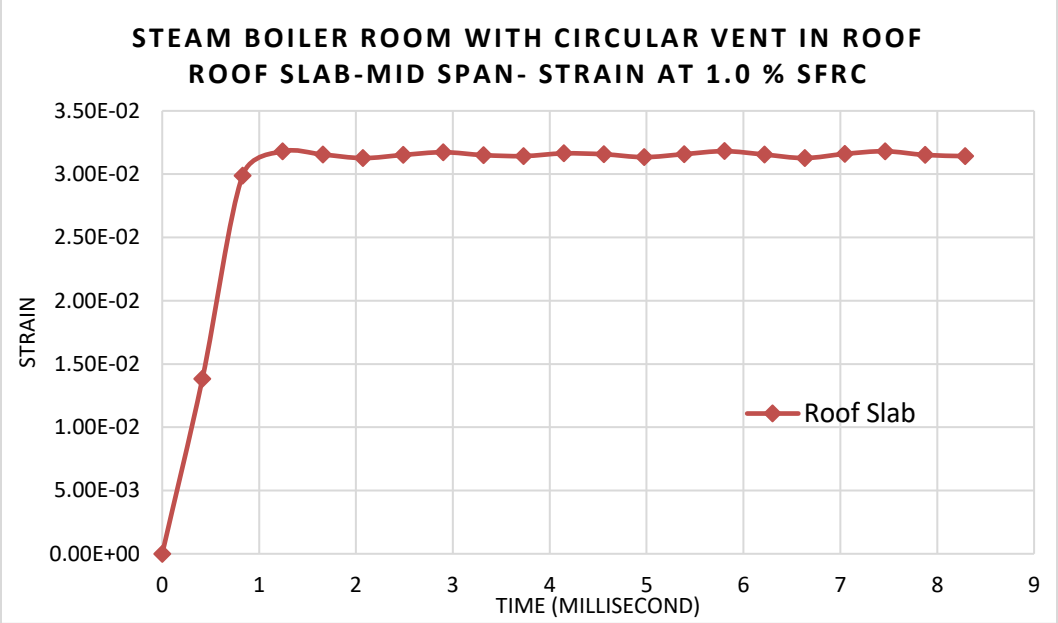

Figure 104 Circular vent in the roof – Strain at Roof Slab at 1.0% SFRC V_f

4.8.3 Parametric Study Comparison- Steam Boiler Room- Rigid Roof vs Frangible Room vs Circular Vent in Roof

Comparison is done with the different arrangements of the roof of Steam Boiler Room for cases: with a rigid roof, with Frangible Roof, and with 4ft Circular Vent in the roof. Comparison is done based on the results found for stresses developed in the structure, deflection, and strain. Concrete with 1.0% SFRC material properties is used for the analysis.

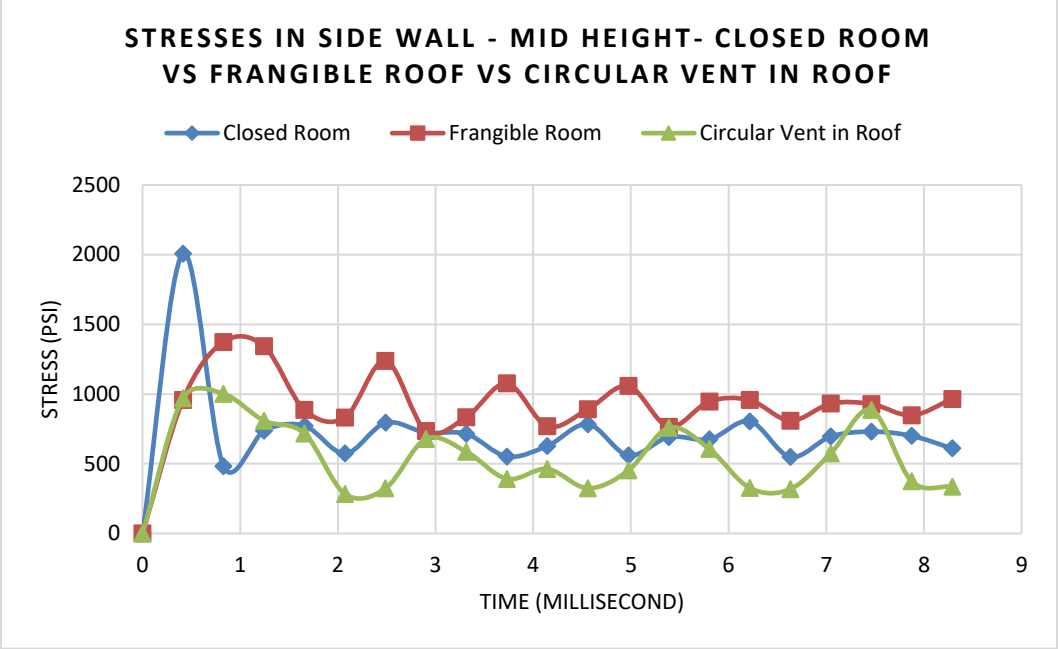

Figure 105 Comparison of Stresses at Side Wall at 1.0% SFRC V_f

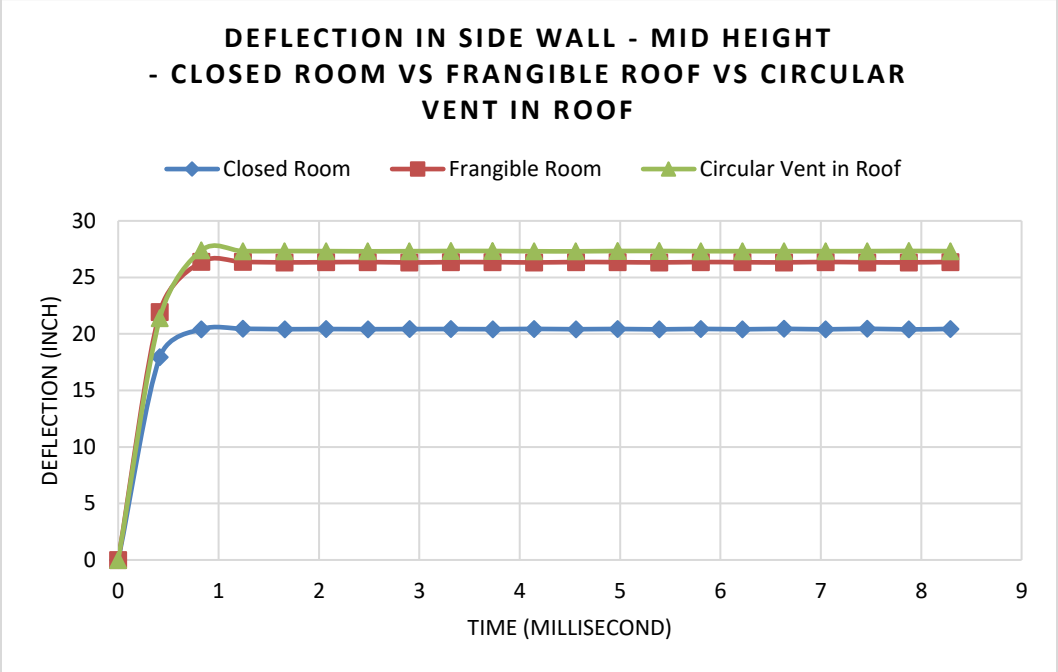

Figure 106 Comparison of Deflection at Side Wall at 1.0% SFRC V_f

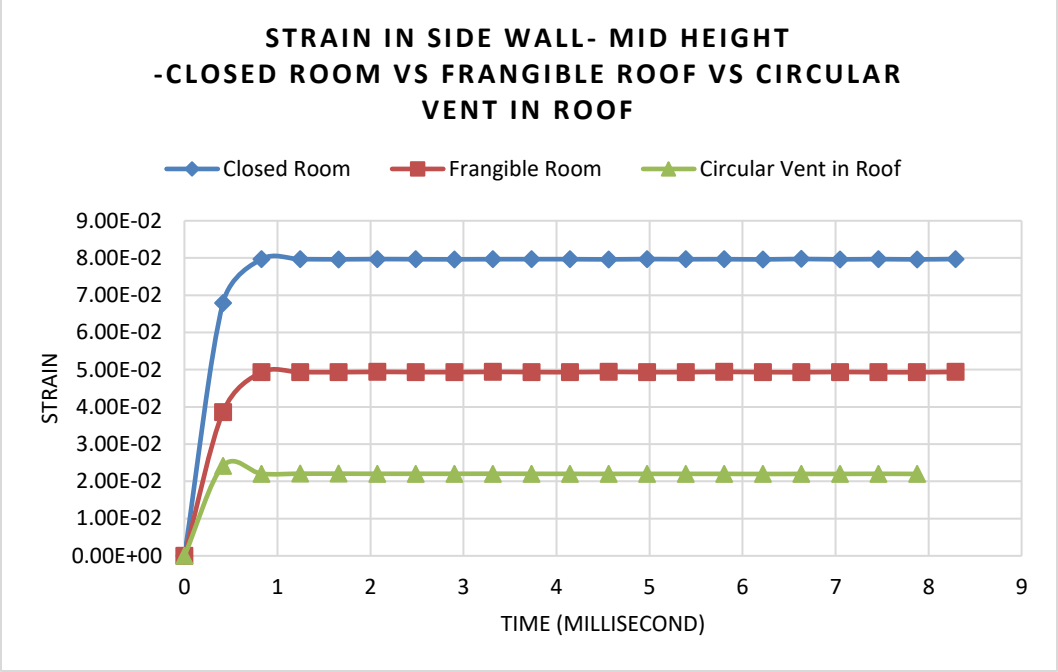

Figure 107 Comparison of Strain at Side Wall at 1.0% SFRC V_f

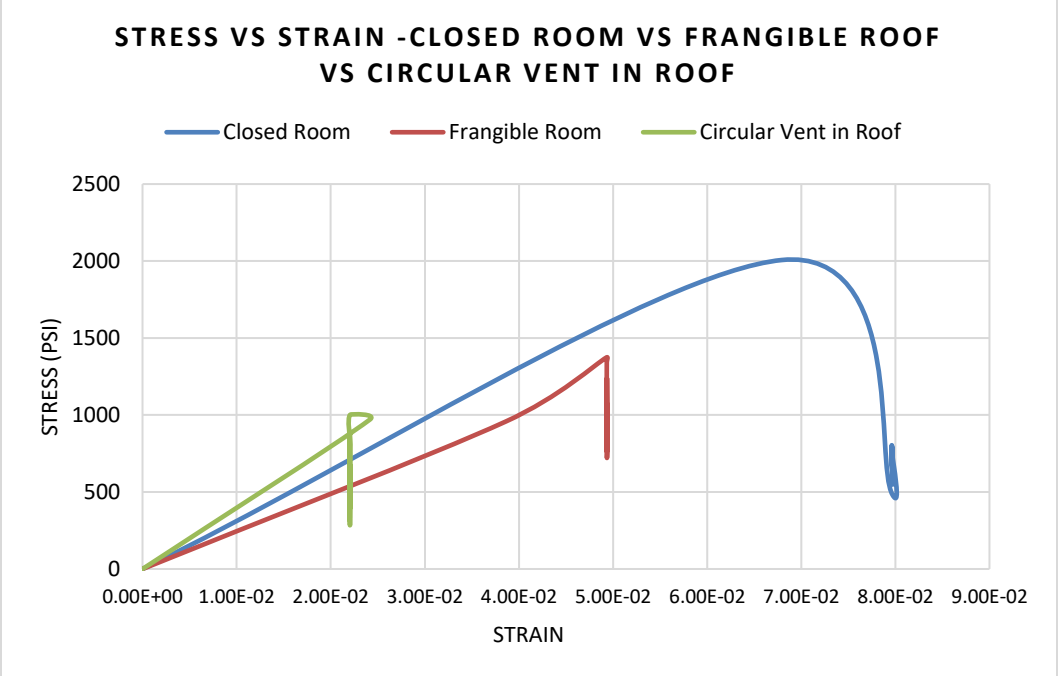

Figure 108 Comparison of Stress Vs Strain at Side Wall at 1.0% SFRC V_f

Table 19: Comparison for Side Wall - Mid-height center results of different arrangements of Steam Boiler Room

Side Wall- Mid Height Center – Stresses, Strain and Deflection Comparison different arrangements of Steam Boiler Room for 1.0% SFRC			
	Closed Room	Frangible Roof	Circular Vent in Roof
Stresses (psi)	2006.680	1374.132	1001.562
% decrease	-	**-31.52%**	**-50.09%**
Strain	0.0797	0.049	0.0241
% decrease	-	**-38.03%**	**-69.71%**
Deflection (inch)	20.4559	26.370	27.391
% increase	-	**28.91%**	**33.91%**

Maximum stresses developed at the side wall due to the steam boiler explosion is found lowest in the case with 4ft diameter Circular vent in roof and highest in the case with a rigid roof. It is found that deflection at the side wall – mid-height is found highest in the case with Circular vent in roof and lowest in the case with the rigid roof because of the rigidity of the roof slab. Correspondingly the strain is significantly reduced in the case with a circular vent in the roof by 69%.

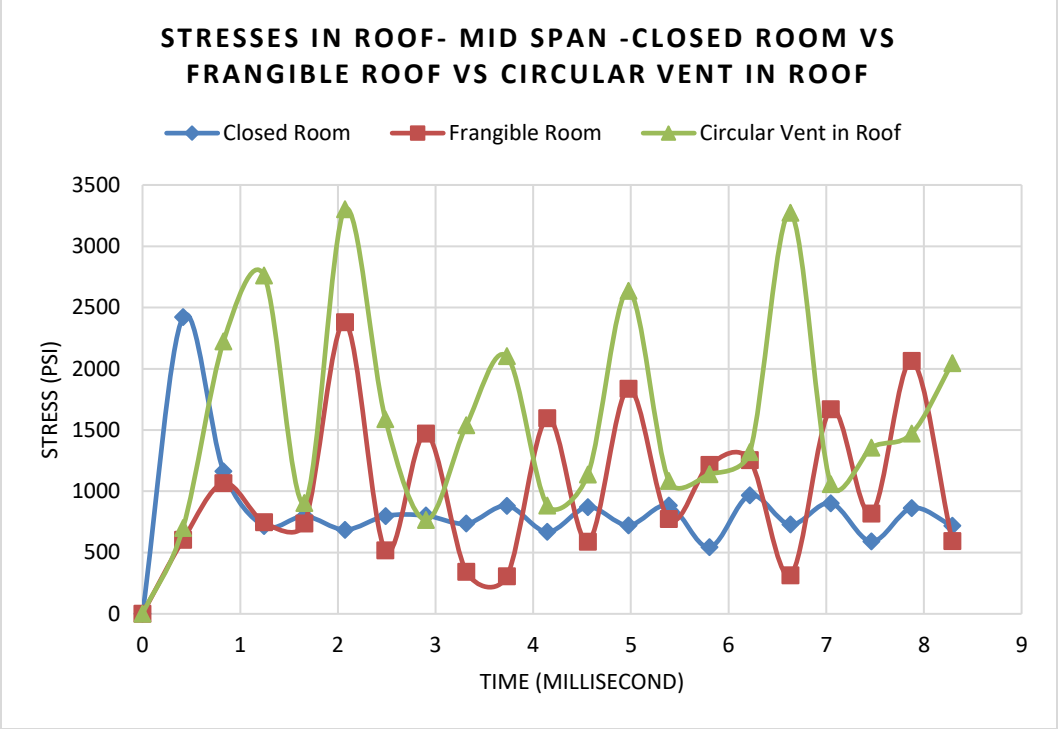

Figure 109 Comparison of Stresses at Roof Slab at 1.0% SFRC Vf

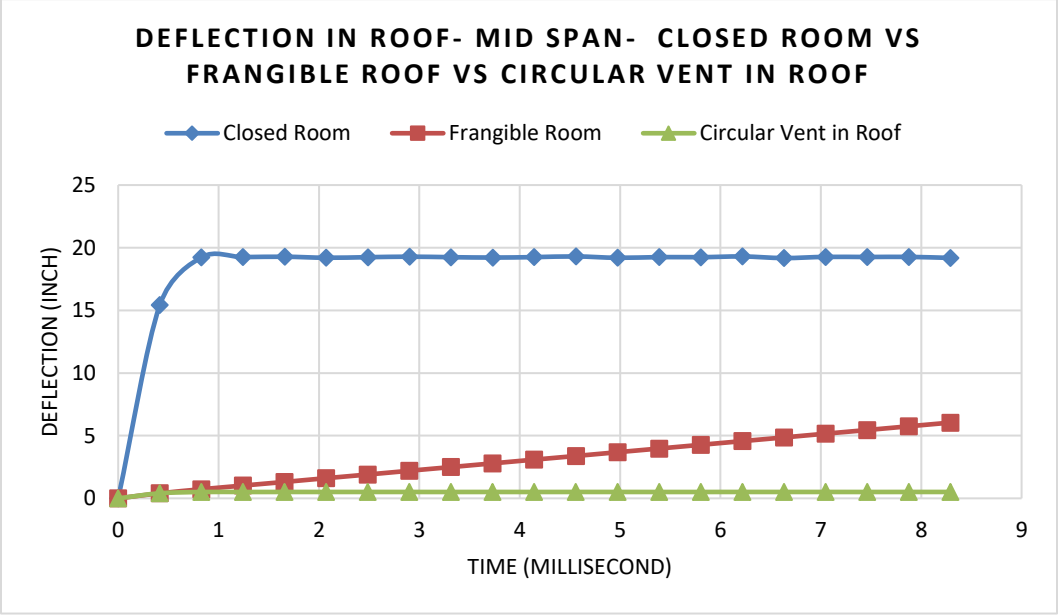

Figure 110 Comparison of Deflection at Roof Slab at 1.0% SFRC Vf

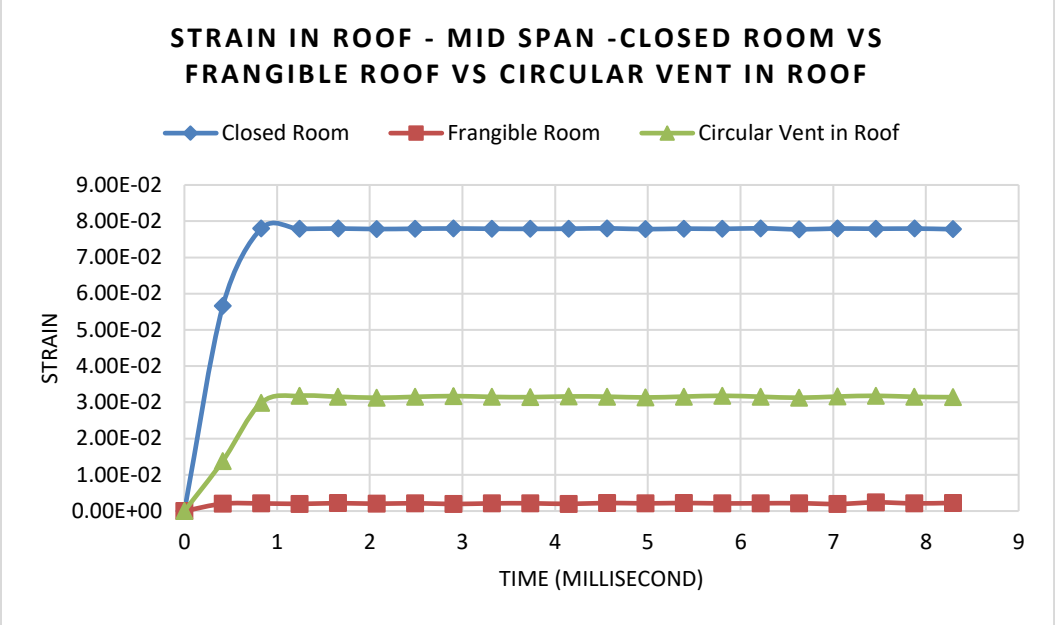

Figure 111 Comparison of Strain at Roof Slab at 1.0% SFRC Vf

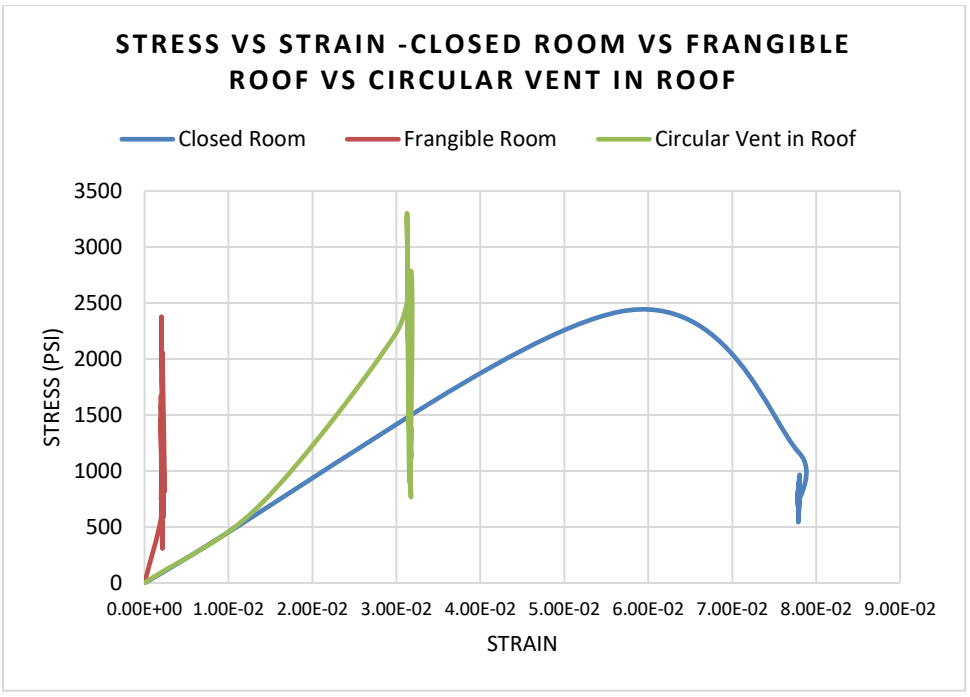

Figure 112 Comparison of Stress Vs Strain at Roof Slab at 1.0% SFRC Vf

Table 20: Comparison for Roof Slab of different arrangements of Steam Boiler Room

Roof Slab – Stresses, Strain and Deflection Comparison different arrangements of Steam Boiler Room for 1.0% SFRC			
	Closed Room	Frangible Roof	Circular Vent in Roof
Stresses (psi)	2422.470	2378.869	3302.457
% increase / decrease	-	**-1.80%**	**36.33%**
Strain	0.0780	0.0023	0.0318
% decrease	-	**-96.94%**	**-59.23%**
Deflection (inch)	19.306	237.941	20.1311
% increase	-	**1132.43%**	**4.27%**

Maximum stresses developed at the roof slab due to the steam boiler explosion is found lowest in the case with a rigid roof and highest in the case with circular vent. It is found that deflection at the roof slab is found highest in the case with a frangible roof and lowest in the case with a rigid roof because of the rigidity of the roof slab. Correspondingly the strain is significantly reduced in the case with a frangible roof by 96%.

Table 21: Comparison for Maximum Stresses, Strain, and Deflection of different arrangements of Steam Boiler Room

Maximum Stresses, Strain and Deflection Comparison different arrangements of Steam Boiler Room for 1.0% SFRC			
	Closed Room	Frangible Roof	Circular Vent in Roof
Stresses (psi)	19957.2	13587	18463
% decrease	-	**-31.92%**	**-7.49%**
Strain	0.381	1.226	1.07900
% increase	-	**221.78%**	**183.20%**
Deflection (inch)	20.492	28.646	27.394
% increase	-	**39.79%**	**33.68%**

Maximum stresses developed at the side wall and foundation joint due to the steam boiler explosion is found lowest in the case with a frangible roof and highest in the case with a rigid roof. It is found that deflection at the side wall – mid-height is found highest in the case with a frangible roof and lowest in the case with a rigid roof because of the rigidity of the roof slab. Correspondingly the strain is increased in the case with a frangible roof.

4.9 Discussion of Results

4.9.1 Steam Boiler -Closed Room for 0.0%, 0.5% and 1.0% SFRC.

In the experimental studies its obtained that the mechanical properties of the concrete have enhanced. Adding 1% of steel fiber in concrete can increase the modulus of elasticity by 11%, compressive strength by 22%, tensile strength by 42%, and modulus of rupture by 32 %. Hence the steel fibers can be used in the concrete mix by volume fraction to mitigate the effect of an accidental explosion. It also enhances the capacity of the structure and provides greater resistance to the dynamic loading condition due to an explosion. By adding 1.0% steel fiber to concrete, the overall capacity of structure can be significantly increased by 26%, the deflection reduced by 23%, and strain reduced by 21%. Damages caused due to an explosion within nearby a building like catastrophic damage to the building's structure, loss of life, and injuries to occupants can be mitigated by using SFRC structures.

4.9.2 Parametric Study Comparison -Steam Boiler Room with a rigid roof, frangible roof & 4 ft circular vent in the roof

The parametric study is carried out to reduce the effect of the explosion on the structure by making different arrangements for the roof, which can help release the energy, mainly with a rigid roof, frangible roof, and 4 ft circular vent in the roof. It is found that maximum stresses developed at the side wall due to the steam boiler explosion is found lowest in the case with 4ft diameter Circular vent in roof and highest in the case with a rigid roof. Also, it is found that deflection at the side wall – mid-height is found highest in the case with Circular vent in roof and lowest in the case with the rigid roof because of the rigidity of the

roof slab. Correspondingly the strain is significantly reduced in the case with a circular vent in the roof by 69%.

The overall maximum stresses developed at the side wall and foundation joint due to the steam boiler explosion is found lowest in the case with a frangible roof and highest in the case with a rigid roof. It is found that deflection at the side wall – mid-height is found highest in the case with a frangible roof and lowest in the case with a rigid roof because of the rigidity of the roof slab. Correspondingly the strain is increased in the case with a frangible roof.

5 CONCLUSIONS

5.1 Conclusions

- By adding 1.0% volume fraction of steel fibers into the concrete design mix will increase concrete's compressive strength by 22%, modulus of rupture by 32%, and the tensile strength by 42%.
- Adding 1.0% volume fraction of steel fibers into the concrete mix will increase the Modulus of Elasticity of Concrete by 11%.
- The addition of steel fibers into the concrete mix design increases its strength but will reduce the workability.
- The effect of an accidental explosion of steam boiler on the surrounding walls significantly reduces by adding 1% steel fibers. Effect on the side wall shows an increase in the capacity of the side wall by 22%, reduce strain by 18% and reduce deflection by 11% under dynamic/ explicit loading (due to an internal explosion of Steam Boiler of capacity 4400 lb (2000 kg)).
- The effect of an accidental explosion of a steam boiler on the roof slab significantly reduces by adding 1% steel fibers. Effect on the roof slab shows an increase in the capacity of the side wall by 35%, reduces strain by 27%, and reduce deflection by 15% under dynamic/ explicit loading.
- Adding 1.0% of steel fibers in concrete will increase the overall strength of the structure by 27%, decrease the strain by 22%, and decrease deflection by 23% under dynamic loading.
- By providing the frangible roof in the Steam Boiler room, stresses decrease by 32%, strain reduces by 38%, and the deflection increases by 29% in side walls. In

the roof slab, stresses decrease by 2%, strain decrease by 97%, and increases the deflection by 1133% because of the frangible roof.

- By providing 4 ft diameter circular vent in roof slab in Steam Boiler room, stresses decrease by 50%, strain decrease by 70%, and increases the deflection by 34% in side walls. In roof slab, stresses increase by 37%, strain reduction by 60%, and increase the deflection by 4%.
- Comparison of Steam Boiler room structure model of Closed Room, Frangible room, and Circular vent in roof concludes that the frangible roof will reduce stresses by 32%, keeping the deflection almost the same in reference to circular vent in the roof. This shows the effect of the explosion of a steam boiler on the boiler room with a frangible roof significantly decreases in the boiler room with a rigid roof.

5.2 Recommendations for Future Work

- Future studies should explore improving the fc', ft, and fr values by increasing the percentage of steel fibers.
- Perform a study with different fiber reinforcement to see the change in mechanical properties of concrete and flexural capacity of concrete.
- Studies can be carried out for the different arrangement of vents in the surrounding walls to reduce the reflected pressure.
- Studies can be carried out for the different arrangements of frangible surrounding walls.
- Test the effect of an accidental explosion of steam boiler on the adjacent building structures.
- FEA studies can be carried out by using the incident wave interaction loading instead of CONWEP loading.
- Design criteria for the steam boiler room can be explored to make the structure safe under the dynamic loading by increasing the thickness of the wall and providing the reinforcement.
- Cost analysis can be carried out for cost-effective design.

Appendix A

Sample Calculations & Formulas

Compression, Tensile, and Modulus of Rupture Calculations

- *Compression Test,*

$$fc' = \frac{P}{\pi r^2}$$

P= Load at Failure

r- radius of the cylinder

Ex. P=37 kips; r=2 in.

$$fc' = \frac{P}{\pi r^2} = \frac{37000\ lbs}{\pi\ \times 2in^2} = 2945\ \text{psi}$$

- *Tensile Strength,*

$$f_t = \frac{2P}{\pi LD}$$

P – Compressive Load at Failure

L- Length of Cylinder

D- Diameter of Cylinder

Ex. P=26 kips; L=12 in.; D=6in.

$$f_t = \frac{2P}{\pi LD}\ = \frac{2\ \times 26000}{\pi\ \times 12\ \times 6} = 232\ \text{psi}$$

- *Modulus of Rupture,*

$$f_r = \frac{PL}{BD^2}$$

$P-$ Load at Failure

$L-$ Beam Span Between Supports

$D-$ Depth of Beam

$B-$ Width of Beam

Ex. P=7 kips; L=20 in.; D= 6in; B=6in.

Appendix B

Positive Phase Wave Parameters

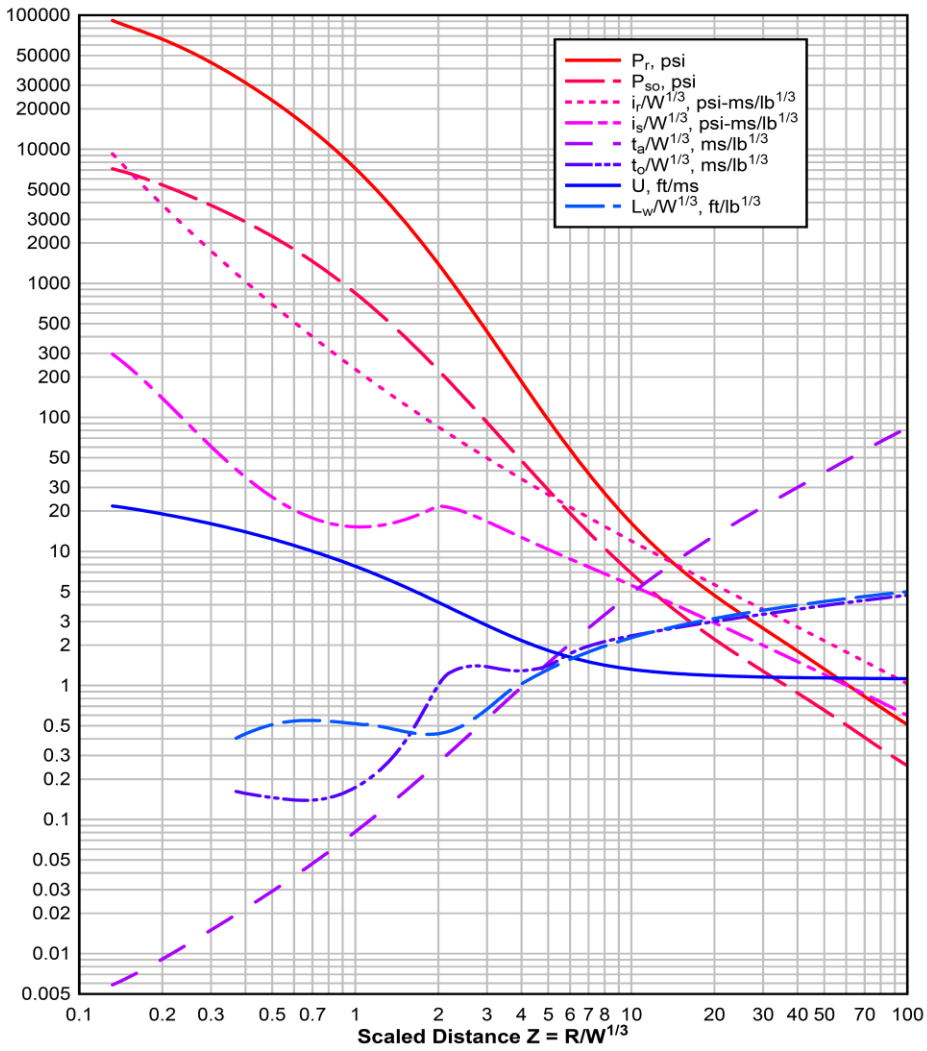

Chart – Positive phase shock wave parameters for a TNT – U*FC* 3-340-02 (2008) [2]

Charge weight = 150 kg = 330.693 lb,

Distance of charge weight to Side wall = 5.577 ft,

Scaled Distance, Z = $\frac{5.577\ ft}{\sqrt[3]{330.693\ lb}} = 0.80653$

Above Chart is used to find the following parameters:

Peak side on over pressure, P_s = 1100 psi,

Peak normally reflected pressure, P_r =11000 psi,

Scaled incident impulse, $i_s / w^{1/3}$ = 15 psi-ms / $lb^{1/3}$,

Incident impulse, i_s = 15 $(330.693)^{1/3}$ = 103.728 psi-ms,

Scaled reflected impulse, $i_r / w^{1/3}$ = 310 psi-ms / $lb^{1/3}$,

Reflected impulse, i_r = 310 $(330.693)^{1/3}$ =2143.729 psi-ms,

Scaled arrival time = $t_A / w^{1/3}$ = 0.06 ms / $lb^{1/3}$,

Arrival time, t_A = 0.06 $(330.693)^{1/3}$ = 0.4149 ms,

Scaled positive phase duration = $t_0 / w^{1/3}$ = 0.15 ms / $lb^{1/3}$,

Positive phase duration, t_0 = 0.15 $(330.693)^{1/3}$ = 1.037 ms ≈ 1 ms (millisecond)

Wave front velocity, U = 9 ft/ms

Scaled wave length of positive pulse $L_w / w^{1/3}$ = 0.55 ft / $lb^{1/3}$

Wave length of positive pulse = 0.55 $(330.693)^{1/3}$ = 3.80 ft.

References

1. Washington, DC: U.S. Department of Defense. 1990. Structures to Resist the Effects of Accidental Explosions (TM 5-1300).
2. Washington, DC: U.S. Department of Defense. 2008. Structures to Resist the Effects of Accidental Explosions (UFC 3-340-02). Washington, DC: U.S. Department of Defense.
3. Dr. Raad Azzawi, MSc Thesis, UoB 1992 “Dynamic behavior of RC barriers in industrial units subjected to the internal explosion”.
4. Dr. Raad Azzawi, Dr. Ali Abolmaali, UTA 2019, “Experimental investigation of steel fiber RC hollow columns under eccentric loading”. Institution of Structural Engineers. Published by Elsevier Ltd.
5. Dr. Raad Azzawi, N.Varughese, 2020 “Flexural behavior of prefelx sfrc-encased steel joist composite beams. Published by Elsevier B.V.
6. ASCE Petrochemical. 1997. Design of Blast Resistant Buildings in Petrochemical Facilities. Reston, VA: Task Committee on Blast Resistant Design, American Society of Civil Engineers.
7. Smith, P., and Hetherington, J., “Blast and Ballistic Loading of Structures, 1st ed,” Butterworth-Heinemann, Oxford, 1994.
8. Kinney, G., and Graham, K., “Explosive Shocks in Air, 2nd ed,” Springer-Verlag, Berlin, 1985.
9. Dusenberry, D., “Handbook for Blast-Resistant Design of Buildings, 1st ed,” John Wiley and Sons, Inc., Hoboken, New Jersey, 2010.
10. Bulson, P., “Explosive Loading of Engineering Structures, 1st ed,” Taylor and Francis Group, London, 1997.

11. Gas Explosion Handbook, Gexon Company, July 2007.
12. Hyde, D., “Users’ Guide for Microcomputer Programs CONWEP and FUNPRO – Applications of TM 5-885-1,” U.S. Army Engineer Waterways Experimental Station, Vicksburg, VA, 1988.
13. Banthia,N,Chokri,K, and Trottier,JF,1995. Impact tests on Cement-Based Fiber Reinforced Composites. ACI Publications, Detroit, USA, SP, 155-9, pp.171-188
14. Khaloo, A R and Kim, N, 1997. “Influence of Concrete and Fiber Characteristics on Behaviour of Steel Fiber Reinforced Concrete under Direct Shear”. ACI Materials Journal, 94, No. 4, pp. 592-601.
15. Johnston, CD, and Zemp, WR, 1991. “Flexural Fatigue performance of Steel Fibre reinforced concrete- Influence of Fibre Content, Aspect Ratio, and Type”. ACI Material Journal, 88, No.4, pp. 374-383
16. Elsaigh, W. A., and Kearsley, E. P. (2006). “Effect of matrix strength on the performance of steel fiber reinforced concrete.” Proc., 3rd Young Concrete Engineers’ Practitioners’ and Technologists’ Conf., Midrand, South Africa.
17. A.M Shende et al. “Comparative Study on Steel Fiber Reinforced cum Control Concrete” International Journal Of Advanced Engineering Sciences And Technologies Vol. No. 6, Issue No. 1, 116 – 120
18. J. Mater. “Mechanical Properties of Steel Fiber Reinforced Concrete”, Journal of Materials in Civil Engineering, Volume 19, Issue 5, 2007
19. Wan Jusoh WA. Hybrid fiber-reinforced composite concrete (HYFRCC). J Civ Eng. 2015;27:466–478.
20. Song W, Yin J. Hybrid effect evaluation of steel fiber and carbon fiber on the performance of the fiber-reinforced concrete. J Eng Res Appl. 2016;9(8):1–12.
21. Mohite, P. M. “History of FEM-Origin of FEM” IIT Kanpur.

22. Abaqus 6.11 Theory Manual (2011).
23. Weck, O. (2005). “CAE-Finite Element Method” Massachusetts Institute of Technology.
24. ASTM C39 Test Method for Compressive Strength of Cylindrical Concrete Specimens
25. ASTM C78 Test Method for Flexural Strength of Concrete
26. ASTM C192 Standard Practice for Making and Curing Concrete Test Specimens
27. ASTM C496 Test Method for Splitting Tensile Strength of Cylindrical Concrete Specimens.
28. Mohamed F. Ibrahim, Hisham A. El-Arabaty, Ibrahim S. Moharram “Effect of a steam boiler explosion on boiler room and adjacent buildings structure,” International Journal of Engineering Science Invention (IJESI), Feb 2019
29. Brode, H.L. (1955). “Numerical Solutions of Spherical Blast Waves.” Journal of Applied Physics. 26 (6), 766-775.
30. Baker, W.E., Cox, P.A., Westine, P.S., Kulesz, J.J., and Strehlow, R.A. (1983). “Explosion Hazards and Evaluation.” Elsevier Scientific Publishing Company, New York.
31. Vasilis Karlos, George Solomos, “Calculation of Blast Loads for Application to Structural Components” European Laboratory for Structural Assessment, December 2013
32. Kingery, C. N., and Bulmash, G. (1984). “Airblast parameters from TNT spherical air burst and hemispherical surface burst.” Technical Rep. ARBRLTR-02555, U.S. Army Armament Research and Development Center, Ballistics Research Laboratory, Aberdeen Proving Ground, Aberdeen, MD.

33. Newmark, Nathan M., 1956. An engineering approach to blast-resistant design (Paper, 2786). ASCE Transactions 121: 45–64. Reston, VA: American Society of Civil Engineers.
34. Nancy Varughese, MSc Thesis, UTA 2019 “Flexural Behavior of Preflex SFRC-Encased Steel Joist Composite Beams”
35. Ezeldin, A. S., and Balaguru, P. N., “Normal- and High-Strength Fiber-Reinforced Concrete under Compression,” Journal of Materials in Civil Engineering, ASCE, V. 4, No. 4, 1992, pp. 415-429. doi: 10.1061/(ASCE)0899-1561(1992)4:4(415)
36. Gao, J.; Sun, W.; and Morino, K., “Mechanical Properties of Steel Fiber-Reinforced, High-Strength, Lightweight Concrete,” Cement and Concrete Composites, V. 19, No. 4, 1997, pp. 307-313. doi: 10.1016/S0958-9465(97) 00023-1
37. Padmarajaiah, S. K., “Influence of Fibers on the Behavior of High Strength Concrete in Fully/Partially Prestressed Beams: An Experimental and Analytical Study,” Indian Institute of Science, Bangalore, India, 1999.
38. Biggs J. M., 1964. Introduction to Structural Dynamics. New York: McGraw-Hill Book Company.
39. Mays, G. C., and P. D. Smith, eds. 1995. Blast Effects on Buildings. London: Thomas Tedford Publications.